HAC REF F7182

MECHANISMS OF RADIATION DAMAGE GENERATED BY IONIZING RADIATION IN OPTICAL WAVEGUIDES

Robert N. Schwartz

Hughes Research Laboratories
3011 Malibu Canyon Road
Malibu, California 90265

September 1988

DAAG29-84-C-0005

Final Report

June 1, 1984 through December 31, 1987

DEPT. OF THE ARMY
ARMY RESEARCH OFFICE
P.O. Box 12211
Research Triangle Park, NC 22709-2211

UNCLASSIFIED
SECURITY CLASSIFICATION OF THIS PAGE

REPORT DOCUMENTATION PAGE

Form Approved OMB No. 0704-0188

1a. REPORT SECURITY CLASSIFICATION: Unclassified	1b. RESTRICTIVE MARKINGS
2a. SECURITY CLASSIFICATION AUTHORITY	3. DISTRIBUTION/AVAILABILITY OF REPORT: Approved for public release; distribution unlimited.
2b. DECLASSIFICATION/DOWNGRADING SCHEDULE	
4. PERFORMING ORGANIZATION REPORT NUMBER(S)	5. MONITORING ORGANIZATION REPORT NUMBER(S): ARO 20676.5-MS
6a. NAME OF PERFORMING ORGANIZATION: Hughes Research Laboratories; 6b. OFFICE SYMBOL (If applicable): HRL	7a. NAME OF MONITORING ORGANIZATION: U.S. Army Research Office
6c. ADDRESS (City, State, and ZIP Code): 3011 Malibu Canyon Road, Malibu, CA 90265	7b. ADDRESS (City, State, and ZIP Code): P.O. Box 12211, Research Triangle Park, NC 27709-2211
8a. NAME OF FUNDING/SPONSORING ORGANIZATION: U.S. Army Research Office; 8b. OFFICE SYMBOL (If applicable)	9. PROCUREMENT INSTRUMENT IDENTIFICATION NUMBER: DAAG29-84-C-0005
8c. ADDRESS (City, State, and ZIP Code): P.O. Box 12211, Research Triangle Park, NC 27709-2211	10. SOURCE OF FUNDING NUMBERS: PROGRAM ELEMENT NO. / PROJECT NO. / TASK NO. / WORK UNIT ACCESSION NO

11. TITLE (Include Security Classification)
Mechanisms of Radiation Damage Generated by Ionizing Radiation in Optical Waveguides

12. PERSONAL AUTHOR(S)
Robert N. Schwartz

13a. TYPE OF REPORT	13b. TIME COVERED	14. DATE OF REPORT (Year, Month, Day)	15. PAGE COUNT
Final	FROM 6/84 TO 12/87	1988, June	132

16. SUPPLEMENTARY NOTATION The view, opinions, and/or findings contained in this report are those of the author and should not be construed as an official Department of the Army position, policy, or decision, unless so designated by other documentation.

17. COSATI CODES		
FIELD	GROUP	SUB-GROUP

18. SUBJECT TERMS (Continue on reverse if necessary and identify by block number)
Optical fibers, radiation damage, mechanisms, germanium-doped silica, heavy metal fluoride glass, optical transmission, EPR

19. ABSTRACT (Continue on reverse if necessary and identify by block number)

Radiation damage generated by ionizing radiation (UV- and γ-radiation) was studied in a variety of optical preforms and fiber-optic waveguides. The materials investigated included germanium-doped silica preforms and fibers, fluorine-doped silica, and heavy metal fluoride glass. Radiation damage and aging effects in bulk and fiber TlBr-TlI (KRS-5) were also investigated. Electron paramagnetic resonance and optical spectroscopies were used to study the centers generated by the ionizing radiation. A parallel study of the intrinsic bonding defects in SiO_2 films grown by a variety of techniques was also carried out.

20. DISTRIBUTION/AVAILABILITY OF ABSTRACT: ☒ UNCLASSIFIED/UNLIMITED ☐ SAME AS RPT ☐ DTIC USERS	21. ABSTRACT SECURITY CLASSIFICATION: Unclassified
22a. NAME OF RESPONSIBLE INDIVIDUAL: Robert N. Schwartz	22b. TELEPHONE (Include Area Code): (213) 317-5595; 22c. OFFICE SYMBOL

DD Form 1473, JUN 86 Previous editions are obsolete. SECURITY CLASSIFICATION OF THIS PAGE

UNCLASSIFIED

1/11

TABLE OF CONTENTS

LIST OF ILLUSTRATIONS

SECTION 1

INTRODUCTION

Fiber-optic waveguides are well known to be sensitive to ionizing radiation such as γ-rays, x-rays, and ultraviolet (UV) photons as well as to energetic particles such as protons, electrons, and neutrons.[1] When optical fibers are exposed to ionizing radiation or energetic particles, defect centers are formed, which, as a result of optical absorption and/or scattering, degrade the transmission characteristics of fiber-optic waveguides. Since fiber-optic waveguides are used in systems that may be exposed to radiation, it is important to understand the origin and microstructure of the resulting color centers in order to develop more radiation-resistant optical fibers.

Moreover, in addition to the defect centers created by exposure to energetic radiation or particles, some defects/color centers are caused by certain methods of fabricating the preforms[2] and by drawing conditions.[3] Improvement of fiber-optic waveguides requires a better understanding of the sources of those defects as well.

The research reported here focused on developing a basic understanding of the structure and mode of formation of radiation-induced defects in the bulk materials used to fabricate fiber-optic waveguides as well as in the optical fibers themselves. Our approach was to identify and structurally characterize the radiation-induced point defects by the use of spectroscopic techniques such as optical and electron paramagnetic resonance (EPR) spectroscopy and to correlate defect formation with material composition, structure, and processing.

In addition to analyzing bulk materials, we carried out a parallel study of the intrinsic defects in SiO_2 films grown by a variety of techniques. Thin-film studies are important not only for providing fundamental information about the nature of defects in silica-based materials, but also for providing detailed information at the molecular level on materials crucial for microelectronic devices, thin-film guided-wave devices, and coatings of optical fibers.

Under Contract DAAG29-84-C-0005, we initiated a collaborative program with Prof. Larry Kevan of the University of Houston to study paramagnetic defects in glassy materials. Two graduate students and one postdoctoral fellow were supported over the period of this contract. Some of the results on the radiation-induced defects in germanium-doped silica described in this report were used in the doctoral thesis (University of Houston, 1985) of Dr. Walee Chamultrat. In addition, the work on radiation-induced centers in heavy-metal fluoride glasses is expected to be presented in the future doctoral thesis of Mr. Guan-Dei Lei.

The results of the research reported here are contained in technical articles that have been published, are in press, or have been submitted for publication. To keep this report to a manageable length, we summarize each paper in Section 2 and present each full-length paper or manuscript as an individual appendix.

SECTION 2

SUMMARIES OF RESEARCH RESULTS

This section summarizes the publications that document our research results and identifies the appendix that presents the complete text of each.

2.1 SUMMARY OF APPENDIX A

"Radiation damage of germanium-doped silica glasses: Spectral simplification by photo- and thermal bleaching, spectral identification and microwave saturation characteristics" [J. Appl. Phys. 59, 2933 (1986)].

Gamma- and UV-induced defect centers in germanium-doped SiO_2 glasses were studied by EPR spectroscopy. In our experiments, we separated the germanium-doped core from the preforms fabricated by the modified chemical vapor deposition technique. We observed that UV irradiation (254 nm) of core samples produces a single type of germanium-related paramagnetic center – the Ge(3) (also called the Ge-E'). On the other hand, γ-irradiation generates several types of germanium-related point defects – the Ge(1), Ge(2), and Ge(3). However, as the γ-irradiated sample is heated or broad-band photoirradiated by a xenon source, the Ge(1) and Ge(2) centers disappear, leaving only the Ge(3) center.

The separated silica cladding was also γ-irradiated and studied by EPR spectroscopy. We observed two types of Si-E' centers, $E'_{\alpha 1}$ and $E'_{\alpha 2}$. At lower radiation doses, one sees significant numbers of both $E'_{\alpha 1}$ and $E'_{\alpha 2}$; at higher doses, however, $E'_{\alpha 2}$ clearly dominates.

In addition, we measured the microwave power saturation at different temperatures in both the core and cladding samples to further differentiate and characterize the various types of radiation-induced point defects. Analysis of the microwave saturation curve of the Ge-E' and Si-E' centers shows that the

characteristic spin relaxation time of the Ge-E' center is ~100 times shorter than that of the Si-E' center. That finding is consistent with an electron spin relaxation mechanism involving modulation of the anisotropic g-tensor.

2.2 SUMMARY OF APPENDIX B

"Electron paramagnetic resonance and optical study of radiation-induced defect centers in doped silica glasses" *Defects in Glasses, [Materials Research Society Symposia Proceedings, Vol. 61:* edited by Frank L. Galeener, David L. Griscom, and Marvin J. Weber (Materials Research Society, Pittsburgh, Penn., 1986), p. 197].

Using optical as well as EPR spectroscopy, we studied the radiation-induced centers in both bulk germanium-doped silica and germanium-doped multimode optical fibers. We also analyzed the defect centers produced by γ- and UV-irradiation in fluorine-doped silica. In both bulk and fibers, γ-irradiation produces several germanium-related centers – the Ge(1), Ge(2), and Ge(3) (or Ge-E'). On the other hand, UV irradiation produces just one type of center – the Ge(3). Significant spectral simplification can be achieved in both bulk and fibers by heating and by broad-band photo-irradiation.

UV-induced optical-loss spectra in the 0.5 to 1.5 μm range were measured as a function of the UV exposure time. We found that the UV-induced loss in germanium-doped multimode silica fibers not only increases with germanium concentration but also shifts to longer wavelengths. In addition, we observed that the UV-induced loss measured at 0.66 μm saturates at long UV exposure times.

Two types of Si-E' centers were observed in γ-irradiated fluorine-doped silica. At lower radiation doses, significant numbers of both $E_{\alpha'_1}$ and $E_{\alpha'_2}$ variants are generated; whereas at higher doses $E_{\alpha'_2}$ is by far the dominant species. In contrast, only the $E_{\alpha'_2}$ variant is produced by UV-irradiation. The photobleached low-gamma-dose fluorine-doped silica sample is also dominated by the $E_{\alpha'_2}$ variant.

2.3 SUMMARY OF APPENDIX C

"Electron paramagnetic resonance studies of intrinsic bonding defects and impurities in SiO_2 thin solid films" *Defects in Glasses, [Materials Research Society Symposia Proceedings, Vol. 61:* edited by Frank L. Galeener, David L. Griscom, and Marvin J. Weber (Materials Research Society, Pittsburgh, Penn., 1986), p. 359].

Recent theoretical[4] and experimental[5] work indicates that the ac electrical transport phenomena in rf-sputtered thin SiO_2 solid films may be controlled by intrinsic bonding defects. We have used EPR spectroscopy to identify possible paramagnetic intrinsic bonding defects in as-deposited thin silica films. Thin films were grown by a variety of techniques, such as electron-beam (E-beam) vacuum deposition, rf sputtering, thermal oxidation of polysilicon, plasma-enhanced chemical vapor deposition (PECVD), and hot- and cold-wall low-pressure chemical vapor deposition (LPCVD). Some of the growth techniques, such as E-beam deposition, rf sputtering, and cold-wall LPCVD, yield thin SiO_2 films with paramagnetic intrinsic bonding defects similar to those observed in bulk radiation-damaged vitreous silica. In contrast, PECVD and hot-wall LPCVD silica films and SiO_2 films formed by oxidizing polysilicon display no room-temperature EPR signal.

We speculate that the paramagnetic point defects in the as-deposited E-beam and rf-sputtered films may result from the activation of preexisting diamagnetic precursor defects by the background radiation (i.e., soft x-rays) and/or the energetic charged particles that are associated with those deposition techniques. In contrast, the CVD techniques have no attendant soft x-rays or energetic particles able to convert diamagnetic precursor defects into paramagnetic states. However, the cold-wall LPCVD reactor contains sufficient hydrogen to form $O_3{\equiv}Si\text{-}H$,

which may be subsequently converted to a paramagnetic center according to the reaction

$$H\bullet + O_3{\equiv}Si\text{-}H \rightarrow O_3{\equiv}Si\bullet + H_2.$$

Here we have introduced the shorthand notation $O_3{\equiv}Si$ to represent three separate covalent bonds to oxygen.

2.4 SUMMARY OF APPENDIX D

"Electron-spin resonance of NO_2 trapped in SiO_2 thin solid films" [J. Appl. Phys. 59, 3231 (1986)].

Certain deposition techniques yield thin solid films of SiO_2 with paramagnetic point defects similar to those found in γ- and x-irradiated bulk vitreous silica. In contrast, we found that the SiO_2 films grown by the PECVD technique show no room-temperature EPR signal in the $g \simeq 2$ region. However, if the PECVD silica film is cooled to 77K, it produces a strong EPR absorption signal with hyperfine structure spread over ~170 G. That signal is assigned to trapped NO_2 radicals, which were incorporated in the film during deposition, probably because plasma-decomposed N_2O was used as a source of oxygen for oxidizing silane to silica.

Further, the temperature-dependent EPR spectra and slow-motional at EPR simulations suggest that the NO_2 radicals undergo axial motional averaging about the y-molecular axis in the plane and parallel to the O-O direction over the temperature range 12 to 87K.

The consequences of NO_2 impurities are not well understood, but they are unlikely to be beneficial for microelectronic devices. Chemically, NO_2 is a strong oxidizer that should contribute to oxidation of the adjacent semiconductor surface during any high-temperature processing. Electronically, NO_2 impurities could conceivably behave as electron traps.

2.5 SUMMARY OF APPENDIX E

"Optical scattering and EPR study of ZBLAN glass: Dependence on preparation and processing methods" [Mater. Sci. Forum 19-20, 275 (1987)].

In recent years, heavy-metal fluoride glasses have been extensively investigated because of their potential use for constructing ultra-low-loss infrared-transmitting optical waveguides. We investigated the influence of glass-processing conditions on optical scattering and, using EPR, studied the types of centers created by ionizing radiation in ZBLAN (ZrF_4, BaF_2, LaF_3, AlF_3, and NaF) glass. Samples of ZBLAN were prepared using several different reactive-atmosphere processing (RAP) schemes such as CF_4-O_2, CCl_4-CF_4-He, CCl_4-O_2, CCl_4-Ar, and CCl_4-He. Light-scattering measurements indicate that samples prepared using CF_4-O_2 yield relatively highly scattering glasses compared to samples processed with CCl_4-Ar or CCl_4-He. It is suspected that oxide-related impurity centers are responsible for the observed high scattering.[6,7]

We also found that the types of radiation-induced centers in ZBLAN glass depend strongly on the glass-processing conditions. For example, ZBLAN glasses processed with CCl_4 yield paramagnetic Cl_2^- centers when γ-irradiated. The Cl_2^- centers are stable at room temperature but absorb in the infrared. We have also observed by EPR a radiation-induced center that is stable even when the glass is heated to 373K. It is believed to be associated with a hole trapped on an oxide-related impurity[8] and may possibly be correlated with the oxygen species responsible for the high scattering levels in ZBLAN glass. In fact, we have observed that the EPR signal intensity of the oxide-related center is lowest in ZBLAN glass processed with either CCl_4-Ar or CCl_4-He.

2.6 SUMMARY OF APPENDIX F

"Radiation-induced paramagnetic defects in heavy metal fluoride glasses" [Radiat. Phys. Chem. 32, 439 (1988)].

A fundamental obstacle to the use of heavy-metal fluoride glasses in fabricating infrared transmitting optical fibers is the presence of oxide anion impurities that have been correlated with scattering loss in the fiber.[9] We investigated the effects of water contamination on the radiation-damage process in heavy-metal fluoride glasses, focusing on the correlation of oxide impurities with the observed radiation-induced paramagnetic defects. We used EPR and electron-spin-echo (ESE) modulation techniques to study the paramagnetic point defects generated by γ-irradiation in both pristine and water-contaminated ZBLAN glass. We found that the radiation-induced center remaining after an irradiated sample was annealed at 393K is not associated with an oxide impurity introduced by water corrosion. Further, ESE modulation results indicate that the hole trap associated with the "central resonance"[9] is complex, involving not only F^- and Al^{3+} ions but also O^{2-}.

2.7 SUMMARY OF APPENDIX G

"Aging effects in bulk and fiber TlBr-TlI" [J. Appl. Phys. 63, 4365 (1988)].

It has long been suspected that the degradation of the optical properties of TlBr-TlI (KRS-5) results from water contamination. Secondary-ion mass spectroscopy (SIMS) and neutron-scattering data indicate that a significant amount of a hydrogen-related impurity accumulates in the surface layers of the crystalline/polycrystalline material. We used a variety of techniques, including SIMS, powder-neutron and x-ray diffraction, and infrared and EPR spectroscopy, to probe the chemical and structural properties of both pristine and aged TlBr-TlI.

Following γ-irradiation at 77K, we observed a radiation-induced EPR spectrum consisting of a strong doublet (~42 G splitting) centered at $g \simeq 2.008$. We believe that the doublet results from the radiolysis of H_2O trapped in the TlBr-TlI material; we assigned it to the •OH radical. This result suggest that the H-bearing impurity is water. EPR at 77K revealed no radiation-induced paramagnetic defects intrinsic to TlBr-TlI following γ-irradiation at 77K.

2.8 SUMMARY OF APPENDIX H

"A simultaneous electron paramagnetic resonance (EPR) and optical absorption study of ultraviolet-induced defect centers in Ge-doped silica fibers" [to be published in J. Appl. Phys., 1988].

Because of its long optical pathlength, the fiber-optic waveguide is a unique medium for studying color centers in low concentration or those with low intrinsic oscillator strength. Optical spectroscopy, on the one hand, is a highly sensitive measurement technique, but it lacks the structural specificity of EPR. Therefore, a combination of both spectroscopic techniques is desirable for probing the defect structure in germanium-doped silica fibers. Simultaneous measurement of both the optical absorption and the EPR in the same fiber sample is also useful for unambiguously determining whether a correlation exists between the color-center absorption and the EPR signal.

To carry out such an experiment, we designed and assembled a coil of optical fiber (see Figure 1) that can be inserted in the microwave cavity of the EPR spectrometer (see Figure 2), thus allowing simultaneous measurement of both the optical absorption and the EPR in the fiber (see Figure 3). Another important feature of this experimental arrangement is the ability to carry out *in situ* UV-irradiation of the optical fiber coil.

M17991

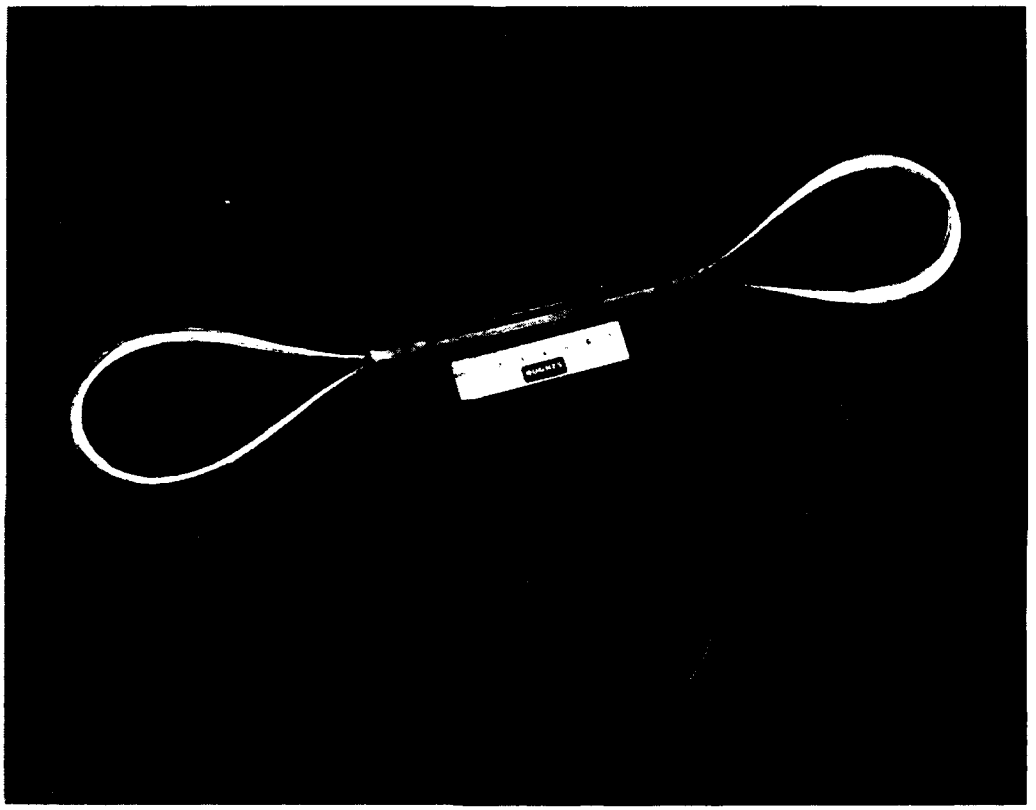

Figure 1. Optical fiber coil.

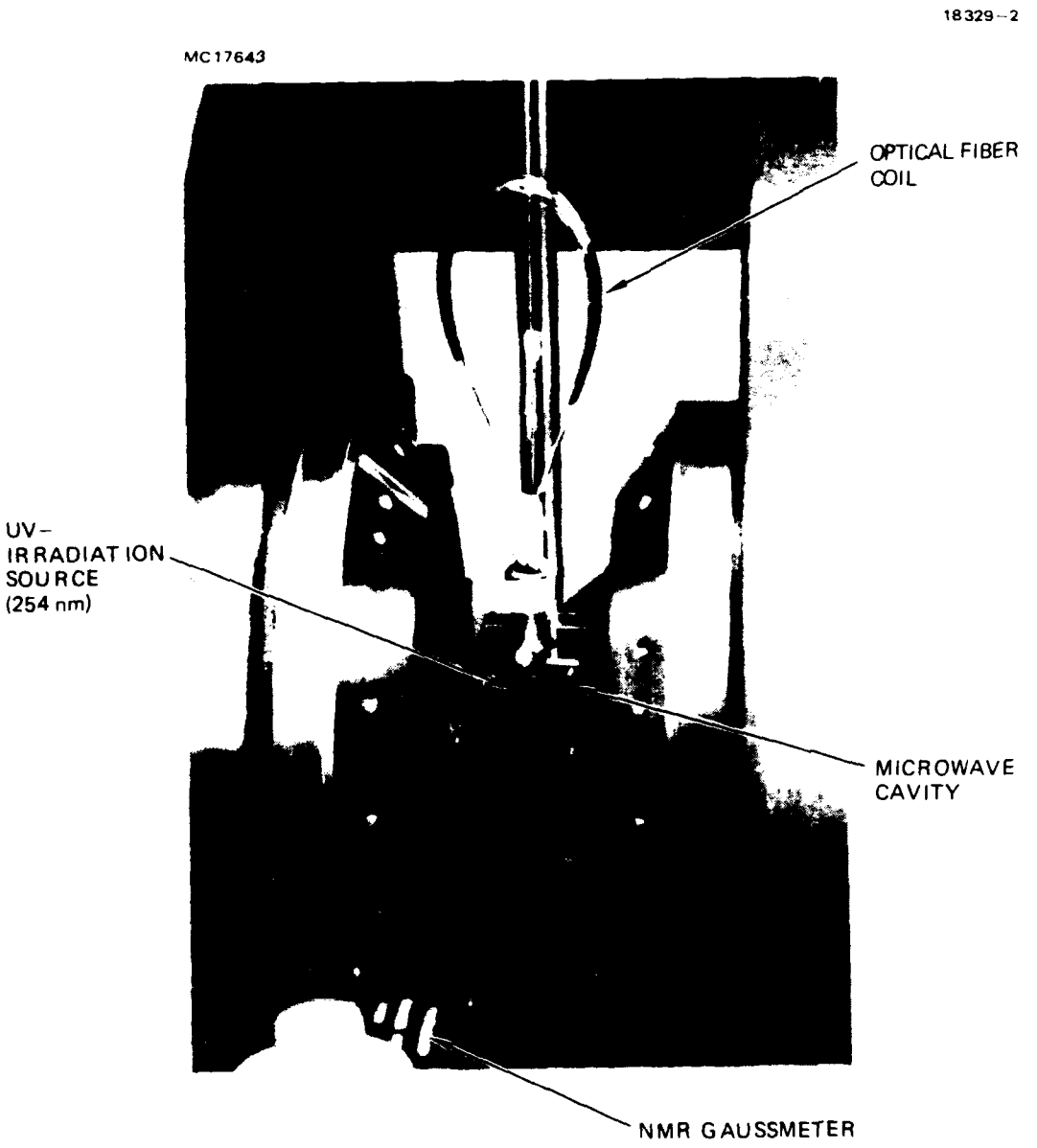

Figure 2. Optical fiber coil in EPR microwave cavity.

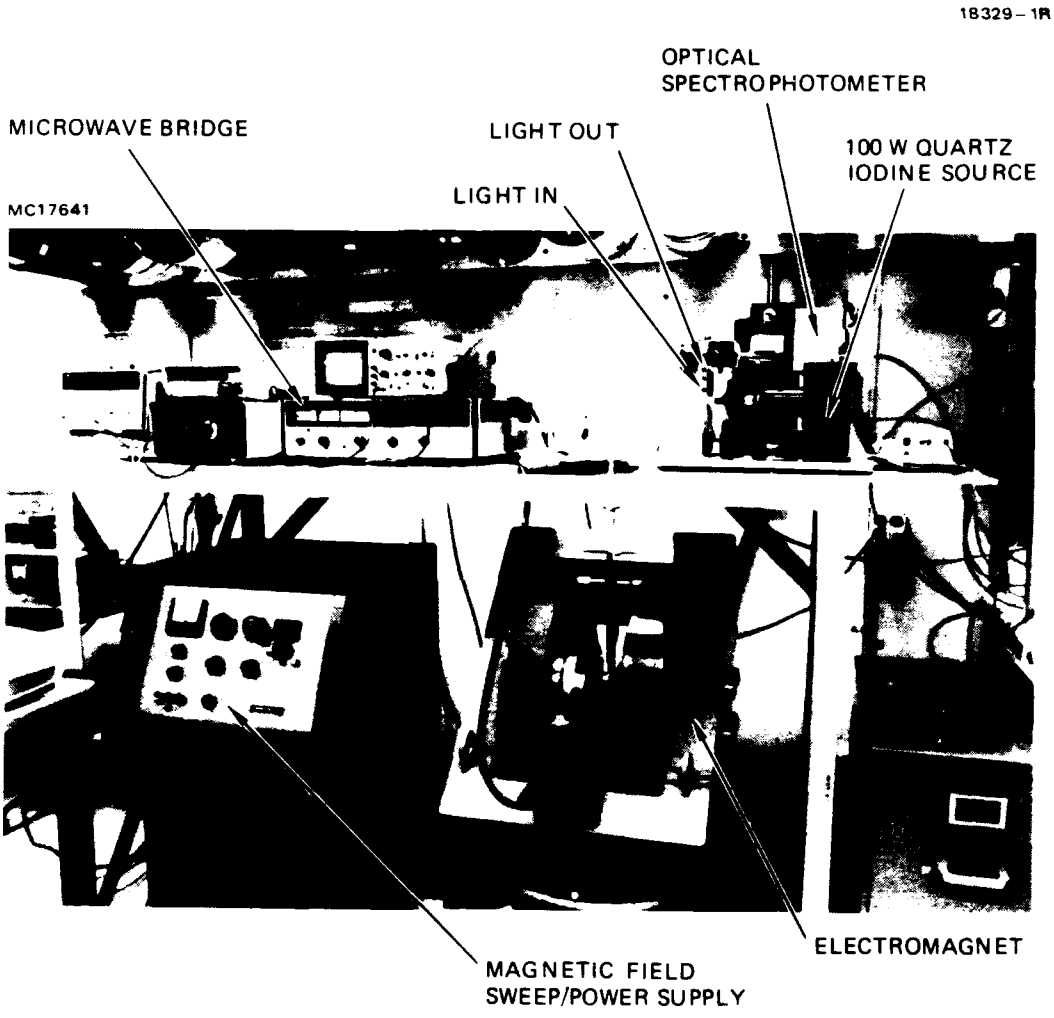

Figure 3. Experimental configuration for simultaneous optical absorption and EPR measurements.

Using the same setup, we measured the optical absorption and EPR in a germanium-doped silica optical waveguide following *in situ* irradiation with 254 nm (4.88 eV) photons. In the irradiated fiber, the EPR signal is dominated by the resonance of the Ge-E′ center. Over the limited range of dose exposure (~5.5 J/cm^2) covered by our experiments, we observed a direct correlation between the radiation-induced growth of the paramagnetic Ge-E′ center and the UV-induced optical loss in the 1.77 to 3.00 eV (700 to 413 nm) spectral region. No UV-induced loss was observed in the near-infrared, i.e., over the range 0.7 to 1.38 eV (1771 to 900 nm).

Our experiments do not indicate whether the UV-induced loss in the visible is owing to the UV optical-absorption-band tails of the Ge-E′ center or the tails associated with one or more different absorbing defects, such as diamagnetic color centers as numerous as the paramagnetic Ge-E′ centers. We conjecture, however, that the UV-induced loss may be associated with the band tails of a diamagnetic electron trap.

SECTION 3

COMPENDIUM

In this section we bring together those portions of the detailed published papers and manuscripts summarized in Section 2 which will not only provide a coherent picture of the nature of the work carried out under this contract but in addition, relate to the broader picture of radiation damage in optical waveguide fibers and bulk optical materials.

An EPR signal assigned to Ge-E' centers was first reported by Weeks and Purcell[8] in electron- and γ-irradiated glassy and crystalline GeO_2. In GeO_2-SiO_2 glasses, Frieble et al.[10] reported four kinds of EPR signals that were due to Ge-associated defect centers. These centers were denoted Ge(0), Ge(1), Ge(2), and Ge(3), with the Ge(3) defect assigned to the Ge-E' center. It was assumed that the Ge(n) centers (n = 1 to 3) consisted of an electron trapped in a dangling bond on the Ge atom (three-fold coordinated) and n next-nearest neighbor Ge atoms bonded through the three bridging oxygens. Our studies of photobleaching and UV-induced defect formation in germanium-doped silica (Appendices A and B) along with the simultaneous study by Watanabe et al.[11] of the ^{73}Ge hyperfine structure associated with the Ge(n) centers in Ge-doped silica fibers suggest that the Ge(1,2) centers are not Ge-E' type defects. A structural model consistent with the ^{73}Ge hyperfine structure data indicates that the Ge(1) center is best described as an unpaired electron localized on a four-coordinated Ge atom substitutional for Si in the silica network. Even though the Ge(1) and Ge(2) centers have similar hyperfine couplings, it is observed that Ge(2) is more stable than Ge(1). Additional work is required in order to sort out the structural distinctions between the Ge(1) and Ge(2) point defects.

Thin SiO_2 dielectric films are technologically important materials currently used in the fabrication of microelectronic

devices and thin-film guided wave devices, and have potential application as coatings of optical fibers. EPR studies of SiO_2 thin films are not only important for providing fundamental information about the electronic structure of the defects (intrinsic and extrinsic) in these silica-based materials but also the factors controlling their formation. Our studies on thin SiO_2 films reported in (Appendices C and D) are unique in that we have studied films grown by a variety of techniques such as E-beam evaporation, rf sputtering, plasma enhanced chemical vapor deposition (PECVD), hot and cold wall low pressure chemical vapor deposition (LPCVD), and thermal oxidation of polysilicon. We find that intrinsic defect formation is extremely fabrication-process dependent. For example, in the E-beam and rf sputtering deposition techniques, a vitreous silica target is bombarded by highly energetic charged particles which produce in the gas phase not only molecular SiO_2, but also charged and neutral atomic and molecular fragments. Thus stable as well as highly reactive species arrive at the surface of the substrate and recombine to form the thin solid film. Under these conditions intrinsic precursor diamagnetic defects, such as oxygen vacancies and peroxy interstitials, are formed. Since the E-beam and rf sputtering deposition techniques are accompanied by soft x rays and energetic particles, electrons and holes are generated, which then become trapped at the appropriate precursor sites leading to the formation of paramagnetic point defects.

Chemical vapor deposition techniques, on the other hand, also involve complex chemical processes in both the gas phase and at the substrate surface. In contrast to the E-beam and rf sputtering techniques, CVD techniques do not have the attendant soft x rays or energetic particles necessary for converting diamagnetic precursor defect sites into paramagnetic states. Paramagnetic defects are observed, however, and it is proposed that their formation is linked with the fact that sufficient

hydrogen is available in the cold wall LPCVD reactor to form $O_3{\equiv}Si\text{-}H$, which is subsequently converted to an $E\beta$ center according to the reaction[12]

$$H^{\circ} + O_3{\equiv}Si\text{-}H \rightarrow O_3{\equiv}Si^{\bullet} + H_2 .$$

Here we have used the notation $O_3{\equiv}Si$ to represent three separate bonds to oxygen.

In recent years complex fluoride glasses based on ZrF_4 have been extensively investigated because of their potential application in ultra-low-loss fiber optic waveguides and laser windows. One of the fundamental materials issues concerning the use of the heavy metal fluoride glasses (HMFG) for optical waveguide applications has been the reduction in the concentration of impurities, such as transition metal and rare-earth group ions and oxide anions, to the parts-per-billion level. Our studies (Appendices E and F) have focused on the oxide anion impurities. Various glass processing procedures have been developed for producing heavy metal fluoride melts with relatively low concentrations of anion impurities, such as OH^- and O^{2-}. One of the more successful methods is the reactive atmosphere processing (RAP)[13] technique, which utilizes a variety of gas mixtures, such as CCl_4/HF, SF_6/He and CF_4/O_2, that are reactive at high temperatures. These reactive component gases are efficient for removing OH^- and O^{2-} impurities from the melt, as well as any H_2O present as impurity in the gases or from outgassing of the system.

Because of the sensitivity of the technique, we have used EPR spectroscopy to detect anion impurities that have been rendered paramagnetic by exposing the HMFG to ionizing radiation. In particular, there is a paramagnetic defect center observed in γ-irradiated HMFG samples annealed at high-temperatures (~393K), which has been suggested[8] to be associated with a hole trapped on an oxide-related impurity (O-center).

Work carried out in our laboratory (Appendix E) and also by Griscom et al.[14] at the Naval Research Laboratory indicates that the O-center EPR signal intensity is increased in $O_{2(g)}$-treated HMFG samples. Griscom and coworkers[14] assign the oxide-related impurity signal to an O_2^- molecular radical anion and suggest that the precursor is an O_2^{2-} ion incorporated in the HMFG as a result of oxidation of metallic iron present in the platinum crucibles used for processing the glass.

In contrast, our results on water-treated HMFG (Appendix F) show that the corrosive attack of water does not lead to an increase in the intensity of the O-center EPR signal. This observation indicates that water-corrosion does not result in the incorporation of precursor O_2^{2-} molecular ions. However, other components of the complex EPR resonance absorption in γ-irradiated water-treated HMFG, in particular the "central resonance," are strongly affected. This observation suggests that the "central resonance," which was initially modeled as a defect consisting of a hole delocalized over several fluorine atoms, may be more complex than originally proposed and thus, may also involve an oxygen anion impurity such as O^{2-}.

Over the past decade, silica-based technology has provided low-loss glasses for fabricating optical fibers. In recent years, however, silica-based optical fibers have come under scrutiny, because it has been demonstrated that nonsilica-based materials have potentially lower transmission losses (i.e., <0.01 dB/km). Of particular importance are materials for fabricating infrared transmitting optical waveguides. One of the most promising materials is polycrystalline thallium bromo-iodide. This material is known to transmit from 0.6 to 40 μm, and due to low intrinsic scattering losses from Rayleigh and Brillouin mechanisms and a multiphonon edge that is shifted to longer wavelengths, it has a theoretical transmittance loss of $\sim 10^{-3}$ dB/km at 10.6 μm.[15] One of the major problems with this material is that the optical loss at 10.6 μm is orders of

magnitude higher than predicted by theory. Also, even though this material has been utilized in the construction of infrared transmitting optical components for ~40 years, nothing is known about its response to ionizing radiation.

Our research (Appendix G) on this potentially important infrared transmitting material represents the first physicochemical study of optical aging in bulk and fiber thallium bromo-iodide. We have used a variety of techniques, including secondary ion mass spectrometry (SIMS), powder neutron and x-ray diffraction, IR, and EPR spectroscopy, to elucidate the chemical and structural basis of optical aging in both bulk and fiber samples. We have found that optical aging is correlated with the accumulation of a H-bearing impurity in the surface layers of the material. It is concluded from EPR and neutron inelastic scattering measurements[16] that the H-bearing impurity is water. Furthermore, we have also observed that impurity-free thallium bromo-iodide is fairly radiation tolerant, with respect to forming intrinsic color centers, when subjected to dose levels up to ~3 Mrad (the highest levels used in our study) of ^{60}Co γ-radiation.[17]

In general, the interaction of high energy radiation (hard radiation), such as x rays and γ rays, or energetic particles, such as neutrons, protons, and electrons, is extremely complex - ranging from the displacement of atoms far from their equilibrium lattice positions as a result of neutron-nucleus collisions, to the generation of secondary fast electrons by Compton scattering of γ-quanta. The end result is the production of transient as well as long-lived defects (color or scattering centers) that deteriorate the optical characteristics of fiber-optic waveguides. In addition to the response of matter to hard radiation, there is an increasing interest in understanding the types of defects created in fiber-optic glasses by low energy photons, such as UV and even longer wavelength photons. This interest has arisen because of the

potential of radiation-induced damage to optical fiber used to transmit high-average-power laser radiation. Also, there is evidence that the UV radiation used for crosslinking prepolymer fiber coatings leads to the formation of color centers in Ge-doped silica fibers, which results in losses approaching several hundred decibel per kilometer over the spectral range of 500 to 1100 nm.

During the course of our research (Appendices A and G) we observed that one of the unique results of using UV photons to create color centers in Ge-doped silica is that only a subset of possible active defect centers is produced thus leading to spectral simplification. In order to obtain detailed information about color center electronic structure and optical loss, we developed a unique technique (Appendix G) to measure simultaneously the optical absorption and the EPR in Ge-doped multimode fiber following in situ irradiation with 254 nm radiation. What we mean by simultaneous is that the experimental arrangement allowed the measurement of both the EPR and optical absorption following in situ UV irradiation on the same sample in the microwave cavity of the EPR spectrometer without disturbing the experimental configuration.

Our main results are: (1) in UV-irradiated (254 nm) fiber the EPR signal is dominated by the resonance of the Ge-E' (Ge(3)) center; (2) over the limited range of dose exposure in our experiments, we observed a direct correlation between the radiation-induced growth of the paramagnetic Ge-E' defect center and the UV-induced optical loss in the visible spectral region (~400 to 750 nm); and (3) no UV-induced loss was observed in the near-infrared spectral region (~900 to 1800 nm). We also carried out some preliminary experiments on the influence of the fiber drawing conditions on the concentration of Ge-E' centers. In general we observed that lower drawing temperatures and lower drawing speeds result in lower concentrations of Ge-E' centers.[18]

Our results are in agreement with the recently published results of Hanafusa et al.,[3] which treats in detail the influence of fiber drawing conditions on color center production.

SECTION 4

STUDENTS SUPPORTED AND DEGREES AWARDED UNDER U.S. ARMY RESEARCH OFFICE SPONSORSHIP

During the course of Contract DAAG29-84-C-0005, we initiated a program of research at the University of Houston, under the direction of Prof. Larry Kevan, to study paramagnetic defects in crystalline and noncrystalline materials by electron paramagnetic resonance spectroscopy. The following graduate students and postdoctoral fellow worked at the University of Houston on research directly related to this contract:

- Graduate Students:

  1. Walee Chamulitrat, Ph.D. thesis, University of Houston, September 1985 (Part I. "Electron Magnetic Resonance Studies of Oxygen Radical Matrix Motions and Interactions in Polymers and on Surfaces." Part II. "Electron Spin Resonance Characterization of Radicals on Silicon Dioxide Surfaces").

  2. Guan-Dao Lei.

- Postdoctoral fellow: Dr Daniella Goldfarb (Ph.D. 1985, Weizmann Institute of Science, Rehovot, Israel).

24 Blank

REFERENCES

1. E.J. Fiebele and D.L. Griscom, in *Treatise on Material Science and Technology,* Vol. 17, Glass II, edited by M. Tomozawa and R.H. Doremus (Academic Press, New York, 1979).

2. E.J. Friebele, D.L. Griscom, and M.J. Marrone, J. Non-Cryst. Solids 71, 133 (1985).

3. H. Hanafusa, Y. Hibino, and F. Yamamoto, Phys. Rev. B 35, 7646 (1987).

4. K. Simakawa and A. Kondo, Phys. Rev. B 27, 1136 (1983).

5. M. Meaudre and R. Meaudre, J. Non-Cryst. Solids 68, 281 (1984).

6. S. Mitachi, S. Sakaguchi, H. Yonezawa, K. Shikano, T. Shigematsu, and S. Takahashi, Jpn. J. Appl. Phys. 24, L827 (1985).

7. T. Nakai, Y. Mimura, O. Shinbori, and H. Tokiwa, Jpn. J. Appl. Phys. 25, L704 (1986).

8. R. Cases, D.L. Griscom, and D.C. Tran, J. Non-Cryst. Solids 72, 51 (1985).

9. T. Nakai, Y. Mimura, H. Tokiwa, and O. Shinbori, J. Lightwave Technol. LT-3, 565 (1985).

10. E.J. Friebele, D.L. Griscom, and G.H. Sigel, Jr., J. Appl. Phys. 45, 3424 (1974).

11. Y. Watanabe, H. Kawazoe, K. Shibuya, and K. Muta, Jpn. J. Appl. Phys. 25, 425 (1986).

12. D.L. Griscom, J. Appl. Phys. 58, 2524 (1985).

13. R.C. Pastor and A.C. Pastor, Mat. Res. Bull. 10, 251 (1975).

14. D.L. Griscom, P. Hart, J.M. Jewell, J.T. Kohli, and J.E. Shelby, J. Non-Cryst. Solids 103, 300 (1988).

15. J.A. Harrington and A.G. Standlee, Appl. Opt. 22, 3073 (1983).

16. A.R. Williams and J.A. Wysocki (unpublished results).

17. R.N. Schwartz and G.D. Lei (unpublished results).

18. R.N. Schwartz (unpublished results).

19. H. Hanafusa, Y. Hibino, and F. Yamamoto, Phys. Rev. B 35, 7646 (1987).

APPENDIX A

RADIATION DAMAGE OF GERMANIUM-DOPED SILICA GLASSES: SPECTRAL SIMPLIFICATION BY PHOTO- AND THERMAL BLEACHING, SPECTRAL IDENTIFICATION AND MICROWAVE SATURATION CHARACTERISTICS

Reprinted from

Journal of
APPLIED PHYSICS

Volume 59 | 15 April 1986 | Number 8

Radiation damage of germanium-doped silica glasses: Spectral simplification by photo- and thermal bleaching, spectral identification and microwave saturation characteristics

Walee Chamulitrat and Larry Kevan
Department of Chemistry, University of Houston, Houston, Texas 77004

Robert N. Schwartz, G. Richard Blair, and Gregory L. Tangonan
Hughes Research Laboratories, 3011 Malibu Canyon Road, Malibu, California 90265

pp. 2933-2939

a publication of the American Institute of Physics

Radiation damage of germanium-doped silica glasses: Spectral simplification by photo- and thermal bleaching, spectral identification and microwave saturation characteristics

Walee Chamulitrat and Larry Kevan
Department of Chemistry, University of Houston, Houston, Texas 77004
Robert N. Schwartz, G. Richard Blair, and Gregory L. Tangonan
Hughes Research Laboratories, 3011 Malibu Canyon Road, Malibu, California 90265

(Received 4 October 1985; accepted for publication 2 January 1986)

Germanium-doped silica glasses are important materials used in the fabrication of preforms from which optical waveguides are drawn. The preforms consist of an outer cladding of silica and an inner core of germanium-doped silica. These separate portions have been subjected to varying types of ionizing radiation and the centers generated have been studied by electron-spin resonance spectroscopy. Core samples show the generation of a single type of germanium E' center in the silica matrix which is surrounded by three next-nearest-neighbor germanium atoms and is specified as Ge(3) after xenon lamp irradiation at room temperature. If γ irradiation is used, several germanium E' centers with varying numbers of next-nearest-neighbor germanium atoms ranging from 0 to 3 are generated and are designated as Ge (n) centers, where $n = 0, 1, 2$, and 3. The Ge(1) and Ge(2) centers disappear after heat treatment at a temperature of ~ 500 K leaving only the Ge(3) center as the most stable of these species. The intensity of the Ge(3) centers after γ irradiation and heat treatment increases in intensity with the γ-irradiation dose to at least ~ 0.5 Mrad. Photobleaching by xenon lamp irradiation of γ-irradiated core samples also decreases the intensity of the Ge(1) and Ge(2) centers. Gamma irradiation of cladding samples generates two different types of silicon E' centers, $E'_{\alpha 1}$ and $E'_{\alpha 2}$. At a lower radiation dose one sees a mixture of $E'_{\alpha 1}$ and $E'_{\alpha 2}$, but at a higher radiation dose, $E'_{\alpha 2}$ dominates. Microwave power saturation data at different temperatures on both the core and the cladding samples are used to further differentiate and characterize these various species. It is found that a relaxation mechanism involving modulation of the g anisotropy is probable.

I. INTRODUCTION

In recent years research on SiO_2-GeO_2 glasses has been intensified because of the potential use of this material in low attenuation optical waveguides for communication. To date, research efforts to develop extremely low-loss as well as radiation-tolerant optical waveguides using germanium-doped silica glass has focused on identifying the paramagnetic defect centers produced by ionizing radiation[1,2] and by fabrication processes.[3,4] These studies have been extremely useful for not only characterizing the radiation response of optical-waveguide glasses but also for understanding the mechanisms of color center formation and for developing means to minimize their formation.[5,6]

Friebele *et al.*[1] identified four germanium-related defects in γ-irradiated germanium-doped silica using electron-spin resonance (ESR) spectroscopy. Since the spectra were complex due to overlapping resonances, detailed spectral simulations were required to determine the g tensor components for each defect center. Further studies of their spectral assignment have not progressed since this original work.

In the present work we demonstrate methods for spectral simplification of the complex spectra in γ-irradiated germanium-doped silica and the use of the progressive microwave power saturation to assist in the spectral assignment of the overlapping resonances in this important system.

II. EXPERIMENT

Optical preform glasses were prepared by the modified chemical vapor deposition technique (MCVD) using $SiCl_4$ and $GeCl_4$ as reagents. The quantities of gas for depositing the glass in Heraeus Amersil TO-8 quartz tubing were controlled by a Tylan gas handling system. The germanium content was determined by both arc-emission and energy-dispersive x-ray analysis and was found to be 8.8 mole % GeO_2. The preforms were cut to separate the core and cladding parts. Each sample had an approximate length of 0.3 cm and a cross section of 0.2 cm diameter. All samples were irradiated at room temperature by ^{60}Co γ radiation at a dose rate of 1.12 Mrad h^{-1}. Core samples were irradiated for various doses up to 1 Mrad, whereas samples of cladding were irradiated to levels as high as 8.8 Mrad. In addition to γ irradiation, photoirradiations were also carried out with a 1-kW xenon arc lamp with the output passed through a 3-cm water filter to filter out infrared radiation. The shortest wavelength component from this source was ~ 250 nm. At 420 nm the light intensity at the sample position from the xenon light source was measured with a radiometer to be 0.017 J s^{-1} cm^{-2}.

Electron-spin resonance (ESR) spectra were obtained at 9.1 GHz with a Varian model E-4 ESR spectrometer with 100-kHz magnetic field modulation. For the microwave

 0021-8979/86/082933-07$02.40

power saturation studies a Varian E-9 ESR spectrometer was used which allows greater variation of the microwave power. Temperature variation was carried out by cold nitrogen gas flow with a Varian variable-temperature accessory. Temperatures were monitored to $\pm$ 1 K with a copper-Constantan thermocouple with a digital voltmeter readout. Spectral g values were calibrated against a Cr^{3+} in MgO standard references with $g = 1.9796$. The g values were also calculated by measuring the microwave frequency with a Hewlett-Packard 5342A microwave frequency counter and the magnetic field with a Varian nuclear magnetic resonance gaussmeter. The g values were determined with an estimated error of $\pm$ 0.0005.

Gamma-irradiated glassy core samples were subjected to subsequent temperature treatment at about 500 K with the flame from a natural gas–oxygen torch. The temperature was monitored using an iron-Constantan thermocouple. Gamma-irradiated core samples were also photobleached by xenon lamp irradiation. ESR spectra were recorded periodically after both heat treatment and photobleaching.

III. RESULTS

Unirradiated core samples show an approximately axially symmetric ESR spectrum with $g_1 = 2.0010$, $g_2 = 1.9949$, and $g_3 = 1.9935$ as shown in Fig. 1(a). After γ irradiation a doublet with a splitting of 119 G was detected as well as a new signal at $g \simeq 2$ as shown in Fig. 1(b). The intensity of this new complex signal versus radiation dose is shown in Fig. 2. The yield increases linearly to about 0.1 Mrad and increases more slowly up to about 1 Mrad.

The ESR spectrum of γ-irradiated bulk cladding material is shown in Fig. 3(a). The $g \simeq 2$ range of this spectrum is shown in more detail in Fig. 3(b) as a function of γ-irradiation dose. One can see that at a lower dose several signals seem to overlap, whereas at a higher dose one apparently axially symmetric signal becomes dominant. This dominant signal can be identified as a silicon E' center.

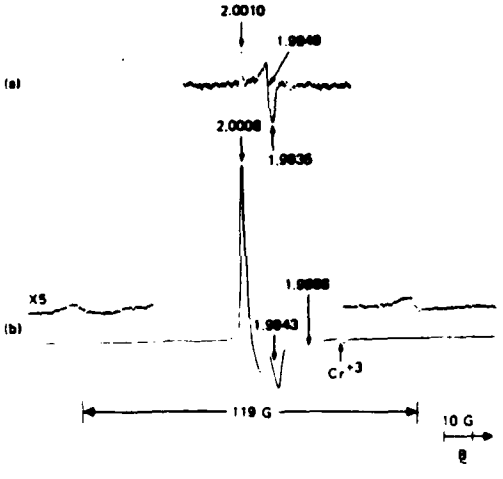

FIG. 1. ESR spectra at room temperature of (a) an unirradiated core sample with signals at $g_1 = 2.0010$, $g_2 = 1.9949$, and $g_3 = 1.9935$, and (b) a γ-irradiated core sample with a 119 G doublet and several overlapping lines. Cr^{3+}/MgO was used as a field marker with $g = 1.9796$.

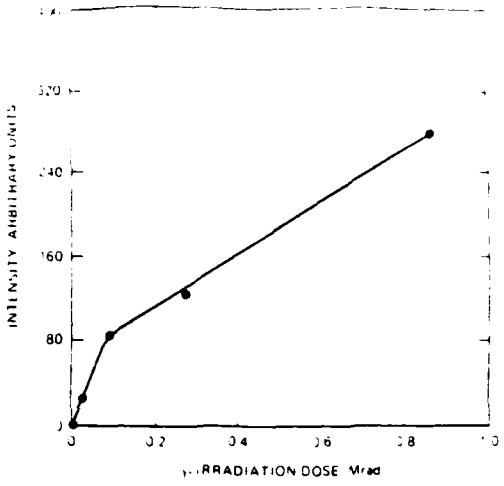

FIG. 2. The dose dependence of a γ-irradiated core sample measured by ESR at $g = 2.0008$. The intensity is normalized per gram of the core sample.

Xenon lamp irradiation of the core samples was found to produce an axially symmetric ESR spectrum as shown in Fig. 4(a). This signal starts to saturate after about 30 h of xenon lamp irradiation as shown in Fig. 5. The signal generated in the core sample is much larger than the signal generated by the same xenon lamp irradiation in the cladding sam-

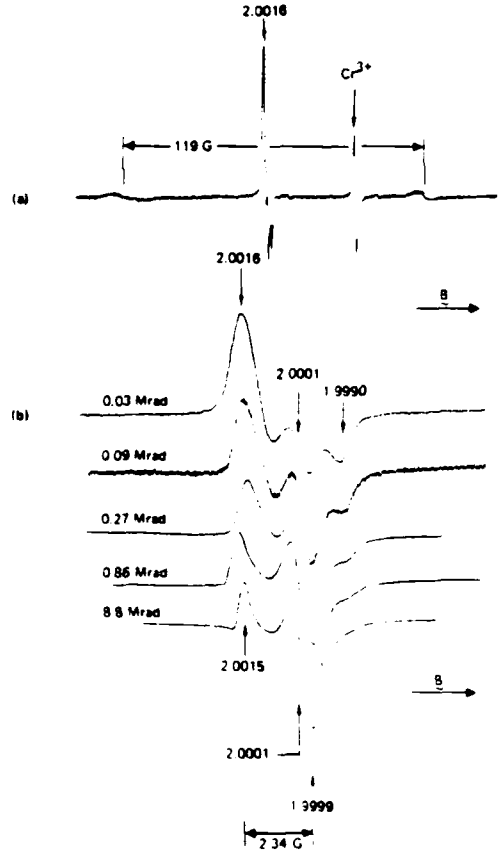

FIG. 3. Room temperature ESR spectra of γ-irradiated cladding samples showing (a) silicon-related defect centers at $g \simeq 2$ and a doublet 119 G, and (b) dose dependence of the $g \simeq 2$ region.

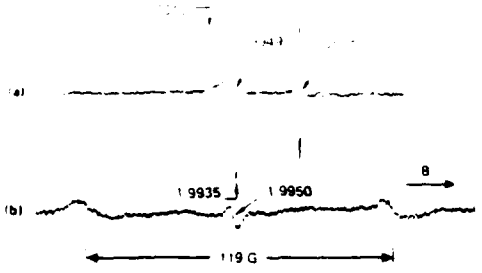

FIG. 4. Room temperature ESR spectra of (a) a core sample xenon lamp irradiated for 3 h showing signals at $g_1 = 2.0010$, $g_2 = 1.9949$ and $g_3 = 1.9935$ and (b) a cladding sample xenon lamp irradiated for 8 h showing a 119 G doublet and an isotropic line with a 5 G peak-to-peak derivative linewidth.

ple as shown in Fig. 4(b). The cladding sample generates a weak 119-G doublet and an isotropic signal near $g = 1.9950$ with a linewidth of 5 G. Gamma-irradiated core samples were subjected to xenon lamp irradiation and ESR spectra were recorded periodically after 15, 30, and 60 min of exposure as shown in Fig. 6. It is seen that the overall signal intensity is significantly reduced except at $g = 1.9943$ which is assigned to the Ge(3) defect center; see below.

It was also found that the γ-irradiated core samples could be heated by an oxy–gas torch at about 500 K to decrease the complexity of the ESR spectra and to generate exclusively the Ge(3) center. The heat treatment was stopped after complete conversion to Ge(3). The intensity of each core sample of the simplified Ge(3) signal with γ-irradiation dose and subsequent heat treatment is shown in Fig. 7. It is seen that the intensity of the signal increases to about 0.5 Mrad before starting to saturate.

Microwave power saturation studies were made to help ascertain which signals are due to the same species. Figure 8 shows power saturation curves for the γ-irradiated sample with measurements done at room temperature at three different spectral positions corresponding to $g = 2.0008$, 1.9943, and 1.9866 [see Fig. 1(b)]. Note that the three saturation curve shapes are different, indicating different species

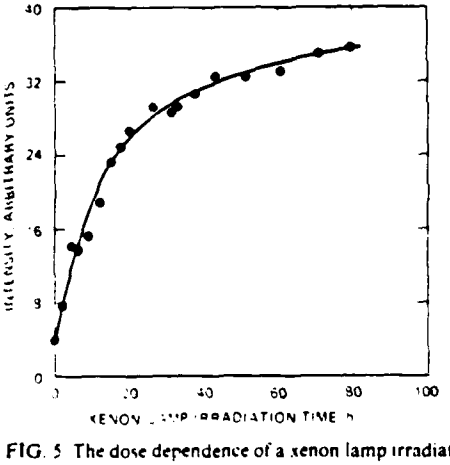

FIG. 5. The dose dependence of a xenon lamp irradiated core sample. The intensity was measured at $g = 2.0010$.

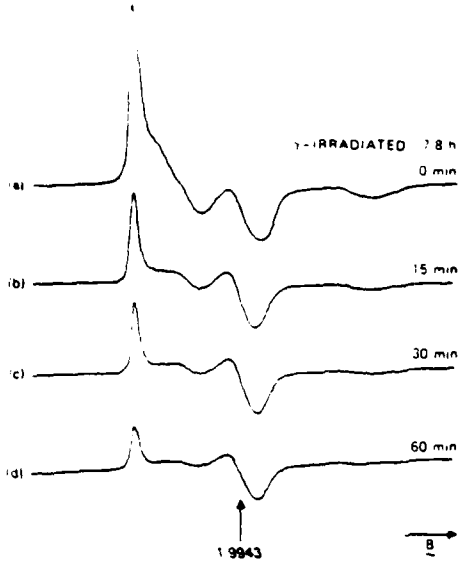

FIG. 6. Room temperature ESR spectra of γ-irradiated core samples showing spectral simplification by photobleaching. All spectra are recorded the same gain.

or different combinations of species. Analogous microwave power saturation curves for resonance signals at $g = 2.0010$ and 1.9949 [see Fig. 4(a)] are shown in Fig. 9 for xenon lamp-irradiated samples. These signals at $g = 2.0010$ and $g = 1.9949$ show the same saturation behavior as the signal at $g = 1.9943$ [see Fig. 8(b)] of the γ-irradiated samples for the entire range of microwave power which suggests that all three signals are due to the same species.

The temperature dependence of the saturation curves for both core and cladding samples were also studied. To characterize the saturation curves the $B_{1/2}$ values were measured, where $B_{1/2}$ corresponds to the microwave magnetic field at which the signal is one-half of what it would be in the absence of power saturation. These values are reported as the square root of milliwatts of incident power into the cavity as measured with a microwave power meter and are designated

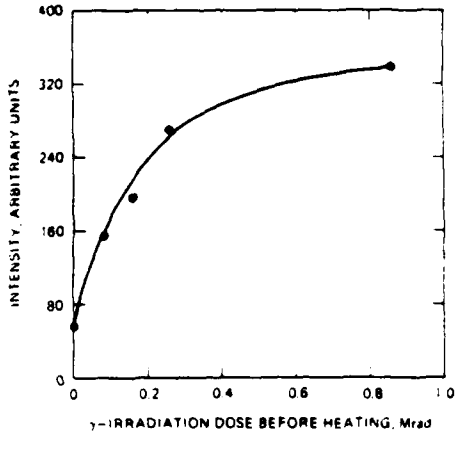

FIG. 7. The γ-dose dependence of the Ge(3) center in the core samples with a 500 K heat treatment following the γ irradiation. The Ge(3) intensity was measured by ESR at $g = 1.9943$ and was normalized per gram of sample

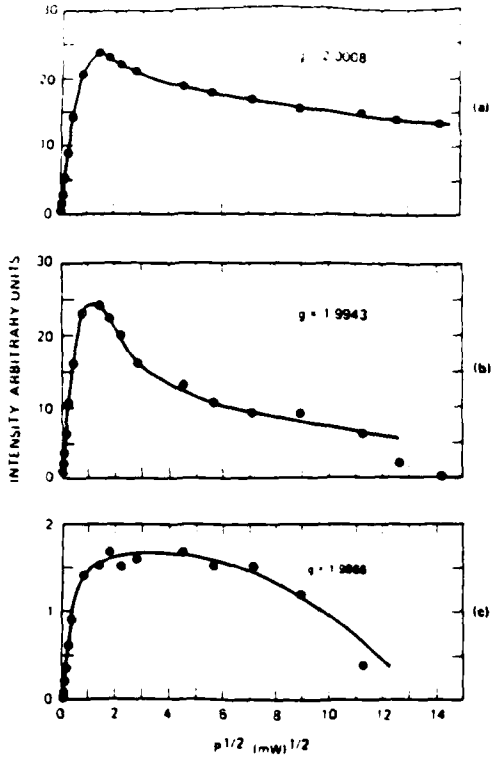

FIG. 8. Microwave power saturation curves of 0.03-Mrad γ-irradiated core samples measured at (a) $g = 2.0008$, (b) $g = 1.9943$, and (c) $g = 1.9866$. The signal positions are shown in Fig. 1(b).

as $(P^{1/2})_{1/2}$. It should be noted that these values correspond to relative measures of the degree of saturation. Values are tabulated for γ-irradiated and xenon lamp-irradiated core samples in Table I and for γ-irradiated cladding samples in Table II at different temperatures.

One can see from Table I that the signal at $g = 1.9943$ of γ-irradiated core samples and the signal at $g = 1.9949$ of xenon lamp-irradiated core samples have about the same

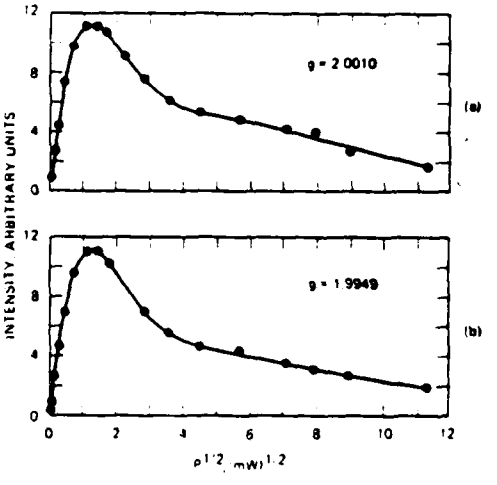

FIG. 9. Microwave power saturation curves of 15-h xenon lamp-irradiated core samples measured at (a) $g = 2.0010$ and (b) $g = 1.9949$. The signal positions are shown in Fig. 4(a).

TABLE I. $(P^{1/2})_{1/2}$ saturation curve values of γ-irradiated and xenon lamp-irradiated core samples. See Figs. 1(b) and 4(a) for signal positions.

γ-irradiated core (0.03 Mrad)

Temp. (K)	$g = 2.0008$	$g = 1.9943$	$g = 1.9866$
77	$0.22 \pm 0.025(\text{mW})^{1/2}$	$0.26 \pm 0.06(\text{mW})^{1/2}$	$0.17 \pm 0.05(\text{mW})^{1/2}$
125	0.81 ± 0.15	0.67 ± 0.15	0.22 ± 0.10
192	0.85 ± 0.05	0.75 ± 0.05	0.70 ± 0.20
298	1.26 ± 0.14	1.19 ± 0.10	1.07 ± 0.25
327	1.72 ± 0.20	1.67 ± 0.07	1.19 ± 0.5

Xenon lamp-irradiated core (3 h of irradiation)

Temp. (K)	$g = 2.0010$	$g = 1.9949$
77	$0.27 \pm 0.05(\text{mW})^{1/2}$	$0.30 \pm 0.07(\text{mW})^{1/2}$
213	0.65 ± 0.07	0.88 ± 0.15
269	0.87 ± 0.05	0.92 ± 0.10
298	1.14 ± 0.12	1.21 ± 0.12
344	1.04 ± 0.20	1.25 ± 0.10

$(P^{1/2})_{1/2}$ values at similar temperatures except perhaps at the highest temperature. Since the $g = 1.9949$ signal is identified as g_2 of the Ge(3) species, this suggests that the $g = 1.9943$ signal can also be so assigned. The signal at $g = 1.9866$ of γ-irradiated core samples has much different saturation characteristics that are apparently from a different center. The signal at $g = 2.0008$ seems to have intermediate behavior.

From Table II the 0.03-Mrad γ-irradiated cladding samples show that the same power saturation values for the signal at $g = 2.0016$ and the signal at $g = 1.9990$ at corresponding temperatures. This suggests that they are due to the same species which corresponds to one type of silicon E' center. The signal at $g = 2.0001$ of the 0.03-Mrad γ-irradiated cladding samples has different saturation characteristics and is assigned to a different type of silicon E' center.

TABLE II. $(P^{1/2})_{1/2}$ saturation curve values of low-dose and high-dose γ-irradiated cladding samples. See Fig. 3(b) for signal positions.

γ-irradiated cladding (0.03 Mrad)

Temp. (K)	$g = 2.0016$	$g = 2.0001$	$g = 1.9990$
77	$0.03(\text{mW})^{1/2}$	$0.03(\text{mW})^{1/2}$	$\cdots(\text{mW})^{1/2}$
180	0.144 ± 0.02	0.12 ± 0.02	0.144 ± 0.02
227	0.22 ± 0.02	0.18 ± 0.02	$\cdots$
298	0.25 ± 0.02	0.14 ± 0.02	0.20 ± 0.02
329	0.33 ± 0.03	0.21 ± 0.03	0.36 ± 0.02

γ-irradiated cladding (8.8 Mrad)

Temp. (K)	$g = 2.0015$	$g = 2.0001$
77	$\sim 0.1(\text{mW})^{1/2}$	$\sim 0.1(\text{mW})^{1/2}$
198	~ 0.1	~ 0.1
252	0.12	0.13
298	0.10	0.12
324	0.11	0.14
376	0.22	0.25

IV. DISCUSSION

A. Core samples

Gamma-irradiated core samples give composite ESR signals at $g \simeq 2$ as shown in Fig. 1(b) and a doublet of 119 G splitting. The doublet has been assigned to an electron trapped at a hydrogen-compensated substitutional germanium center.[7] The photobleaching, heat treatment, and power saturation experiments confirm that there are at least two species in the $g \simeq 2$ region. These species seem analogous to silicon E' centers in pure silica.[8] In germanium-doped silica four germanium E' centers have been assigned which differ in the number of next-nearest germaniums from $n = 0$ to 3.[1] These centers are denoted as Ge(n). In germanium-doped silica the dominant centers produced by γ irradiation are germanium E' centers instead of silicon E' centers because of the higher electronegativity of germanium.

Friebele *et al.*[1] have assigned three principal g-tensor components to each of the Ge(n) centers by spectral simulation. From these values we make the assignments in Fig. 1(b) of $g = 1.9866$ to Ge(2) and $g = 1.9943$ to Ge(0) and/or Ge(3). The $g = 2.0008$ line in Fig. 1(b) is considered to be a superposition of several Ge(n) species. These assignments are consistent with the power saturation data shown in Fig. 8. A recent work by Hanafusa *et al.*[3] showed that the axially symmetric signal at $g_1 = 2.0010$, $g_2 = 1.9949$, and $g_3 = 1.9935$ assigned to Ge(3) was induced in the GeO_2-doped silica optical fibers by drawing.

The defect center signal in unirradiated core samples shown in Fig. 1(a) is assigned to Ge(3) based on the g values of Friebele *et al.*[1] When a sample is subjected to xenon lamp irradiation for several hours this Ge(3) signal seems to be generated exclusively as in Fig. 4(a).

We have found that the complex spectra generated in the γ-irradiated samples can be simplified by heating and by photoirradiation with a xenon lamp. Figure 6 shows the effect of xenon lamp irradiation for times up to 1 h on a γ-irradiated core sample. This photoirradiation time is too short to generate significant Ge(3) from the photoirradiation alone. Note that the $g = 1.9943$ line intensity remains about constant during 1-h photoirradiation while all the other spectral features decrease in intensity. The net result appears to be a disappearance of the various other Ge(n) species leaving only Ge(3). Totally analogous behavior is observed for heating a γ-irradiated sample to about 500 K.

We conclude that the Ge(3) species is more stable to both heat and broadband photoexcitation than the other Ge(n) species. It is also noteworthy that significant spectral simplification of γ-irradiated germanium-doped silica can be achieved. One might expect that a Ge(3) species would be more stable than other Ge(n) species due to the higher total electronegativity of the center.[1] This also implies that there is little, if any, contribution to the simplified spectrum [Fig. 6(d)] after heat treatment or photoirradiation.

In Fig. 7 it is shown that γ irradiation followed by heat treatment generates Ge(3) as a function of irradiation dose and, in addition, shows that the Ge(3) signal tends to reach a saturation intensity at about 1 Mrad. This is similar to the finding of Weeks and Purcell[9] but differs from that of Friebele *et al.*[1]

B. Cladding samples

Gamma-irradiated cladding samples show different apparent signals in the $g \simeq 2$ region at different doses and also the 119 G doublet. At a low 0.03-Mrad gamma dose the spectrum in Fig. 3(b) looks relatively complex and will be assigned to at least two different silicon E' centers. Interestingly, at higher doses above 1 Mrad the spectrum simplifies to one that can be assigned to a single silicon E' center with axial g anisotropy. An axially symmetric signal with $g_\perp = 2.0001$ and $g_\parallel = 2.0015$ is identifiable as the silicon E' center.[10] The spectrum at low-gamma dose seems identical with the spectrum of x-irradiated Suprasil quartz in Fig. 3 of Ref. 10. This spectrum was decomposed into two different E' centers termed $E'_{\alpha 1}$ and $E'_{\alpha 2}$. Thus we conclude that the same two E' centers are generated in the cladding at low dose. From the g values given for $E'_{\alpha 1}$ and $E'_{\alpha 2}$ (Ref. 10) we can identify the dominant center in the cladding at high gamma dose as $E'_{\alpha 2}$.

$E'_{\alpha 1}$ is postulated to be a center formed by displacing a bridging oxygen atom from its normal bonding position.[10] The displaced oxygen atom is stabilized by bonding to a nearby oxygen atom to form a peroxy linkage. In this model the $E'_{\alpha 1}$ center is characterized by a rhombic g tensor. Griscom[10] postulated that $E'_{\alpha 2}$ is obtained from $E'_{\alpha 1}$ by a redistribution of electron spin to an adjacent silicon center. He argues that the resulting geometry is consistent with an axially asymmetric g tensor.

The xenon lamp-irradiated cladding sample gives the same 119 G doublet as observed in the γ-irradiated cladding sample and a singlet at $g = 1.9950$ with a linewidth of 5 G as shown in Fig. 4(b). The 119 G doublet has been assigned by Vitko[7] to an electron trapped at a hydrogen-compensated substitutional germanium site. It is interesting that the photoirradiation does not generate E' centers in cladding samples. It is also interesting that the 119 G doublet is generated by both γ irradiation and photoirradiation in the cladding but only by γ irradiation in the core.

C. Microwave saturation studies

The analysis of microwave power saturation curves helps to confirm the assignment of the ESR signals of the core and cladding samples. For γ-irradiated core samples the saturation curves at different g-value positions are different as shown in Fig. 8, which indicates that more than one species with different saturation behavior is present. From Fig. 9 the $g_\perp$ ($= 1.9949$) and $g_\parallel$ ($= 2.0010$) lines assigned to Ge(3) in a photoirradiated core sample show the same saturation behavior. This supports their assignment to a single species. Further support is shown in Table I where the $(P^{1/2})_{1/2}$ values as a function of temperature show good correlation. Note that the saturation behavior of the $g = 1.9943$ signal in the γ-irradiated core [Fig. 8(b)] is the same as that of both signals in the photoirradiated curves (Fig. 9). This strongly indicates that all these signals belong to the same species, namely Ge(3).

Gamma-irradiated cladding samples give $E'_{\alpha 1}$ and $E'_{\alpha 2}$ centers at low dose and only $E'_{\alpha 2}$ at high dose. Saturation data for high dose given in Table II show that signals at

$g = 2.0015$ and $g = 2.0001$ have the same behavior. This supports the assignment of these signals to the same species assigned as $E'_{\alpha 2}$. The results on low-dose samples show that all spectral positions at $g = 2.0016$, $g = 2.0001$, and $g = 1.9990$ do not have the same saturation behavior which indicates that at least two species are present; the one at $g = 2.0001$ has similar saturation characteristics to that of species $E'_{\alpha 2}$.

The saturation curve for photoirradiated core was fit to the following expression for homogeneous broadening[11]:

$$Y'_m = AP^{1/2}/(1 + KP)^{3/2}, \quad (1)$$

where A and K are adjustable parameters, Y'_m is the intensity of the first derivative signal, and P is the incident microwave power. The parameter K is calculated from $[1 + K(P)_{1/2}]^{3/2} = 2$, where $(P^{1/2})_{1/2}$ is the square root of the microwave power at which the signal intensity is one-half of what it would be in the absence of saturation. Figure 10(a) shows that the calculated homogeneous broadening saturation curve does not fit the experimental curve. So we conclude that Ge(3) centers show nonideal inhomogeneous broadening. For comparison, a similar analysis was carried out for the high-dose cladding samples and the results are shown in Fig. 10(b). These results indicate that the high-dose signals, which we have assigned to $E'_{\alpha 2}$, are inhomogeneously broadened. Recently, a microwave saturation study of the silicon E' center in glassy SiO_2 was done by Griscom[12] and he also concluded that the silicon E' center signals are inhomogeneously broadened.

From the power saturation expression

$$B_{1/2} = 1/(T_1T_2)^{1/2} \quad (2)$$

and the relation

$$B_{1/2} \propto (P^{1/2})_{1/2}, \quad (3)$$

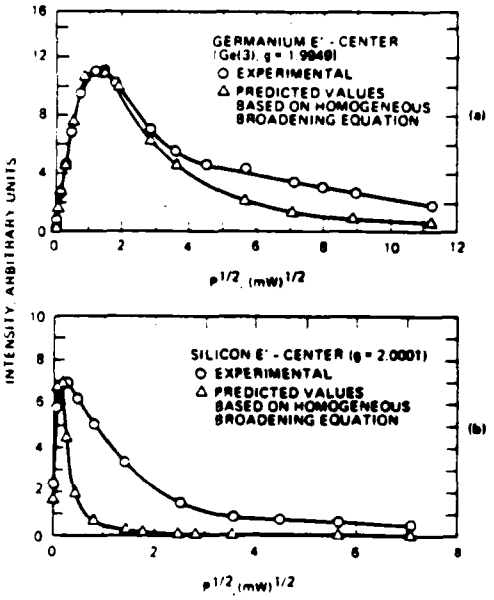

FIG. 10. Microwave power saturation curves for (a) xenon lamp-irradiated (15 h) core sample measured at $g = 1.9949$ and (b) γ-irradiated (8.8 Mrad) cladding sample measured at $g = 2.0001$. See Fig. 4(a) for core signal position and Fig. 3(b) for cladding signal position (8.8 Mrad).

one can take a ratio using Eqs. (2) and (3) to obtain

$$(T_1T_2)_{Ge}/(T_1T_2)_{Si} = [(P^{1/2})_{1/2}]^2_{Si}/[(P^{1/2})_{1/2}]^2_{Ge}. \quad (4)$$

Here, T_1 and T_2 are the longitudinal and transverse electron spin relaxation times, respectively.

From Tables I and II at room temperature, $[(P^{1/2})_{1/2}]_{Si} = 0.12$ and $[(P^{1/2})_{1/2}]_{Ge} = 1.21$ and therefore one gets

$$(T_1T_2)_{Ge} \simeq 10^{-2}(T_1T_2)_{Si}. \quad (5)$$

This shows that germanium E' centers, specifically Ge(3) centers embedded in a glassy SiO_2 host, have shorter spin relaxation times than silicon E' centers.

This result is of particular importance because two different molecular paramagnetic species are coupled to the same molecular host lattice and this provides an opportunity to correlate spin relaxation with radical structure. Aleksandrov[13,14] has developed a theory of paramagnetic relaxation in magnetically dilute molecular solids for the case where a many-electron radical is coupled via a spin-lattice interaction to the phonon spectrum of the solid. In this theoretical treatment, specific harmonic as well as anharmonic phonon modes leads to orientational (rotational) oscillations of the radical in the lattice. These rotational oscillations modulate the orientation of the radical with respect to the external magnetic field and therefore cause the spin quantization axis to fluctuate in a random manner. Aleksandrov[13,14] obtains general expressions for the spin-lattice relaxation time and the line shapes for the case of a radical with an anisotropic g tensor.

T_1^{-1} and T_2^{-1} are both proportional to $(\Delta g)^2$, where Δg is the maximum difference between the three principal g values.[13,14] For Ge(3), $\Delta g = 0.0075$ and for Si(E'), $\Delta g = 0.0016$. Thus, at constant temperature

$$(T_1T_2)_{Ge} \simeq [(\Delta g)_{Si}/(\Delta g)_{Ge}]^4(T_1T_2)_{Si}$$
$$\simeq 0.2 \times 10^{-2}(T_1T_2)_{Si}. \quad (6)$$

This is in reasonable agreement with the experimental result given in Eq. (5) and supports a dominant relaxation mechanism involving modulation of the g anisotropy.

Since the g anisotropy to first order is directly proportional to the spin-orbit coupling constant, it is also instructive to make a prediction on this basis. Literature values at the spin-orbit coupling constants are given as 940 cm^{-1} for Ge (Ref. 15) and 142 cm^{-1} for Si.[16] Thus $(142/940)^4 = 0.05 \times 10^{-2}$ which is the same order of magnitude as the value in Eq. (6).

V. CONCLUSIONS

We have found how to create Ge(3) defect centers by ultraviolet radiation of core samples of germanium-doped silica. Gamma irradiation also increases the intensity of Ge(3). As the dose increases, the species Ge(1) and Ge(2) are also produced. As the γ-irradiated core sample is heated or photobleached, the Ge(1) and Ge(2) centers disappear, leaving the Ge(3) signal unchanged. Microwave power saturation confirms that the Ge(3) species is formed by both γ irradiation and ultraviolet radiation of core samples. Microwave power saturation also confirms that more than one species is formed in γ-irradiated cladding samples at low

gamma dose while at higher dose one species, identified as $E'_{\alpha 2}$, becomes dominant. Analysis of the saturation curves of the dominant Ge(E') and Si(E') centers shows that the Ge(E') center has a characteristic relaxation time ~ 100 times shorter than the Si(E') center. This is consistent with a relaxation mechanism involving modulation of the g anisotropy.

ACKNOWLEDGMENTS

We thank the Army Research Office under contract DAAG29-84-C-0005 for partial support of this research. The power saturation studies were supported by the National Science Foundation. The authors wish to thank M. R. Vince for preparing the germanium-doped preforms.

[1]E. J. Friebele, D. L. Griscom, and G. H. Sigel, Jr., J. Appl. Phys. **45**, 3424 (1974).
[2]H. Itoh, M. Shimizu, Y. Ohmori, and M. Nakamura, J. Non-Cryst. Solids 70, 439 (1985).
[3]Y. Hibino and H. Hanafusa, Jpn. J. Appl. Phys. Lett. 22, 700 (1983); Appl. Phys. Lett. **45**, 614 (1984).
[4]G. Kordas, R. A. Weeks, and D. L. Kinser, J. Non-Cryst. Solids **69**, 293 (1985).
[5]A. W. Guryanov, D. D. Gusovskii, E. M. Dianov, L. S. Kornienko, E. P. Nikitin, A. O. Tybaltovskii, V. F. Khopin, P. V. Chernov, and A. S. Yushin, J. Quantum Electron **9**, 768 (1979).
[6]E. J. Friebele, C. G. Askins, M. E. Gingerich, and K. L. Long, Nucl. Instrum. Methods **B1**, 355 (1984).
[7]J. Vitko, Jr., J. Appl. Phys. **49**, 5530 (1978).
[8]R. A. Weeks, J. Appl. Phys. **27**, 1376 (1956); C. M. Nelson and R. A. Weeks, J. Am. Ceram. Soc. **43**, 396 (1960).
[9]R. A. Weeks and T. A. Purcell, J. Chem. Phys. **43**, 483 (1965).
[10]D. L. Griscom, Nucl. Instrum. Methods **B1**, 481 (1984).
[11]C. P. Poole, *Electron Spin Resonance* (Interscience, New York, 1967), pp. 705.
[12]D. L. Griscom, Phys. Rev. **B20**, 1823 (1979).
[13]I. V. Aleksandrov, Sov. Phys. JETP **21**, 580 (1965).
[14]I. V. Aleksandrov, Teor. Eksp. Khim. **1**, 80 (1965); I. V. Aleksandrov, Teor. Eksp. Khim. **1**, 93 (1965).
[15]J. R. Morton, J. R. Rowlands, and D. H. Whiffen, National Physical Laboratory (UK), Circ. No. BPR 1.3, 1962.
[16]D. S. McClure, J. Chem. Phys. **17**, 905 (1949).

APPENDIX B

ELECTRON PARAMAGETIC RESONANCE AND OPTICAL STUDY OF RADIAITON-INDUCED DEFECT CENTERS IN DOPED SILICA GLASSES

Electron Paramagnetic Resonance and Optical Study of Radiation-Induced Defect Centers in Doped Silica Glasses

Robert N. Schwartz, Gregory L. Tangonan, G. Richard Blair, Walee Chamulitrat, and Larry Kevan

MRS

Reprinted from Materials Research Society Symposia Proceedings Volume 61, *Defects in Glasses*, Frank L. Galeener, David L. Griscom, and Marvin J. Weber, editors.

ELECTRON PARAMAGNETIC RESONANCE AND OPTICAL STUDY OF RADIATION-INDUCED DEFECT CENTERS IN DOPED SILICA GLASSES

ROBERT N. SCHWARTZ*, GREGORY L. TANGONAN*, G. RICHARD BLAIR*,
WALEE CHAMULITRAT** AND LARRY KEVAN**
*Hughes Research Laboratories, Malibu, CA 90265
**Department of Chemistry, University of Houston
Houston, TX 77004

ABSTRACT

Gamma- and UV-induced defect centers in germanium and fluorine doped silica have been studied by electron paramagnetic resonance (EPR) spectroscopy. The complex spectrum at g≈2 in γ-irradiated germanium doped glass corresponds to a superposition of resonances from several germanium E′-centers. In UV-irradiated samples, however, the EPR spectrum is dominated by only one type of germanium E′-center. Significant spectral simplification of γ-irradiated germanium doped silica can be achieved by heating or broadband photoirradiation. Similar results are observed in multimode germanium doped core optical fibers. UV-induced optical loss spectra in the 0.5-1.5 μm wavelength range were also measured in these core fibers as well as the growth kinetics of the UV-induced absorption. Gamma-irradiation of fluorine doped silica generated two different types of silicon E′-centers, $E'_{\delta 1}$ and $E'_{\delta 2}$. At lower radiation dose one sees a mixture of $E'_{\delta 1}$ and $E'_{\delta 2}$, but at higher radiation dose $E'_{\delta 2}$ dominates. A spectrum dominated by the $E'_{\delta 2}$ variant is also observed in UV-irradiated samples and in photobleached low gamma dose samples.

INTRODUCTION

Radiation damage in doped-silica glasses which are useful for optical waveguides has been the subject of numerous investigations [1]. In general most studies have been concerned with the radiation damage produced by high energy ionising radiation such as X-rays and γ-rays or energetic particles including neutrons and electrons. The interaction of high energy radiation with glassy materials is a rather complex phenomenon which depends on many factors including the type of ionising radiation or particles used and the microstructure of the glass [2]. One mode of forming paramagnetic defects, for example, involves the interaction of ionising radiation with the glass to form electrons and holes which are subsequently trapped at preexisting flaws in the glass network [3].

In contrast to the extensive literature on the radiation damage produced by high energy stimuli, the literature on the effects of UV radiation on doped-silica glasses is limited. Recent experiments, however, indicate that radiation-induced optical losses occur in epoxy coated germanium doped optical fibers as a result of using UV radiation for crosslinking the prepolymer liquid coating material [4]. In this article we report on the radiation effects in doped silica preform glasses and single multimode fibers exposed to xenon lamp and UV radiation. The photogeneration and photobleaching of paramagnetic single point defects will be discussed as well as the UV-induced optical loss in fibers.

Mat. Res. Soc. Symp. Proc. Vol. 61 • 1986 Materials Research Society

EXPERIMENTAL

Optical preforms with GeO_2/SiO_2 and P/SiO_2 cores were made by the modified chemical vapor deposition (MCVD) technique. Silica layers doped with germanium or fluorine were deposited inside a Heraeus Amersil T0-8 quartz tube using $GeCl_4$ as the source of germanium and CCl_2F_2 as the fluorine source. Doped core preforms were formed by collapse of the substrate tubing and were sleaved with an additional quarts tube (T0-8) before being drawn into fiber. The fibers were pulled to a diameter of 175 μm using a resistance furnance.

Electron paramagnetic resonance (EPR) spectra were obtained with a Varian E-9 X-band spectrometer employing 25 kHz magnetic field modulation. Spectral g-values were determined using a Cr^{3+} in MgO standard reference with g=1.9796. The g-values were also calculated by measuring the magnetic field with a Varian nuclear magnetic resonance guassmeter and the microwave frequency with a Hewlett-Packard 5342A automatic microwave frequency counter. The estimated error in the measured g-values is ±0.0003.

All irradiations were carried out at room temperature. The preforms were cut to separate the core and cladding parts and the separate portions were subjected to various types of ionising radiation. Gamma-irradiation was achieved using a ^{60}Co source with a dose rate of 1.12 Mrad h^{-1}. Broadband photo-irradiation was carried out with a 1 kW xenon arc lamp with the output passed through a 3 cm water cell to filter out infrared radiation; the shortest wavelength component was ~0.250 μm. The light intensity at the sample position from the light source was measured with a radiometer to be 1.7×10^{-2} J s^{-1} cm^{-2} at a wavelength of 0.42 μm. The UV source was a Pen-Ray (11SC-1) lamp with a quarts envelope. The light intensity at the sample was estimated to be ~1 mJ s^{-1} cm^{-2}, with 92 % of the spectral output at λ = 0.254 μm.

The evaluation of the UV induced loss of optical fibers was carried out using a standard spectral insertion loss apparatus. For these experiments six multimode step-index germanium doped core fibers were studied with 0.185<NA<0.30. The fiber samples, typically 100 m long and wound on a 25 cm diameter drum, were uncoated and kept in the dark prior to measurement. The experimental run consisted of UV-irradiating a small region of the spool which was 5 cm in length and included 60 turns of fiber (the total length of fiber exposed was 3 m). The throughput signal at 0.66 μm was monitored during the irradiations, thus providing a time dependent measure of the peak value of the induced UV loss. The spectral runs were completed in the following way. Prior to any UV-irradiation a spectral insertion loss spectrum of the whole length of fiber was taken. The UV-induced loss scan was then performed. Without disturbing the input coupling, the fiber was severed leaving approximately 20 m and this segment of the fiber was recoupled to the spectrometer/detector optics for the normalisation scan. The spectral insertion loss results for the two runs were then subtracted and plotted, thereby eliminating the common absorption peaks due to OH (3 to 10 ppm). An InGaAs detector was used for the spectral runs over the 0.50 to 1.50 μm range.

RESULTS

Shown in Fig. 1a is the approximately axially symmetric EPR spectrum of an unirradiated germanium doped core sample. The spectrum displayed in Fig. 1b was observed following room temperature γ-irradiation (0.03 Mrad). This spectrum exhibits more structure in the g=2 region as well as a weaker doublet with a splitting of 119 G.

Xenon lamp-irradiation of the germanium doped core samples was found to produce an axially symmetric EPR spectrum as shown in Fig. 2a. The intensity of this signal versus xenon lamp-irradiation time is plotted in Fig. 3 where it should be noted that the signal starts to saturate after about 30 h of

irradiation. Figure 2b shows the EPR spectrum of a xenon lamp-irradiated cladding sample. Clearly discernable is the weak 119 G doublet and an isotropic signal at g=1.9950 with a linewidth of 5 G. We have observed that the signal generated in the cladding sample is significantly smaller than the signal generated by the same xenon lamp-irradiation in the core sample.

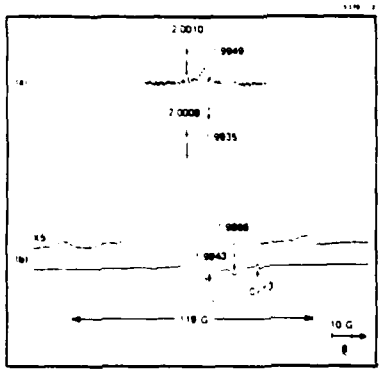

Fig. 1. EPR spectra obtained at room of germanium doped core (a) unirradiated and (b) γ-irradiated. Cr^{3+}/MgO was used as a field marker at g=1.9798.

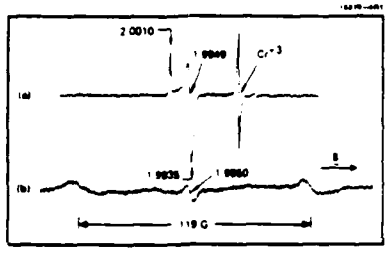

Fig. 2. Room temperature EPR spectra of Xe lamp-irradiated samples (a) germanium doped core and (b) silica cladding.

Gamma-irradiated germanium doped core samples were subjected to xenon lamp-irradiation and EPR spectra were recorded after 15, 30 and 60 min intervals of exposure. As shown in Fig. 4 spectral simplification has resulted with a pronounced decrease in signal intensity occuring at g=2.0004; whereas, at g=1.9943, the signal intensity has remained unchanged. It was found that spectral simplification could also be achieved by heating γ-irradiated core samples in an oxy-gas torch to a temperature of ~500 K.

Exposure of germanium doped core material to UV radiation produced EPR spectra which were much simpler than those obtained by γ-irradiation, but more complex than the spectra produced by only xenon lamp-irradiation. Shown in Fig. 5a is a spectrum obained from a UV-irradiated core sample; subsequent xenon lamp-irradiation simplifies the spectrum as shown in fig. 5b. Similar results were observed in multimode germanium doped core fibers drawn from the preform material from which the above core samples were obtained. Figure 6a shows the EPR spectrum after UV-irradiation and Fig. 6b the spectrum after subsequent xenon lamp-irradiation.

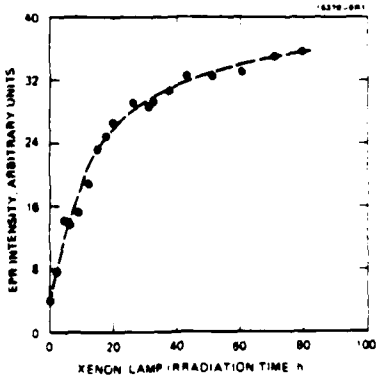

Fig. 3. EPR signal intensity at g=2.0010 versus xenon lamp-irradiation time for germanium doped core material.

Additional insight into UV radiation effects in the optical fibers was gained by measuring the spectral insertion loss in fibers with different numerical apertures (NA) and exposed to various levels of UV radiation. Shown in Fig. 7 are insertion loss spectra for optical fibers with NA=0.2 and NA=0.3 UV-irradiated for 10 min. The value of the NA was determined by the amount of germanium in the core; i.e.,the NA is proportional to square root of the germanium concentration. As can be seen from Fig. 8, the absorption band in the 0.60-0.70 μm region shifts to longer wavelengths with increasing NA. This trend was observed over the complete range of NA studied. In Fig. 8 the optical density measured at λ=0.66 μm is displayed as a function of the UV exposure time for fibers with NA=0.2 and NA=0.3. It is apparent that for a given exposure time, the fiber with the larger NA shows the greatest loss and that pronounced saturation occurs after ~4 min of exposure to UV radiation; whereas the the lower NA fiber shows a smaller loss and a more gradual approach to saturation over the same time interval.

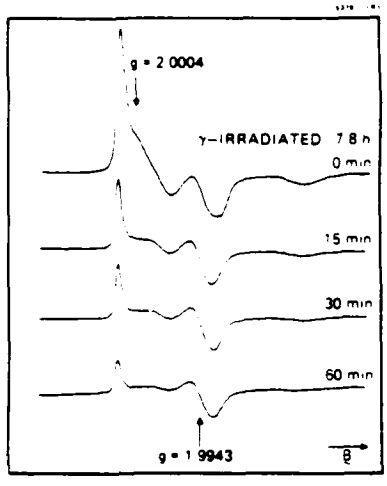

Fig. 4. EPR spectra at room temperature of γ-irradiated germanium doped core sample following Xe lamp-irradiation. All spectra are recorded at the same gain.

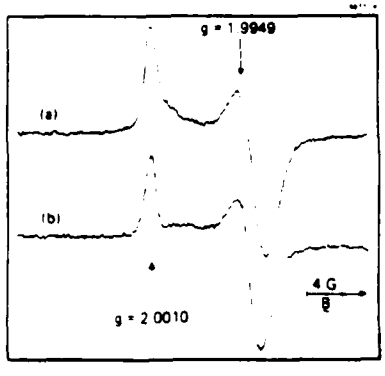

Fig. 5. EPR spectra obtained at room temperature of germanium doped core sample (a) UV-irradiated and (b) after Xe lamp-irradiation of (a).

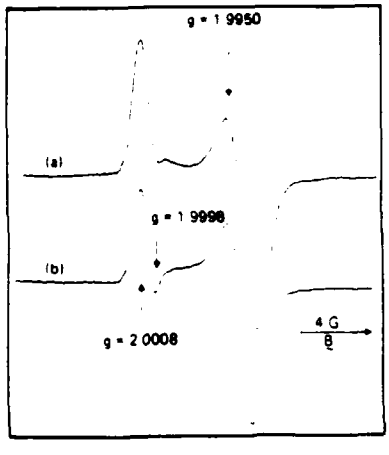

Fig. 6. Room temperature EPR spectra of germanium doped core optical fiber (a) UV-irradiated and (b) after Xe lamp-irradiaton of (a).

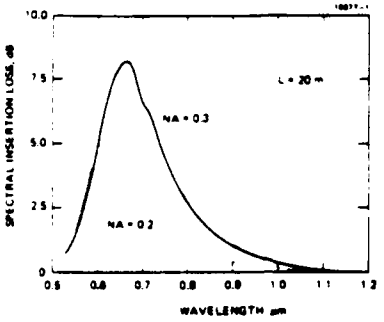

Fig. 7. UV-induced loss spectra of multimode germanium doped core fibers with NA=0.2 and NA=0.3.

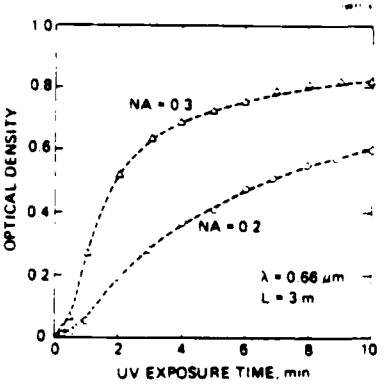

Fig. 8. Growth of the UV-induced loss at 0.66 μm in multimode germanium doped core fibers with NA=0.2 and NA=0.3 measured in situ during steady state UV-irradiation.

The effects of γ-irradiation and UV-irradiation in fluorine doped optical glasses were also investigated. Low dose (0.03 Mrad) γ-irradiated samples give EPR signals at g≈2 and a strong 119 G doublet as shown in Fig. 9a. The EPR signal in the g≈2 region is a composite spectrum (Fig. 9b) which simplifies to an axially symmetric spectrum when irradiated with a UV source (Fig. 9c). In addition, the 119 G doublet is irreversibly photobleached upon exposure to UV radiation. On the other hand, if a fluorine doped silica sample is γ-irradiated to a dose of ~0.5 Mrad, the 119 G is observed; however, the resonance at g≈2 is identical to the spectrum in Fig. 9c. Finally, the spectrum given in Fig. 9c was also observed in fluorine doped samples without the generation of the 119 G doublet when irradiated by UV photons alone.

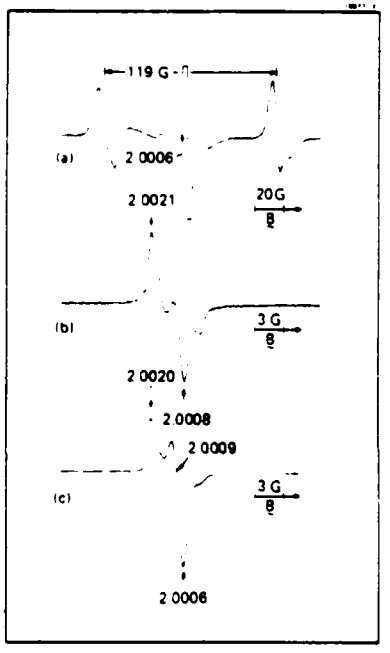

Fig. 9. EPR spectra obtained at room temperature of γ-irradiated (0.03 Mrad) fluorine doped silica glass (a) large magnetic field sweep showing the 119 G doublet, (b) reduced magnetic field sweep showing the details of the center line at g≈2 in (a), and (c) spectrum of g≈2 region following UV-irradiation.

DISCUSSION

The EPR of radiation damaged germanium doped optical glasses has been studied in depth by several groups [5-7]. Friebele and coworkers [5] assigned the composite spectrum shown in Fig. 1b in the g=2 region to several germanium E'-centers with varying numbers of next nearest-neighbor germanium atoms ranging from 0 to 3. These centers were designated as Ge(n) centers, where n=0,1,2, and 3. Recently, we have carried out microwave power saturation measurements at different temperatures to further differentiate and characterise these various Ge(n) species [8]. The 119 G doublet indicated in Fig. 1b (as well as in Figs. 2b and 9c) has been assigned by Vitko [9] to an electron trapped at a hydrogen compensated substitutional germanium (electron localised in Ge sp^3 hybrid orbital) center.

The spectrum of the unirradiated germanium doped core sample shown in Fig. 1a is assigned to Ge(3) based on the g-values of Friebele and coworkers [5]. The Ge(3) species is exclusively generated when core samples are subjected to xenon lamp-irradiation (Fig. 2a). In addition, we also observed that the composite EPR spectrum generated in γ-irradiated core samples could be simplified by photoirradiation with a xenon lamp and by heating. These results are summarised in Fig. 4. The important feature to note in this figure is that the intensity of the g=1.9943 resonance remains constant during photoirradiation while all the other spectral features decrease in intensity. It is also important to point out that the photoirradiation time is too short to generate a signficant number of Ge(3) centers by xenon lamp-irradiation alone. Thus, the net result appears to be the disappearance of the various other Ge(n) species by photoionisation with sub-bandgap radiation, leaving only Ge(3). As pointed out above, totally analogous behavior (spectral simplification) is also observed by heating γ-irradiated core samples to ~500 K.

UV irradiation (0.254 μm) of germanium doped core samples produced composite EPR spectra; however, the Ge(3) center is the most prominent component (Fig. 5). A small amount of Ge(1) and Ge(2) may be present as evidenced by the high-field shoulder on the g=2.0010 line in Fig. 5a. As observed in the γ-irradiated core samples, only Ge(3) centers remain after photoirradiation with the xenon source. Similar results were also observed in UV-irradiated single germanium doped core fibers (Fig. 6). The resonance at g=1.9998 in the spectrum shown in Fig. 6b is associated with photogenerated silicon E'-centers in the cladding or fluorine doped barrier layer.

We conclude from the discussion above that in germanium doped silica the Ge(3) species is most stable to both heat and broadband photoexcitation than the other Ge(n) species. Based on electronegativity arguments [5,10], it is expected that the Ge(3) center should be the most stable of the Ge(n) centers.

The addition of index-modifying dopants to silica to form optical waveguides results in significant changes in the optical response of the glass. For example, in unirradiated germanium doped silica fiber, the absorption at ~0.60 μm is weak (loss < 20 dB/km) and attributed to drawing-induced defects of the silica network [11]. As shown in Fig. 7, UV-irradiation produces a strong absorption band in the 0.63-0.67 μm range which is a factor of ~200 times larger than the silica drawing-induced peak in the unirradiated fiber [4]. It is also clear in Fig. 7 that the UV-induced absorption band not only increases with germanium concentration (increasing NA), but in addition, shifts to longer wavelengths. The saturation behavior of the UV-induced absorption measured at 0.66 μm with UV exposure time clearly depends on the NA (Ge concentration) of the fiber as illustrated in Fig. 8. For the high NA fiber, the change in the UV-induced loss with time is initially very dramatic, followed by pronounced saturation at longer exposure times. In contrast, preliminary EPR measurements on the growth of Ge(3) centers in the same fibers indicate a linear dependence on the UV exposure

time over the same time interval. Recent work,however, has shown a good correlation between the radiation-induced optical loss and the EPR of γ-irradiated doped-core optical fibers [11].

Gamma-irradiated fluorine doped silica samples show different apparent signals in the g≈2 region at different doses and also the 110 G doublet. At low 0.03 Mrad gamma dose the spectrum in Fig. 9b is complex and is assigned to at least two different silicon E'-centers. When exposed to UV radiation this spectrum simplifies to a single silicon E'-center with axial g-anisotropy as shown in Fig. 9c. This spectrum is also observed in fluorine doped silica samples subjected to ~0.5 Mrad γ-irradiation or exposed to UV radiation alone. Griscom [12] observed a similar composite spectrum in X-irradiated Suprasil silica and proprosed that the spectrum was due to two E'-center variants termed $E'_{\alpha 1}$ and $E'_{\alpha 2}$. Thus we conclude that the same two variants $E'_{\alpha 1}$ and $E'_{\alpha 2}$ are generated in fluorine doped silica at low gamma dose. Based on the g-values given for $E'_{\alpha 1}$ and $E'_{\alpha 2}$ [12], we identify the defect center responsible for the spectrum in Fig. 9c as the $E'_{\alpha 2}$ variant.

CONCLUSIONS

We have observed that in germanium doped silica UV-irradiation (0.254 μm) produces one type of germanium E'-center whereas, γ-irradiation generates several related germanium E'-centers designated as Ge(n) where n=0,1,2, and 3. As the γ-irradiated sample is heated or photobleached the Ge(0), Ge(1), and Ge(2) centers disappear leaving only the Ge(3) center. Similar results were also observed in multimode step-index germanium doped core optical fibers. We have also found that the UV-induced loss band in doped core fibers not only increases with germanium concentration but in addition, shifts to longer wavelengths. Furthermore, we have observed that the growth kinetics of the UV-induced loss saturates at longer UV exposure times. Two types of silicon E'-centers were observed in γ-irradiated fluorine doped silica. At low dose a mixture of $E'_{\alpha 1}$ and $E'_{\alpha 2}$ variants are generated, whereas at higher dose $E'_{\alpha 2}$ is the dominant species. In constrast, only the $E'_{\alpha 2}$ variant is produced by UV-irradiation alone. A photobleached low gamma dose sample is also dominated by the $E'_{\alpha 2}$ variant.

ACKNOWLEDGEMENTS

We thank the Army Research Office for support of this research under contract number DAAG29-84-C-0006. The authors wish to thank M.R. Vince and V.L. Jones for their technical assistance.

REFERENCES

1. E.J. Friebele, C.G. Askins, M.E. Gingerich and K.I. Long, Nucl. Instr. and Meth. B1, 355 (1984).
2. E.J. Friebele and D.L. Griscom, in: Treatise on Materials Science and Technology, Vol. 17, Glass II, eds, M. Tomozawa and R.H. Doremus (Academic Press, New York, 1979) p. 257.
3. D.L. Griscom, J. Non-Crystalline Solids, 73, 51 (1985).
4. L.L. Blyler, Jr., F.V. DiMarcello, J.R. Simpson, E.A. Sigety, A.C. Hart, Jr., and V.A. Foertmeyer, J. Non-Crystalline Solids 38 and 39, 165 (1980).

5. E.J. Friebele, D.L. Griscom, and G.H. Sigel, Jr., J. Appl. Phys. 45, 3424 (1974).
6. G. Kordas, R.A. Weeks, and D.L. Kinser, J. Non-Crystalline Solids 69, 293 (1985).
7. H. Itoh, M. Shimizu, Y. Ohmori and M. Nakamura, J. Non-Crystalline Solids 70, 439 (1985).
8. V. Chamulitrat, L. Kevan, R.N. Schwartz, G.R. Blair, and G.L. Tangonan, submitted to the J. Appl. Phys.
9. J. Vitko, Jr., J. Appl. Phys. 49, 5530 (1978).
10. J.P. Hagon, M. Jaros and A.M. Stoneham, J. Phys. C, 18, 4957 (1985).
11. A.N. Gur'yanov, D.D. Gusovskii, E.M. Dianov, L.S. Kornienko, E.P. Nikitin, A.O. Rybaltovskii, V.F. Khopin, P.V. Chernov and A.S. Yushin, Sov. J. Quantum Electron. 9, 768 (1979).
12. D.L. Griscom, Nucl. Instr. and Meth. B1, 481 (1984).

APPENDIX C

ELECTRON PARAMAGNETIC RESONANCE STUDIES OF INTRINSIC BONDING DEFECTS AND IMPURITIES IN SiO_2 THIN SOLID FILMS

Electron Paramagnetic Resonance Studies of Intrinsic Bonding Defects and Impurities in SiO_2 Thin Solid Films

Robert N. Schwartz, Marion D. Clark, Walee Chamulitrat, and Larry Kevan

MRS

Reprinted from Materials Research Society Symposia Proceedings Volume 61, *Defects in Glasses*, Frank L. Galeener, David L. Griscom, and Marvin J. Weber, editors.

ELECTRON PARAMAGNETIC RESONANCE STUDIES OF INTRINSIC BONDING DEFECTS AND IMPURITIES IN SiO_2 THIN SOLID FILMS

ROBERT N. SCHWARTZ*, MARION D. CLARK*, WALEE CHAMULITRAT** AND LARRY KEVAN**
*Hughes Research Laboratories, Malibu, CA 90265
**Department of Chemistry, University of Houston,
Houston, TX 77004

ABSTRACT

Electron paramagnetic resonance (EPR) spectroscopy has been used to identify paramagnetic intrinsic bonding defects and impurities in as-deposited thin solid SiO_2 films. Thin films grown by E-beam vacuum deposition, RF sputtering, thermal oxidation of polysilicon, plasma enhanced chemical vapor deposition (PECVD), and low pressure chemical vapor deposition (LPCVD) techniques have been examined. Some of the growth techniques yield films that have paramagnetic centers similar to those found in bulk radiation-damaged vitreous SiO_2. A new temperature dependent EPR center was observed in PECVD SiO_2 films and has been assigned to trapped NO_2. Slow-motional EPR lineshape theory was used to analyse the temperature dependent spectra.

INTRODUCTION

The ability to grow thin film dielectric materials free of intrinsic bonding defects and impurities is of major practical importance for the development of electronic devices utilising compound semiconductor substrates such as InP, GaAs, and (Hg,Cd)Te. In general, the performance of a device is strongly correlated with the thin film microstructure, including defect and impurity molecular structure. Electron paramagnetic resonance (EPR) spectroscopy is a well established technique for not only detecting, but also, determining the electronic structure of paramagnetic point defects and impurities [1]. While there exists an extensive literature on the EPR of defects and impurities in bulk insulators, EPR studies in thin film dielectrics is rather sparse [2-4].

Two molecular models have been proposed for the intrinsic bonding defects in bulk amorphous silica ($a\text{-}SiO_2$): (1) the vacancy-bridge model [5,6] and (2) the valence-alternation pair model [7,8]. In the vacancy-bridge model the peroxy linkage and the oxygen vacancy are the dominant precursor defects and are the analogs of the Frenkel vacancy-interstitial defect pair formed in crystalline solids [9]. Ionising radiation generates electron-hole pairs in the material with the holes subsequently trapped by the peroxy linkage and the oxygen vacancy to form paramagnetic peroxy radicals [10] and E'-centers [11]. It is also possible to create these paramagnetic centers by highly energetic ionising radiation which, by knock-on or radiolytic processes, generate atomic displacements in the originally defect-free bonding network.

The valence-alternation pair model predicts that the main defects are charged over- and undercoordinated oxygen sites, neutral undercoordinated paramagnetic silicon centers, and neutral undercoordinated paramagnetic oxygen centers. While overwhelming support for the vacancy-bridge model is provided by EPR measurements, recent electronic structure calculations [12] suggest that valence-alternation defects are also present in bulk $a\text{-}SiO_2$, but at a much lower concentration.

Mat. Res. Soc. Symp. Proc. Vol. 61 • 1986 Materials Research Society

Recent theoretical [13] and experimental [14] work suggest that AC electrical transport phenomena in RF sputtered SiO_2 thin films may be controlled by valence-alternation pair defects. Since in the RF sputtering technique the vitreous silica target is not only destroyed but in addition, the films are also exposed to attendant soft X-rays and energetic particles, it is not too suprising that a high density of bonding defects is formed in the film. However, whether these intrinsic defects are the vacancy-bridge type or the valence-alternation variety is still an open question.

In this article we summarise our EPR results on intrinsic bonding defects and impurities in SiO_2 thin films grown by a variety of techniques. This information is extremely important for developing an understanding of the types of defects generated as well as the processing factors controlling their formation.

EXPERIMENTAL

Thin films of SiO_2 were grown by plasma enhanced chemical vapor deposition (PECVD), low pressure chemical vapor deposition (LPCVD), E-beam vacuum deposition, RF sputtering,and thermal oxidation of polycrystalline silicon techniques. The films were deposited on approximately 7.5 x 3 mm^2 polished Spectrosil (15 mil thick) fused quarts substates and were approximately 0.5 μ thick.

The PECVD system was designed and constructed at the Hughes Research Laboratories. The plasma is inductively coupled and excited at 13.56 MHz. The system was optimised for SiO_2 deposition at 300°C using N_2O and SiH_4 diluted with He. The films were deposited at a rate of 100 Å/min at a radiofrequency power of 40 W. LPCVD films were grown in the same cold wall reactor by pyrolytic reaction of O_2 with SiH_4. Oxygen, diluted with He and two sources of silane, one diluted with He and the other with Ar,were used to control the flow of the reactant gases. The films were grown at 300°C without RF excitation at a rate of 100 Å/min. A conventional hot wall reactor system was also used to grow LPCVD SiO_2 films by the pyrolytic reaction of oxygen with silane. In this system the reactant gases were used without further dilution by a carrier gas. The films were grown at a rate of 170 Å/min at 450°C. The SiO_2 films formed by thermal oxidation utilised CVD polysilicon. The polysilicon films were grown on polished Spectrosil substrates in a hot wall CVD reactor filled with SiH_4 (0.3 torr). Throughout the deposition the temperature was maintained at 657°C and the growth rate was 111 Å/min. The subsequent thermal oxidation was carried out at approximately 950°C.

The E-beam vacuum deposited films were grown in a modified Airco Temescal CV-8 E-beam machine. During depositon the chamber was back-filled with oxygen to a pressure of approximately $6x10^{-4}$ torr. Heraeus Amersil Spectrosil fused quarts was used as the evaporation source. During the deposition the substrates were maintained at approximately 100°C and the deposition rate was about 276 Å/min. A modified Materials Research Corporation sputtering system was used for growing the RF sputtered films. This is a RF planar diode type plasma system operating at 13.56 MHz and configured with an 8 inch high purity fused silica target. Argon was used as the sputtering gas for all depositions. The substrates were placed on a water cooled SiO_2-coated copper pallet which was at ground potential during unbiased deposition and maintains the substrates below 100°C throughout film growth. The films were deposited at a rate of 100 Å/min under both biased and unbiased conditions.

EPR spectra were obtained with a Varian E-9 spectrometer equipped with a Hewlett-Packard 5342A automatic microwave frequency counter and a Varian NMR gaussmeter for magnetic field measurement. EPR at 77 and 4.2 K were recorded in quarts insertion dewars. For variable temperature measurements between 4.2 and 165 K an Air Products LTD Helitran unit inserted into the microwave cavity

was used. The sample temperature was stabilized using an Artronix 5301 temperature controller to drive the heater in the Helitran unit. The Artronix controller monitored the temperature near the sample with a 50 Ω,0.25 W carbon resitor. The temperature was measured by a chromel-iron doped gold (0.07 atomic % iron) thermocouple placed directly above the sample in the cavity while recording EPR spectra. The variation in temperature with the position of the thermocouple in the microwave cavity was noted and the appropriate corrections were made in the recorded temperatures.

RESULTS

Shown in Fig. 1 are EPR spectra recorded at 77 K of as-deposited E-beam and straight(unbiased) RF sputtered SiO_2 thin films. The spectra are overmodulated in order to improve the signal-to-noise and therefore, the recorded lineshapes are severely distorted. The intense single line resonsance at g=2.0006 is close to that expected for a defect center with the unpaired spin localized in a sp^3 hybrid orbital, e.g.,a silicon E'-center. The weak signal at g=2.0070 may possibly be due to the peroxy radical. More resolved spectra are obtained, as shown in Fig. 2, by reducing the level of the magnetic field modulation. These spectra are in the g=2.0006 region and exhibit the typical amorphous EPR lineshape of a paramagnetic center possessing an axially symmetric g tensor.

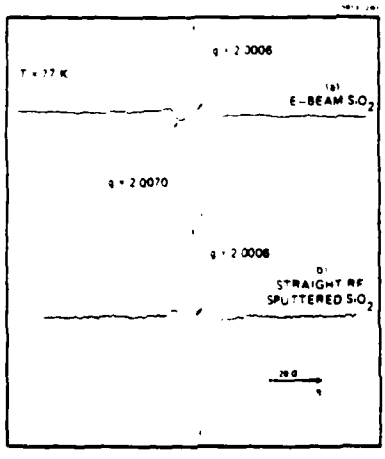

Fig. 1. EPR spectra (overmodulated) at 77 K of (a) E-beam vacuum evaporated SiO_2 and (b) straight (unbiased) RF-sputtered SiO_2.

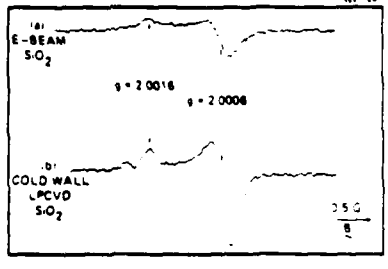

Fig. 2. Room temperature EPR in g=2 of (a) E-beam deposited SiO_2 and (b) cold wall LPCVD SiO_2.

Previous studies [1,15] have established that the various properties such as mechanical, optical and electrical of RF sputtered SiO_2 thin films are strongly influenced by the substrate bias conditions during film growth. The effect of bias on the film microstructure is not well understood; however, EPR does provide evidence that there is a significance difference in the intrinsic defect density in films deposited with and without bias. As seen in Fig. 3 the g=2.0006 resonance of the biased sputtered SiO_2 film is reduced by a factor of five relative to that of the straight sputtered film.

The as-deposited SiO_2 thin films grown by the chemical vapor deposition technique exhibit some interesting characteristics. For example, the cold wall LPCVD films give strong EPR resonances at g=2.0006 and g=2.0067 (see

Fig. 4) ,whereas no EPR is observed in the SiO_2 films grown in the hot wall LPCVD system (see Fig. 5a,b). We have also observed that annealing the cold wall LPCVD sample in N_2 at 300°C for 1 h leads to an irreversible loss of the EPR spectrum. As shown in Fig. 5c, no EPR is observed in SiO_2 films formed by thermal oxidation of CVD polycrystalline silicon.

In contrast to some of the other films studied,the EPR specta displayed in Fig. 6 of PECVD SiO_2 films shows no room temperature signal in the g≈2 region. However,if the sample is cooled to about 105 K a strong EPR signal with hyperfine structure spread over approximately 170 G is observed [4]. As shown in Fig. 7 the observed spectral lineshapes depend strongly on temperature. If we assume that the 4.2 K spectrum is close to the rigid limit, then we can use this spectrum to obtain the g and A tensor components (Fig. 8b). Listed in Table I are the spin Hamiltonian parameters for the paramagnetic species observed at low PECVD SiO_2 films as well as those for NO_2 trapped in other matrices. It is on the basis of the close similarity of the measured components of the g and A tensors with those for NO_2 in other matrices that we assign the EPR spectrum in PECVD SiO_2 films to trapped NO_2 radicals [4].

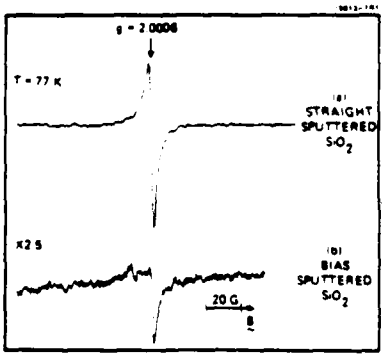

Fig. 3. EPR spectra (overmodulated) of RF-sputtered SiO_2 (a) straight (unbiased; cathode power 300 W) and in (b) biased (cathode power ~300 W and substrate power ~150 W) conditions.

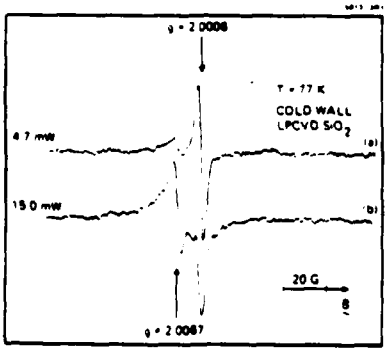

Fig. 4. EPR spectra (overmodulated and power broadened) obtained at 77 K for cold wall LPCVD SiO_2 at two different microwave powers (a) 4.7 mW and (b) 15.0 mW.

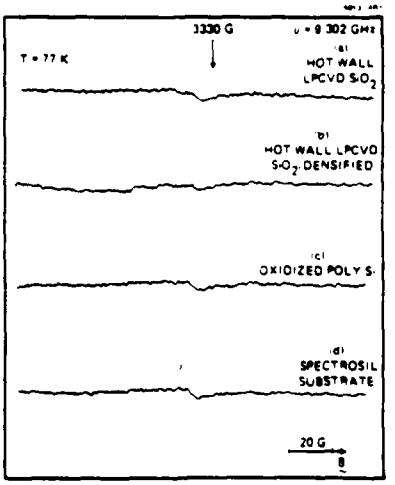

Fig. 5. EPR spectra measured at 77 K for SiO_2 thin films grown by (a) hot wall LPCVD (b) hot wall LPCVD densified at 900°C and (c) thermally oxidized CVD polysilicon. The spectrum from the Spectrosil substrate is shown in (d).

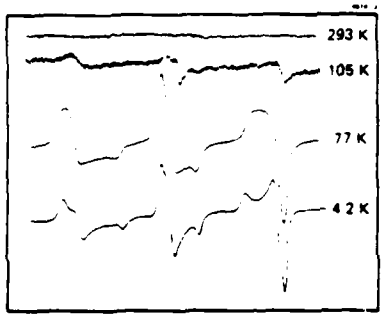

Fig. 6. EPR spectra of PECVD SiO_2 at various temperatures.

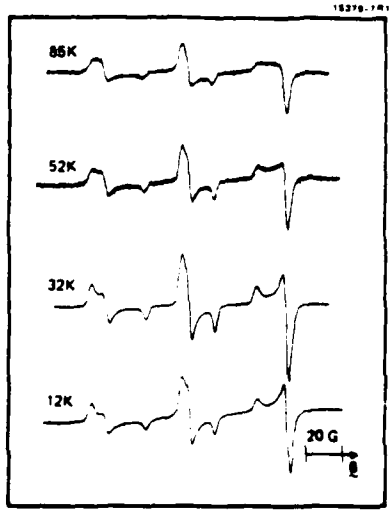

Fig. 7. Variable temperature EPR spectra of NO_2 trapped in PECVD SiO_2.

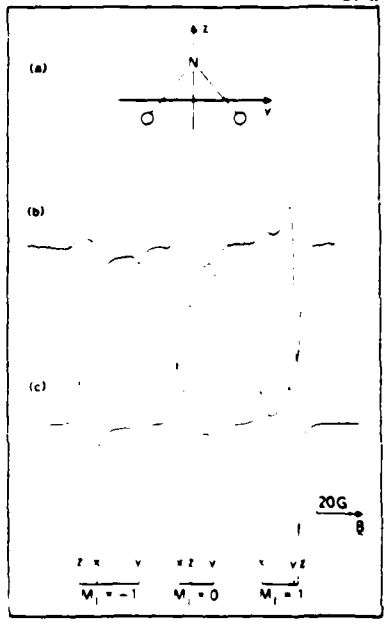

Fig. 8. (a) Molecule-fixed coordinate system for NO_2, (b) EPR spectrum of NO_2 trapped in PECVD SiO_2 at 4.2 K and (c) theoretical rigid-limit spectrum calculated using the spin Hamiltonian parameters given in Table I. The intrinsic linewidth used for the calculation was 1.8 G.

DISCUSSION

The work presented here represents an EPR survey of of the paramagnetic defects and impurities in SiO_2 thin films grown by a variety of techniques. Detailed computer simulations, similar to those performed in bulk glasses [1,10,11,16], of SiO_2 thin film EPR spectra are tractible and are in progress. Even without the benefit of spectral simulations, however, clues regarding the types of defects and impurities present as well as processing factors controlling defect/impurity production may be discerned.

Table I. Spin Hamiltonian parameters for NO_2 in various matrices.

MATERIAL	g			A, G			A_{ISO}, G
	g_{xx}	g_{yy}	g_{zz}	A_{xx}	A_{yy}	A_{zz}	
1 PECVD SiO_2 (4.2 K)	2.0067	1.0029	2.0029	50.1	46.6	66.5	53.0
2 NO_2/VYCOR (4.0 K)	2.0061	1.0013	2.0017	50.1	46.7	66.5	53.0
3 NO_2/RF SPUTTERED SiO_2 (4.2 K)	2.0068	1.0014	2.0023	50.0	47.0	66.0	54.3
4 $NaNO_2$ (77 K, γ-IRRADIATED SINGLE CRYSTAL)	2.0057	1.0010	2.0016	49.4	46.8	67.0	54.7

1 PRESENT WORK
2 REFERENCE 21
3 REFERENCE 3
4 H ZELDES AND R LIVINGSTON J CHEM PHYS 35 563 (1961)

To date the mechanism of defect formation in SiO_2 thin films is still an open question. For example, in the E-beam or RF sputtering deposition technique, a vitreous silica target is bombarded by highly energtic charged particles which produce in the gas phase not only molecular SiO_2, but also charged and neutral atomic and molecular fragments [17]. In addition, since the deposition chambers normally used are not ultra high vacuum systems, H_2O and H_2 contamination usually cannot be avoided. Thus stable as well as highly reactive species arrive at the surface of the substrate and recombine to form a dense silica. It is not too suprising that under these conditions precursor defects such as oxygen vacancies and peroxy intersitials are formed. Since the E-beam and RF sputtering deposition techniques are accompanied by soft X-rays and energetic particles, electrons and holes are generated which then become trapped at the appropriate precursor sites leading to the formation of paramagnetic point defects.

Our EPR measurements shown in Fig. 2a of E-beam silica films clearly indicate that the g tensor of the point defect is nearly axially symmetric with $g_{\parallel}$=2.0016 and $g_{\perp}$=2.0006. These g-values indicate that the defect is one of the E'-center variants, possibly E'_{β} or E'_{γ} [16]. The E'_{γ} variant can be ruled out because the attendant background radiation and energtic particles do not have sufficient energy to create this center [16]. The production of E'_{β} implies the reaction of atomic hydrogen with a precursor species such as a positively charged three-fold coordinated silicon species ($O_3{\equiv}Si^+$) [16,18] or more realistically, a Si-H group, e.g., $O_3{\equiv}Si$-H [19]. Here we have introduced the shorthand notation $O_3{\equiv}Si$ to represent three separate bonds to oxygen. Detailed computer simulations (specifically, obtaining g-value distributions), thermal annealing studies and isotopically labled (^{17}O and ^{29}Si) films will assist in distinguishing between E'_{β} and E'_{γ}.

Chemical vapor deposition techniques, on the other hand, also involve complex chemical processes in both the gas phase and at the subststrate surface. In contrast to the E-beam and RF sputtering methods, CVD techniques do not have the attendant soft X-rays or energetic particles which are necessary for converting diamagnetic precursor defect sites into paramagnetic states. However, as displayed in Fig. 4, the cold wall LPCVD SiO_2 films exhibit resonances at g=2.0006 and g=2.0067. The microwave power saturation behavior of the g=2.0067 signal is different from the g=2.0006 resonance and therefore, provides clear evidence that at least two different radicals are present. It is also interesting to note that the g=2.0067 signal saturates at higher microwave powers. This type of behavior is expected if the spin

relaxation times T_1 and T_2 are proportional to $(\Delta g)^{-2}$, where Δg is the maximum difference between the three principal g-values [20].

By reducing the microwave power and the magnetic field modulation levels, the powder averaged EPR lineshape (Fig. 2b) corresponding to a center with an axially symmetric g tensor is clearly revealed and it is proposed here that it is an $E\acute{\beta}$ variant. The basis for this assignment is that sufficent hydrogen is available in the cold wall LPCVD reactor to form $O_3{\equiv}Si\text{-}H$ which is subsequently converted to the $E\acute{\beta}$ center according to the reaction [19]:

$$H^{\circ} + O_3{\equiv}Si\text{-}H \rightarrow O_3{\equiv}Si^{\bullet} + H_2.$$

As pointed out above, annealing cold wall LPCVD SiO_2 films at 300°C for 1 h resulted in the irreversible loss of the spectrum. Similar results were observed over the same temperature range for the $E\acute{\beta}$ center in high-purity fused silica (Spectrosil) [16].

The NO_2 incorporated in the PECVD SiO_2 films occurs most likely as a result of using plasma decomposed N_2O as the source of oxygen for oxidising SiH_4 to silica. As shown in Fig. 7, as the temperature is raised from 4.2 to 77 K the spectral features corresponding to the x and z components of the g and A tensors become less resolved whereas, the y components remain clearly discernable, even up to 102 K. These observations are indicative of a temperature dependent motional averaging process which averages the x and z components of the g and A tensors.

In order to assess the role of motional averaging on the EPR spectra of NO_2 trapped in PECVD SiO_2, slow-motional spectral simulations were carried out assuming an anisotropic Brownian diffusion model [21] and using the spin Hamiltonian parameters listed in Table I. A Brownian diffusional model was chosen only because the computer program ran more efficiently with this model. Shown in Fig. 9 are simulated spectra for various rotational diffusion rates ($R_{||}$,$R_{\perp}$) with $R_{||}$ first along the y molecular axis (left panel) and then along z (right panel). For these simulations $R_{||}/R_{\perp} = 10$, where $R_{||}$ and $R_{\perp}$ are the rotational diffusion constants parallel and perpendicular to the molecular-fixed axis system shown in Fig. 8a where axial symmetry is assumed. These simulations clearly show that with $R_{||}$ parallel to the y molecular-fixed axis, the y spectral components are clearly resolved in all the hyperfine components (i.e., M_I=0,±1) even at high rotation rates (i.e., shorter rotational correlation times). However, with $R_{||}$ parallel to the z axis, the y tensor components are less discernable at shorter correlation times because of motional averaging of the x and y components. We have also observed that the NO_2 spectra in PECVD SiO_2 films vary less dramatically with temperature over the whole temperature range

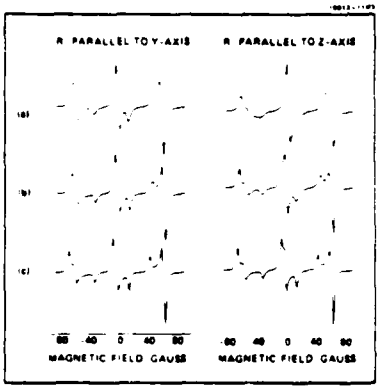

Fig. 9. Theoretical NO_2 slow-motional EPR spectra for various correlation times. Left panel is for $R_{||}$ parallel to the y-molecule fixed axis and right panel for $R_{||}$ along the z axis. See text for details. (a) $R_{||}=7.5\times10^{7}$ s^{-1}, $\tau=7.03\times10^{-9}$ s, (b) $R_{||}=2.5\times10^{7}$ s^{-1}, $\tau=2.11\times10^{-8}$ s and (c) $R_{||}=5.0\times10^{6}$ s^{-1}, $\tau=1.05\times10^{-7}$ s. The spin Hamiltonian parameters used are listed in Table I. A Lorentzian lineshape with an intrinsic linewidth of 1.8 G was used in all simulations.

studied than that for NO_2 on Vycor glass [22]. These results indicate that the motion of NO_2 in PECVD silica is more restricted than on porous Vycor glass.

CONCLUSIONS

The results of the present EPR study indicate that E-beam, RF sputtering, and cold wall LPCVD deposition techniques yield SiO_2 films with paramagnetic intrinsic bonding defects similar to those observed in bulk vitreous silica. PECVD SiO_2 films, on the other hand, display no room temperature EPR signal; however, when the films are cooled below approximately 105 K, a spectrum attributed to trapped NO_2 is observed.

ACKNOWLEDGEMENTS

The authors wish to thank H.L. Garvin (HRL) for helpful discussion concerning this work and for preparing the RF sputtered films, and to P.G. Reif (HRL) for depositing the E-beam films. This work was supported by the Army Research Office under contract number *DAAG29-84-C-0005*.

REFERENCES

1. D.L. Griscom, J. Non-Crystalline Solids 73, 51 (1985) and references therein.
2. T.W. Hickmott and J.E. Baglin, J. Appl. Phys. 50, 317 (1979).
3. E.J. Friebele, D.L. Griscom, and T.W. Hickmott, J. Non-Crystalline Solids 73, 351 (1985).
4. E.N. Schwartz, M.D. Clark, W. Chamulitrat, and L. Kevan, submitted to the J. Phys. Chem.
5. K.L. Yip and W. Beall Fowler, Phys. Rev. B 11, 2327 (1975).
6. A.H. Edwards and W. Beall Fowler, Phys. Rev. B26, 6649 (1982).
7. G.N. Greaves, J. Non-Crystalline Solids 32, 295 (1979).
8. G. Lucovsky, Phil. Mag. B 41, 457 (1980).
9. N.W. Ashcroft and N.D. Mermin, Solid State Physics (Saunders College, Philadelphia, 1976).
10. E.J. Friebele, D.L. Griscom, M. Staplebrock, and R.A. Weeks, Phys. Rev. Letters 42, 1346 (1981).
11. D.L. Griscom, Phys. Rev. B 22, 4192 (1980).
12. E.P. O'Reilly and J. Robertson, Phys. Rev. B 27, 3780 (1983).
13. K. Simakawa and A. Kondo, Phys. Rev. B 27, 1138 (1983).
14. M. Meaudre and R. Meaudre, J. Non-Crystalline Solids 68, 281 (1984).
15. T.W. Hickmott, J. Appl. Phys. 42, 2543 (1971).
16. D.L. Griscom, Nucl. Instr. and Meth. B 1 481 (1984).
17. J.W. Coburn and E. Kay, Appl. Phys. Letters 18, 435 (1971).
18. D.L. Griscom, J. Non-Crystalline Solids 68, 301 (1984).
19. D.L. Griscom, J. Appl. Phys. 58, 2524 (1985).
20. I.V. Aleksandrov, Soviet Phys. JETP 21, 580 (1965); Teor. Eksp. Khim. 1, 80,93 (1965).
21. J.H. Freed, G.V. Bruno and C.F. Polnaszek, J. Phys. Chem. 75, 3385 (1971).
22. M. Shiotani and J.H. Freed, J. Phys. Chem. 85, 3873 (1981).

APPENDIX D

ELECTRON-SPIN RESONANCE OF NO_2 TRAPPED IN SiO_2 THIN SOLID FILMS

Reprinted from

Journal of
APPLIED PHYSICS

Volume 59 | 1 May 1986 | Number 9

Electron-spin resonance of NO_2 trapped in SiO_2 thin solid films

Robert N. Schwartz and Marion D. Clark
Hughes Research Laboratories, Malibu, California 90265
Walee Chamulitrat and Larry Kevan
Department of Chemistry, University of Houston, Houston, Texas 77004

pp. 3231-3234

a publication of the American Institute of Physics

Electron-spin resonance of NO_2 trapped in SiO_2 thin solid films

Robert N. Schwartz and Marion D. Clark
Hughes Research Laboratories, Malibu, California 90265

Walee Chamulitrat and Larry Kevan
Department of Chemistry, University of Houston, Houston, Texas 77004

(Received 12 December 1985; accepted for publication 20 January 1986)

Electron-spin-resonance spectroscopy has been used to detect the presence of NO_2 in thin amorphous films of SiO_2 grown by the plasma enhanced chemical vapor deposition technique. Temperature dependent spectra were observed over the range 4.2–165 K. Based on the experimental spectra and theoretical spectral simulations we found that in the temperature range of 12–87 K NO_2 is undergoing axial-motional averaging about the axis in the molecular plane parallel to the O–O direction.

I. INTRODUCTION

The ability to deposit insulating thin solid amorphous films such as SiO_2, Si_3N_4, and Al_2O_3 free of impurities and defects has important practical applications. The purpose of the present work is to investigate possible impurities in SiO_2 thin films grown by the plasma-enhanced chemical vapor deposition (PECVD) technique. Electron-spin-resonance (ESR) spectroscopy can be used to identify paramagnetic impurities.

ESR spectra have been reported for SiO_2 thin films formed by radio frequency sputtering techniques.[1] Strong room temperature ESR in the $g \simeq 2$ spectral region is found but has not yet been convincingly assigned to specific species. We have also found room-temperature ESR signals in SiO_2 films generated by electron beam vacuum evaporation as well as sputtering techniques.[2] Work is in progress to better characterize these signals which appear similar to ones generated in γ-irradiated bulk amorphous SiO_2 such as E' centers,[3] nonbridging oxygen-hole centers,[4] and peroxy radicals.[5]

In contrast to the above techniques, we find that the PECVD preparation of SiO_2 films shows no strong room-temperature ESR signal in the $g \simeq 2$ region. However, if the PECVD SiO_2 sample is cooled to 77 K a strong ESR absorption signal with hyperfine structure spread over ~ 170 G is observed. Here we analyze this spectrum, assign it to trapped NO_2 radicals, and characterize its temperature-dependent motional averaging.

II. EXPERIMENT

Thin films of SiO_2 were deposited in a plasma-enhanced chemical vapor deposition system which was designed and constructed at the Hughes Research Laboratories.[6] The plasma is inductively coupled and excited at 13.56 MHz. The system was optimized for SiO_2 deposition at 300 °C using N_2O and SiH_4 diluted with He. SiO_2 films approximately 0.5 μm thick were deposited at a rate of 100 Å/min at a radio-frequency power of 40 W on polished Spectrosil (15 mil thick) fused quartz substrates.

ESR spectra were recorded at X band with a Varian E-9 spectrometer equipped with a Hewlett–Packard 5342A automatic microwave frequency counter and a Varian NMR gaussmeter for magnetic field measurement. The amplitude of the magnetic field modulation was adjusted so that line-shape distortion was found. In addition, the microwa power was adjusted so that no power-related line-shape distortion occurred. ESR spectra were recorded at 4.2 K b immersing the sample in liquid helium contained in a quar insertion Dewar. For variable temperature measurements between 4.2 and 165 K, an Air Products LTD Helitran unit inserted into the microwave cavity was used. The samp temperature was stabilized using an Artronix 5301 temper ture controller to drive the heater in the Helitran unit. The Artronix controller monitored the temperature near tl sample with a 50-Ω, 0.25-W carbon resistor. The temper ture just above the sample was measured by a chromel-iron doped gold (0.07-at. % iron) thermocouple while recordir ESR spectra. For temperatures below 40 K the thermoco ple position read 1 K higher than the sample temperature whereas above 40 K the thermocouple read 2 K higher. The reported temperatures are the corrected thermocouple rea ings. Electron-spin echo (ESE) spectra were obtained at 4 K on a home-built spectrometer operating at typical pulse powers of 100 W.[7]

III. RESULTS AND DISCUSSION

A. Experimental spectra

ESR spectra of PECVD SiO_2 thin films were record at various temperatures ranging from 4.2 to 165 K. As shown in Fig. 1 the observed spectral line shapes deper strongly on temperature. Similar spectra have recently bee reported for NO_2 in various matrices by other workers.[8-10] The lowest temperature achieved in our experiments was 4 K and at this temperature the spectrum of NO_2 in PECV SiO_2 is not as well resolved as that reported for NO_2 on crushed Vycor[8] and for NO_2 trapped in radio frequency (rf) sputtered SiO_2.[10] This may be due to residual-motional e fects or be associated with a distribution of binding sites wit slightly varying spin Hamiltonian parameters. Electron-spin echo measurements of the phase memory time support th latter interpretation; see below.

If we assume that the 4.2 K spectrum is close to the rigid limit then we can use this spectrum to obtain the g and A tensor components [Fig. 2(b)]. Listed in Table I are th

 0021-8979/86/093231-04$02.40

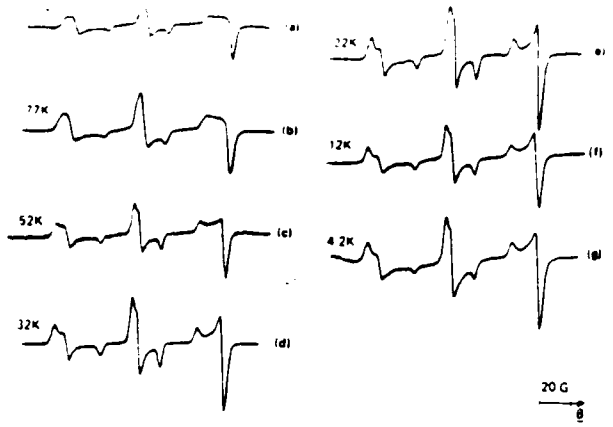

FIG. 1. Variable temperature ESR spectra of NO_2 in PECVD SiO_2 at (a) 85 K, (b) 77 K, (c) 52 K, (d) 32 K, (e) 22 K, (f) 12 K, and (g) 4.2 K.

spin Hamiltonian parameters for the paramagnetic species in PECVD SiO_2 thin films as well as those for NO_2 in various media. It is on the basis of the close similarity of the measured components of the g and A tensors with those for NO_2 in other matrices that we assign the ESR spectrum in

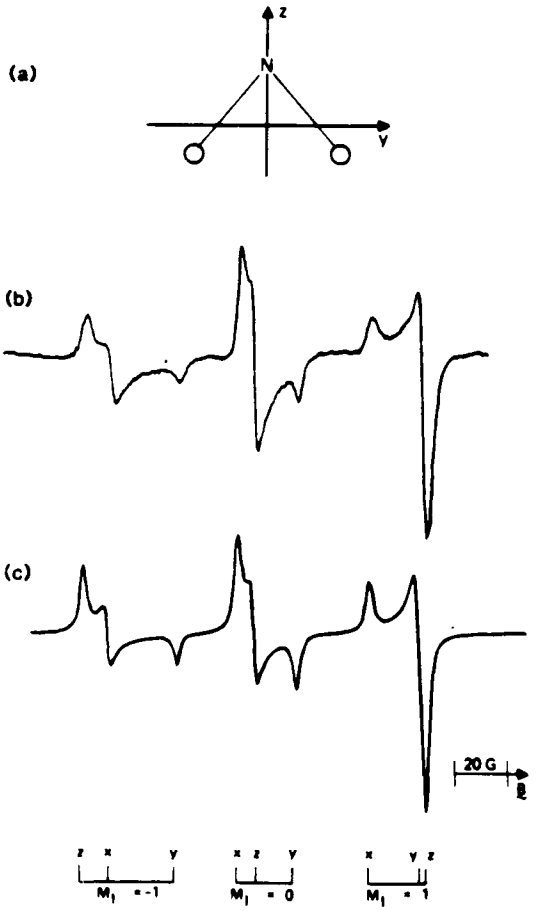

FIG. 2. (a) Coordinate system for NO_2, (b) ESR spectrum of NO_2 in PECVD SiO_2 at 4.2 K, and (c) theoretical rigid-limit spectrum. See text for details. The spin Hamilton parameters used in the calculations are listed in Table I and the intrinsic linewidth was 1.8 G

TABLE I. Summary of spin Hamiltonian parameters for NO_2

Material	g[a]			A, G[b]			a_{iso}, G
	g_{xx}	g_{yy}	g_{zz}	A_{xx}	A_{yy}	A_{zz}	
NO_2/PECVD SiO_2[c] (4.2 K)	2.0057	1.9920	2.0020	50.1	45.8	65.5	53.8
NO_2/Vycor[d] (4.8 K)	2.0051	1.9913	2.0017	50.1	45.7	65.5	53.8
NO_2/$NaNO_2$[e] (77 K, γ-irradiated single crystal)	2.0057	1.9910	2.0015	49.4	46.8	67.9	54.7
NO_2/rf sputtered SiO_2[f] (4.2 K)	2.0059	1.9914	2.0023	50.0	47.0	66.0	54.3

[a] Estimated error is ± 0.0003.
[b] Estimated error is ± 0.5 G.
[c] Present work.
[d] Ref. 8.
[e] H. Zeldes and R. Livingston, J. Chem. Phys. 35, 563 (1961).
[f] Ref. 10.

PECVD thin SiO_2 films to trapped NO_2 radicals.

As the temperature is increased changes occur in the line shapes as well as line positions. From 4.2 to 77 K the spectral features corresponding to the x and z components of the g and A tensors become less resolved; however, the y components remain clearly discernible [compare Fig. 2(c) with Fig. 1]. The y components are still observable up to ~ 102 K. These observations are indicative of a temperature dependent motional-averaging process which averages the x and z components of the g and A tensors. In order to pursue this line of reasoning we have carried out spectral simulations using the slow-motional ESR theory developed by Freed, Bruno, and Polnaszek.[11]

As the temperature is increased above 102 K the intrinsic linewidth significantly broadens with concomitant reduction in the signal-to-noise and at approximately 165 K the lines are broadened beyond detection. This apparent loss of signal is reversible in that NO_2 spectra are again observed if the thin film is cooled below ~ 165 K. The observed reversible intrinsic line broadening may possibly be associated with the rapid exchange of NO_2 with its dimer N_2O_4 as discussed by earlier workers.[8,12] We have also observed an irreversible reduction in the NO_2 ESR spectrum following heating the sample in O_2 at 400 °C for 1 h and a total loss of signal when heated to 500 °C in O_2 for the same length of time. This irreversible effect may be due to the loss of NO_2 from the PECVD SiO_2 thin film when heated to higher temperatures.

B. Theoretical spectra

Rigid-limit and slow-motional ESR spectral simulations of the NO_2 trapped in PECVD SiO_2 thin films were carried out using modified versions of the programs developed by Freed and co-workers.[11,13] In general, the quality of the agreement between the experimental and computed spectra are only fair. However, the quality of the fits is comparable to that obtained for NO_2 in Vycor.[8] Nevertheless, insight concerning the dynamics of the NO_2 radicals

trapped in the SiO_2 films may be obtained from the simulations. The spectral fits do not enable one to distinguish between the various molecular models of motional averaging.

Shown in Fig. 2(b) is the experimental spectrum and in Fig. 2(c) the best fitting rigid-limit spectral simulation of NO_2 trapped in PECVD SiO_2. For the simulations the g and A tensor components listed in Table I were used along with a Lorentzian line shape with an intrinsic linewidth of 1.8 G. The reason the fit is not better in the center component may be associated with a distribution of local binding sites with slightly different g and A tensor components. The experimental center component could also be distorted by the presence of an additional overlapping paramagnetic center. A reasonable candidate might be the silicon E' center. However, its ESR signature should be clearly discernible at room temperature[3] and no such resonance is observed from PECVD SiO_2 films.

In order to assess the role of motional averaging on the ESR spectra above 4.2 K, slow-motional spectral simulations were carried out assuming an anisotropic Brownian diffusion model and using the spin Hamiltonian parameters listed in Table I. There is no significance to picking a Brownian diffusion model instead of other diffusion models. Note that the spectra recorded at temperatures in the range 12–85 K where motional effects become important clearly display the y components in all three hyperfine components (see Fig. 1). These results indicate that the preferred axis for motional averaging is the y molecular axis. Shown in Figs. 3(a) and 3(b) are simulated spectra for various rotational diffusion rates ($R_\parallel$, $R_\perp$) with $R_\parallel$ first along y and then along z. For these simulations $R_\parallel/R_\perp = 10$, where $R_\parallel$ and $R_\perp$ are the rotational diffusion constants parallel and perpendicular to the molecular-fixed axis system shown in Fig. 2(a) where axial symmetry is assumed. These simulations clearly show that for the case of $R_\parallel$ parallel to y the y components are clearly resolved in all the hyperfine components even at high rotation rates (i.e., shorter rotational correlation times), whereas for $R_\parallel$ along z, the y components are less discernible at shorter correlation times due to the motional averaging of the x and y components.

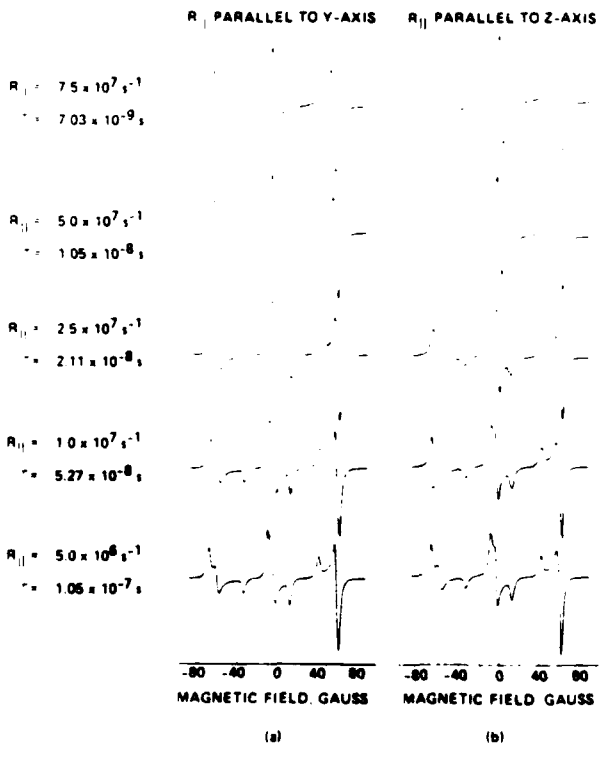

FIG. 3. Theoretical NO_2 spectra calculated for various rotational diffusion rates using slow-motional ESR theory: (a) NO_2 rotating about its y axis and (b) NO_2 rotating about its z axis. See text for details. The spin Hamiltonian parameters used are in Table I. A Brownian diffusion model was assumed and a Lorentzian lineshape with an intrinsic linewidth of 1.8 G was used in all simulations.

Another important feature of this work is the temperature sensitivity of the observed ESR spectra of NO_2 trapped in PECVD SiO_2. We have found that the NO_2 spectra in PECVD silica vary less dramatically with temperature over the whole temperature range studied than that for NO_2 on crushed Vycor.[8] For example, the observed NO_2 spectrum in PECVD silica at 52 K is very similar to that observed at about 23 K for NO_2 on Vycor. These results indicate that the motion of NO_2 is more restricted in PECVD silica than in Vycor glass.

C. Electron-spin echo measurements

Electron-spin echo (ESE) measurements of NO_2 trapped in PECVD SiO_2 were made in order to determine if motional effects contribute to the observed line shape at 4.2 K. From the overall two-pulse ESE decay one extracts the phase memory time T_M which is related to the relaxation processes in the spin system.[14] However, the connection between T_M and the spin-lattice and spin-spin relaxation time is complicated in solids.[15] If the phase memory time is dominated by local field fluctuations arising from modulation of the g and A tensors by radical motion, then T_M should exhibit a M_I dependence.[15] Progress has been made in relating T_M to motional effects both theoretically[16,17] and

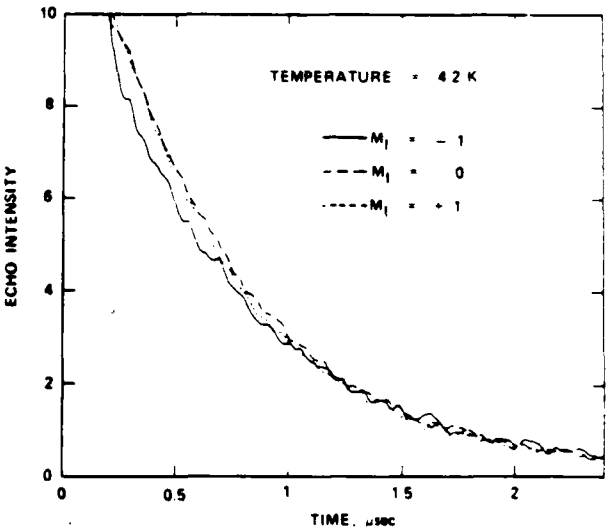

FIG. 4. Two-pulse electron-spin echo envelope decay of NO_2 in PECVD SiO_2 at 4.2 K.

experimentally.[18] In particular Stillman *et al.*[18] have demonstrated that T_M is a direct measure of the rotational correlation time in the slow-motional regime and that the phase memory time can be used to distinguish between various models of rotational diffusion.

Shown in Fig. 4 are the observed two-pulse ($\pi/2 - \pi$) spin-echo decay envelopes for the three NO_2 hyperfine components at 4.2 K. These measurements were made with the magnetic field set on each component to give the largest two-pulse spin echo. It is clear from this figure that the $\pi/2 - \pi$ echo decay envelopes for the three hyperfine components are the same and yield a phase memory time $T_M \sim 1\ \mu$s. Since T_M is independent of M_I we conclude that motional effects do not strongly influence the observed line shape at 4.2 K. It is more plausible that the NO_2 radicals are situated in a distribution of sites with slightly varying **g** and **A** tensors which leads to the discrepancy between the theoretical and observed ESR spectra at 4.2 K.

IV. CONCLUSIONS

The results of the present ESR study confirm the presence of NO_2 in PEVD silica films. The NO_2 is incorporated in the film during deposition most likely as a result of using plasma decomposed N_2O as a source of oxygen for oxidizing silane to silica. In simulating the 4.2 K NO_2 ESR spectra in PECVD silica it is important to take into account variations in the **g** and **A** tensor components due to a distribution of NO_2 binding sites to obtain better fits. From the temperature dependent spectra it is concluded that the NO_2 radicals undergo axial motional averaging about the y molecular axis in the molecular plane and parallel to the O–O direction over the temperature range 12–87 K. It is also concluded that the motion of NO_2 in PECVD silica films is more hindered than in crushed Vycor.

ACKNOWLEDGMENTS

We thank the Army Research Office under Contract DAAG29-84-C-0005 for partial support of this research. The electron-spin echo studies were supported by the National Science Foundation.

[1] T. W. Hickmott and J. E. Baglin, J. Appl. Phys. **50**, 317 (1979).
[2] R. N. Schwartz, M. D. Clark, W. Chamulitrat, and L. Kevan, in *Defects in Glasses*, edited by F. L. Galeener, D. L. Griscom, and M. J. Weber (Materials Research Society, Pittsburgh, PA) (in press).
[3] D. L. Griscom, Phys. Rev. B **22**, 4192 (1980).
[4] M. Stapelbroek, D. L. Griscom, E. J. Friebele, and G. H. Sigel, Jr., J. Non-Cryst. Solids **32**, 313 (1979).
[5] E. J. Friebele, D. L. Griscom, M. Stapelbrock, and R. A. Weeks, Phys. Rev. Lett. **42**, 1346 (1981).
[6] M. D. Clark and C. L. Anderson, J. Vac. Sci. Technol. **21**, 453 (1982).
[7] T. Ichikawa, L. Kevan, and P. A. Narayana, J. Phys. Chem. **83**, 3378 (1980); P. A. Narayana and L. Kevan, J. Magn. Reson. **46**, 84 (1982).
[8] M. Shiotani and J. H. Freed, J. Phys. Chem. **85**, 3873 (1981).
[9] M. Iwaizumi, S. Kubota, and T. Isobe, Bull. Chem. Soc. Jpn. **44**, 3227 (1971).
[10] E. J. Friebele, D. L. Griscom, and T. W. Hickmott, J. Non-Cryst. Solids **71**, 351 (1985).
[11] J. H. Freed, G. V. Bruno, and C. F. Polnaszek, J. Phys. Chem. **B**, 3385 (1971).
[12] J. H. Lunsford, J. Colloid Interface Sci. **26**, 355 (1968).
[13] C. F. Polnaszek, Ph.D. thesis (Cornell University, 1976).
[14] L. Kevan and R. N. Schwartz, eds. *Time Domain Electron Spin Resonance* (Wiley-Interscience, New York, 1979).
[15] I. M. Brown, in *Time Domain Electron Spin Resonance*, edited by L. Kevan and R. N. Schwartz (Wiley-Interscience, New York, 1979), Chap. 6; K. M. Salikhov and Yu D. Tsvetkov, *ibid.*, Chap. 7.
[16] A. E. Stillman and R. N. Schwartz, J. Chem. Phys. **69**, 3532 (1978).
[17] L. J. Schwartz, A. E. Stillman, and J. H. Freed, J. Chem. Phys. **77**, 5410 (1982).
[18] A. E. Stillman, L. J. Schwartz, and J. H. Freed, J. Chem. Phys. **73**, 3502 (1980); **76**, 5658 (1982).

APPENDIX E

OPTICAL SCATTERING AND EPR STUDY OF ZBLAN GLASS: DEPENDENCE ON PREPARATION AND PROCESSING METHODS

Materials Science Forum Volumes 19-20 (1987), pp. 275-286.

OPTICAL SCATTERING AND EPR STUDY OF ZBLAN GLASS: DEPENDENCE ON PREPARATION AND PROCESSING METHODS*

R.N. Schwartz, M. Robinson and G.L. Tangonan
HUGHES RESEARCH LABORATORIES
3011 Malibu Canyon Road
Malibu, CA 90265 (USA)

INTRODUCTION AND SUMMARY

It is well known that the physical properties of fluorozirconate glass (FZG) are strongly dependent on raw material purity and glass processing techniques [1]. For example, FZG simply prepared in a protective inert atmosphere like dry argon, nitrogen, or helium shows colored defects permeating the entire bulk of the sample. These defects are attributable to the reduction of Zr^{4+} to Zr^{3+} and Zr^{2+}. In this paper, we describe results of He-Ne laser optical scattering evaluation, and electron paramagnetic resonance (EPR) studies of γ-irradiated bulk ZBLAN, in investigating various raw materials and glass preparatory techniques, as related to glass quality and physical properties. High purity starting materials and a variety of reactive atmosphere processing (RAP) methods [2] (including CCl_4-Ar, CCl_4-O_2, CCl_4-CF_4, and CF_4-O_2) were used. EPR was used to detect radiation-induced species such as F_2^-, F_2^0, FCl^-, and Zr^{3+} and suspected oxygen-related centers.

STARTING MATERIALS

In this study, fluoride glass components were typically prepared by nonaqueous conversion of oxide or carbonate to fluoride with dry HF [3]. Using ZrO_2, for example, the chemical reaction is $ZrO_{2(s)} + 4HF_{(g)} \rightarrow ZrF_{4(s)} + 2H_2O(g)$. This reaction proceeds rapidly at room temperature to give ZrF_4 with a trace of $ZrF_4 \cdot H_2O$. Sublimation of this product at 825°C gives highly transparent (to 8 μm) needles of ZrF_4 for use in the glass preparation. AlF_3 is prepared by the same technique at 700°C and sublimed at 1350°C to give a clearer and transparent product to about 8 μm in the IR. BaF_2, NaF, and LaF_3 are prepared at room temperature with dry HF, and the yield is quantitative. These materials are then melted in dry HF and soaked for several hours at 1400°C, 1100°C, and 1600°C, respectively, then slowly cooled

to room temperature. In this treatment, impurities such as transition metal fluorides are volatilized from the system, and large water-white crystalline ingots form. Shown in Figure 1 are all of the ZBLAN starting materials prepared by such methods.

GLASS PROCESSING

Glasses for this study were prepared in the controlled environment of an apparatus represented in Figure 2. We used a vitreous carbon crucible for non-oxygen containing atmospheres, and a platinum crucible when O_2 was part of the melt environment. The crucible is loaded with chunks of fluorides of proper proportions to realize the glass formulation, and then inserted into the closed-ended silica tube. The top end of the silica tube is composed of a standard-taper ground-glass joint that permits input of any gas compatible with the crucible and the silica envelope at 800 to 900°C, the glass-melt processing temperature. The silica tube is heated in a nichrome cylindrical heater, and the temperature is measured by a thermocouple at the bottom of the tube. The melt is rapidly cooled and the glass is formed by removing the envelope from the heater; removal is easy because the apparatus is connected to the gas source and neutralizing trap with flexible Teflon input gas lines. Annealing occurs in another nichrome heater nearby, which is set at the annealing temperature.

OPTICAL SCATTERING EVALUATION

We used a direct technique to measure the scattering. The He-Ne laser input beam is focused through the test sample, which is immersed in index-matching liquid. The lens focal length is sufficient to make the beam size essentially constant over the field of view of the collection optics, which consists of a 1-mm-diameter fiber held 5 cm away from the sample. The fiber is recessed within a stainless steel tube to limit the field of view and thereby eliminate stray light. The fiber output is detected with a photomultiplier tube.

Our setup allows the sample to be moved relative to the fixed alignment of the input beam and the field of view of the fiber probe. By adding some light shielding and taking precautions to prevent reflections, we can easily detect the weak scattering from a silica reference piece with S/N of >30, and with 5 mW of laser power. Moving the sample transverse to the beam direction, we obtain a scan of the scattered power with distance.

The scattering results from our best sample are shown in Figure 3, with the scattering level measured for a Suprasil rod used as a reference line. The scattering range is 0.9-to-2-times that of the reference for this sample. An independent evaluation by the Naval Research Laboratory showed that (in scattering defect density) this sample is equivalent to the better glasses made there.

These results are for the best CCl_4-He sample produced. Typical scattering ratios for the different types of processing are listed below.

TABLE I.

Scattering Level	Processing Type
0.9-3	CCl_4-He
1.5-3	CCl_4-Ar
3-10	CF_4-O_2

In general, CCl_4-He and CCl_4-Ar provide low scattering results (we have processed only a few samples with CCl_4-Ar so far). Certainly the samples with CF_4-O_2 processing are consistently worse.

ELECTRON PARAMAGNETIC RESONANCE RESULTS

Recently, the effects of ionizing radiation on the properties of heavy metal fluoride glasses have been studied using both optical and EPR spectroscopies. In particular, we, as well as others, have observed that the nature and stability of the defects produced by ionizing radiation are strongly dependent on the glass preparation techniques.

One successful RAP scheme, which produces high-quality fluorozirconate glasses, utilizes the reactive atmosphere of CCl_4 and He. These reactive component gases are efficient for removing OH^- and $O^=$ impurities and for preventing the reduction of the metal fluoride. This procedure, however, has a serious drawback, because CCl_4 introduces Cl^- impurities into the melt by replacing OH^- with Cl^-. The added Cl^- is deleterious because it produces a higher crystallization tendency and also reduces the resistance to attack from environmental moisture. Furthermore, recent EPR studies indicate that IR absorbing centers, such as Cl_2^- and FCl^-, are generated in radiation-damaged fluorozirconate glasses.

Figure 4 shows EPR spectra of ZBT (ZrF_4, BaF_2, and ThF_4), prepared at HRL and γ-irradiated at 77°K. The spectrum in Figure 4(a) was obtained at 77°K, immediately following γ-irradiation and prior to warming. Indicated in the spectrum are the lines associated with the F_2^-, F_i°, and Zr^{3+} centers, which have been recently reported by other workers [4-7]. Here, F° corresponds to an interstitial, fluorine-related center (V_k center), formed by trapping a hole on a nonbridging fluorine, which subsequently moves to an interstitial position. And, F_2^-, characterized by the two outer lines in the EPR spectrum, represents a fluorine molecular-radical anion (V_k center), formed by hole-trapping, nonbridging fluorines. When the sample is warmed to room

temperature, the F_2^- and F^0 centers disappear, simultaneously, with the appearance of new spectral features. As shown in Figure 4(b), the new features are assigned to the molecular-anion radicals FCl^- and Cl_2^- [7]. In particular, the Cl_2^- center is not only quite stable, but also has an optical absorption spectrum in the IR [8]. Clearly, chlorine is a potential poison for radiation-hard heavy-metal fluoride glasses, so material processes that do not introduce chlorine into these glasses are required.

RAP methods have been developed for preparing high-purity fluorozirconate glasses without introducing Cl^-. In these processing schemes, the fluorozirconate melt is formed in the presence of a reactive atmosphere consisting of moisture-free oxygen and CF_4. The oxygen prevents reduction of ZrF_4, whereas the CF_4 functions as a reactive fluorine component, replacing any oxygen-anion impurities with F^-.

We have used EPR spectroscopy to study radiation-induced centers in ZBLAN (ZrF_4, BaF_2, LaF_3, AlF_3, and NaF) glass prepared using this RAP scheme. Figure 5(a) shows the spectrum following γ irradiation at 77°K, and before warming. Clearly identified are the lines associated with Zr^{3+}, F_2^-, and F^0. As shown in Figure 5(b), after warming to room temperature, the F_2^- and F^0 centers disappear. It is also important to note that the spectral features corresponding to the FCl^- and Cl_2^- hole-type centers are absent. When the sample is heated at 373°K for about 15 min, a new signal is readily distinguishable, as shown in Figure 5(c). Based on the recent work of Cases et al. [6], and taking into account the possibility of trace amounts of water in the starting and processing materials, we associate this EPR signal with a hole-type oxygen center such as O^-.

Recent light scattering studies indicate that FZG fibers [9] and bulk glasses [10,11] with higher loss have a higher oxygen content. It has been suggested that oxygen is in the form of oxides that generate either structural imperfection centers--composed of alien substances resulting from oxide segregation--or crystallines--generated by segregation or nucleation of oxides. Since EPR of γ-irradiated materials provides a unique diagnostic for low concentrations of suspected paramagnetic oxygen impurities, measurements were made on ZBLAN glass samples processed in a variety of ways. Figure 5 is the EPR spectra recorded at 77°K in the g~2 region of γ-irradiated (at 77°K; ~3 Mrad) ZBLAN samples, following warming to 373°K for about 15 min: (a) CF_4-O_2, (b) CCl_4-CF_4-He, (c) CCl_4-O_2, (d) CCl_4-Ar, and (e) CCl_4-He. Note that two general spectral patterns are evident: one pattern is associated with samples processed with CF_4, and the other with samples processed with CCl_4. We should also point out that the samples were not only roughly the same weight, but were also exposed to the same γ-ray dose (~3 Mrad); however, the signals from the samples processed with O_2 were more than ten times stronger than those processed with either He or Ar.

CONCLUSIONS

Samples prepared using CF_4-O_2 yield relatively high scattering glasses, compared to samples processed with CCl_4-Ar or CCl_4-He. EPR spectra appear to be sensitive to the glass processing conditions. In particular, the EPR signal intensity of the oxide-related center is lowest in ZBLAN glasses processed with either CCl_4-Ar or CCl_4-He. Samples will be prepared with ^{17}O, which has a nuclear spin of I=5/2. The hyperfine structure, resulting from the coupling of the unpaired electron spin with the ^{17}O nuclear spin, will be invaluable for characterizing the electronic structure of the paramagnetic "oxide center."

*This work was supported in part by Naval Research Laboratories under contract N00014-85-C-2524 and the Army Research Office contract DAAG29-84-C-0005.

REFERENCES

1. M. Robinson, Mater. Sci. Forum 5, 19 (1985).

2. R.C. Pastor and A.C. Pastor, Mat. Res. Bull. 10, 251 (1975).

3. M. Robinson, J. Cryst. Growth 75, 184 (1986).

4. P.E. Pisanich, L.E. Halliburton, L.N. Feuerheim, and J.M. Silbey, J. Non-Cryst. Solids 70, 37 (1985).

5. T. Tanimura, W.A. Silbey, M. Suscavage, and M. Drexhage, J. Appl. Phys. 58, 4544 (1985).

6. R. Cases, D.L. Griscom, and D.C. Tran, J. Non-Cryst. Solids 72, 51 (1985).

7. D.L. Griscom and D.C. Tran, J. Non-Cryst. Solids 72, 159 (1985).

8. M. Hass and D.L. Griscom, J. Chem. Phys. 51, 5185 (1969).

9. S. Mitachi, S. Sakaguchi, H. Yonezawa, K. Shikano, T. Shigematsu, and S. Takanashi, Jpn. J. Appl. Phys. 24, L827 (1985).

10. T. Nakai, Y. Mimura, H. Tokiwa, and O. Shinbori, J. Lightwave Technol. LT-3, 565 (1985).

11. T. Nakai, Y. Mimura, O. Shinbori, and H. Tokiwa, Jpn. J. Appl. Phys. 25, L704 (1986).

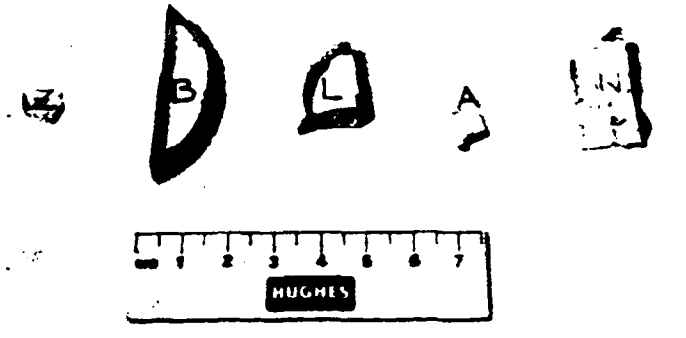

Figure 1. ZBLAN glass starting materials ZrF_4, BaF_2, LaF_3, AlF_3, and NaF

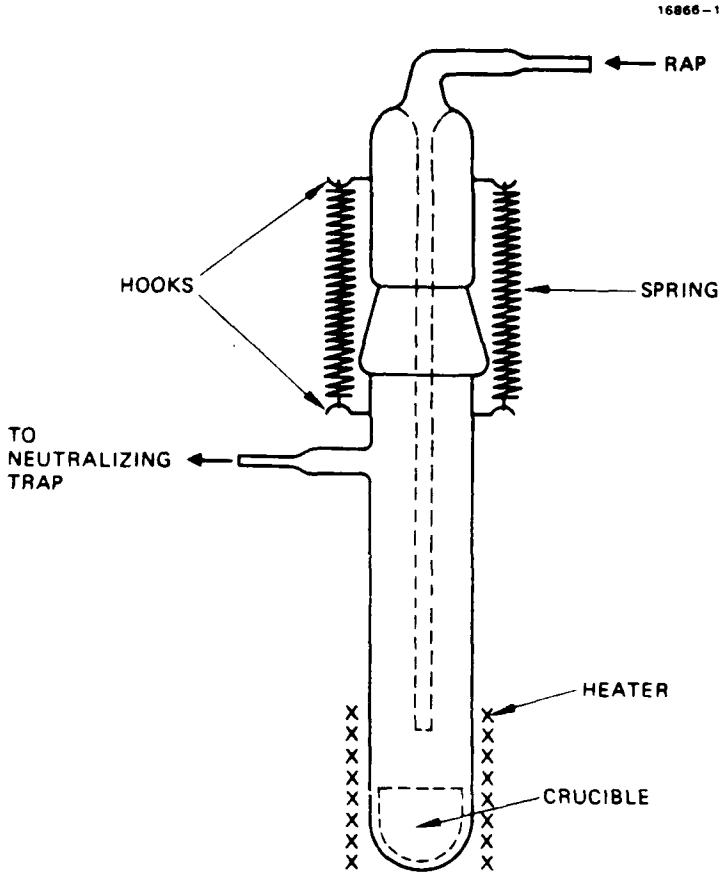

Figure 2. Schematic of the silica envelope for fluoride glass formation.

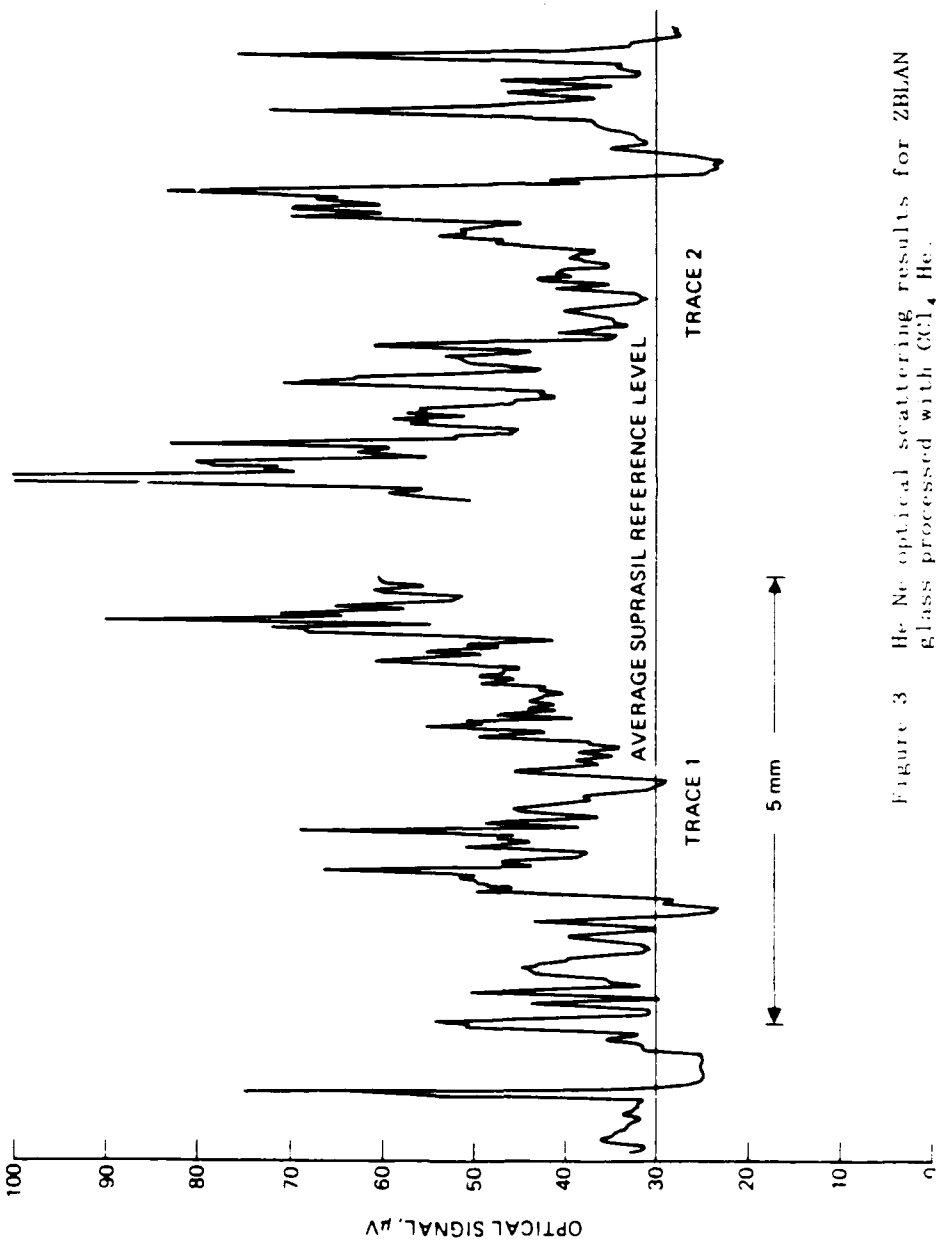

Figure 3 He-Ne optical scattering results for ZBLAN glass processed with CCl_4 He.

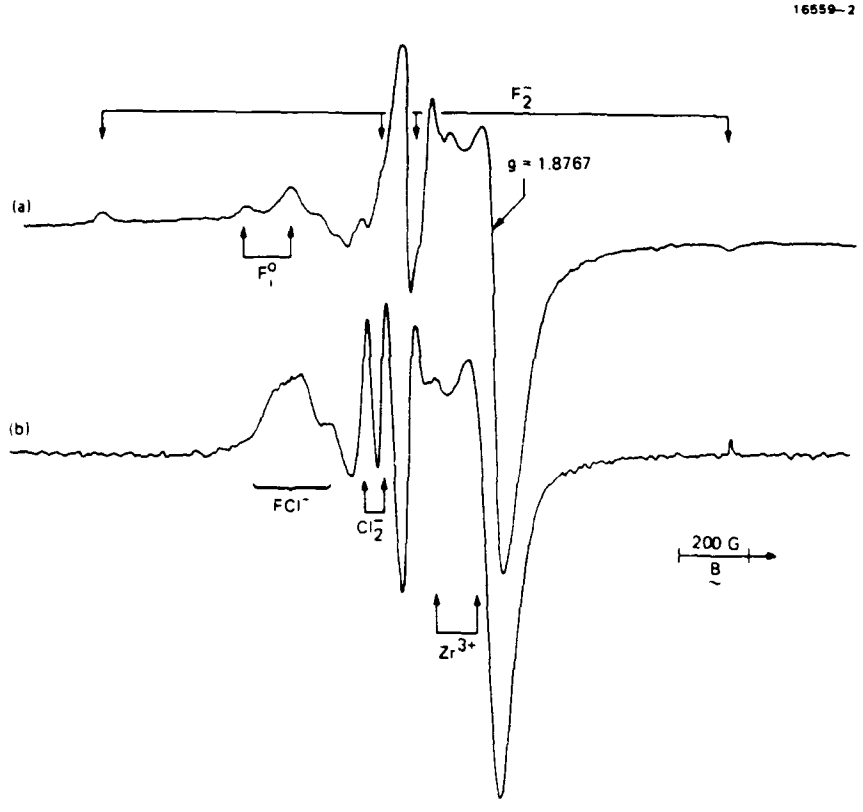

Figure 4. EPR spectra obtained at 77°K of HRL ZBT γ-irradiated at 77°K: (a) prior to warming and (b) following warming to room temperature.

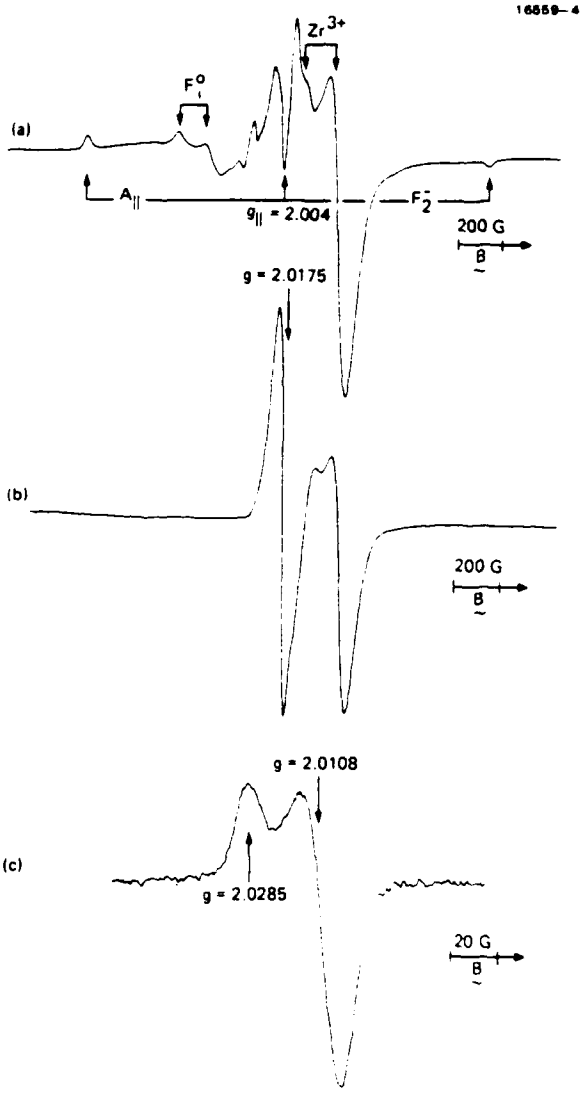

Figure 5. EPR spectra of HRL ZBLAN γ-irradiated at 77°K: (a) spectrum at 77°K following γ-irradiation, (b) spectrum at 77°K following warming to room temperature, and (c) spectrum at 77°K after warming to 373°K.

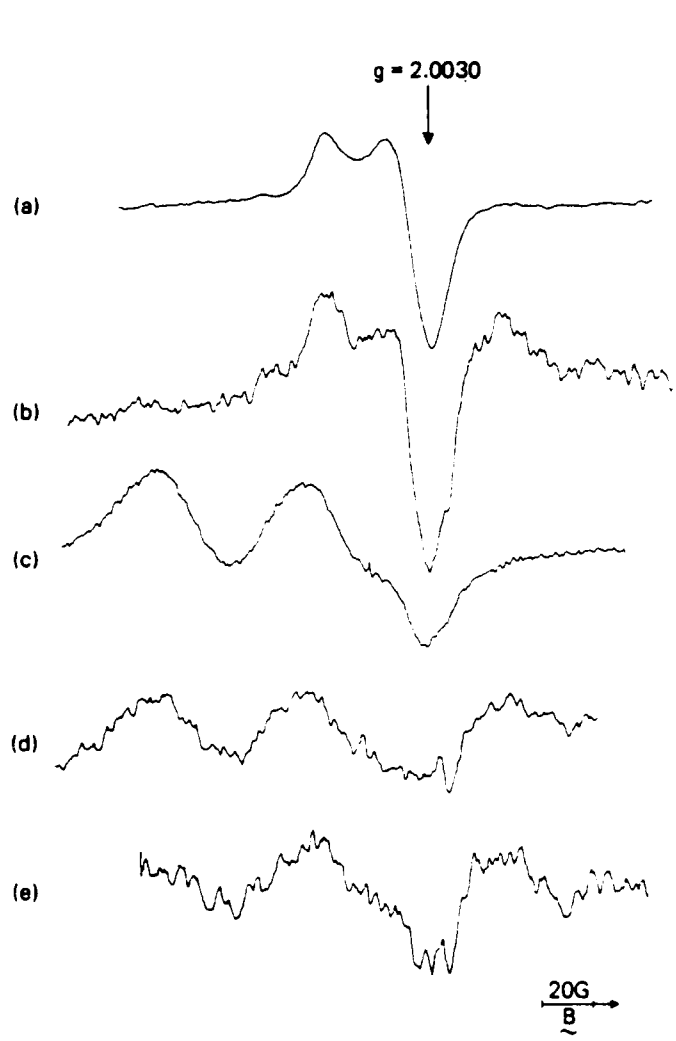

Figure 6. EPR spectra of γ-irradiated HRL ZBLAN samples recorded at 77°K following warming to 373°K: (a) CF_4-O_2; $G=5\times10^3$; (b) CCl_4-CF_4-He, $G=4\times10^4$; (c) CCl_4-O_2, $G=6.3\times10^3$; (d) CCl_4-Ar, $G=4\times10^4$; and (e) CCl_4-He, $G=5\times10^4$. G=spectrometer gain.

APPENDIX F

RADIATION-INDUCED PARAMAGNETIC DEFECTS IN HEAVY METAL FLUORIDE GLASSES

Radiat. Phys. Chem. Vol. 32, No. 3, pp. 439–442, 1988
Int. J. Radiat. Appl. Instrum. Part C
Printed in Great Britain.

0146-5724/88 $3.00 + 0.00

RADIATION-INDUCED PARAMAGNETIC DEFECTS IN HEAVY METAL FLUORIDE GLASSES

ROBERT N. SCHWARTZ,[1] MORT ROBINSON,[1] GUAN-DAO LEI[2] and LARRY KEVAN[2]
[1]Hughes Research Laboratories, 3011 Malibu Canyon Road, Malibu, CA 90265, U.S.A.
[2]Department of Chemistry, University of Houston, Houston, TX 77004, U.S.A.

(*Received* 30 *July* 1987)

Abstract—Ionizing radiation-induced defects in heavy metal fluoride glass have been studied by electron paramagnetic resonance (EPR) and electron spin echo (ESE) modulation techniques. Both pristine as well as water-contaminated glass samples were investigated. EPR measurements indicate that the radiation-induced defect observed after annealing at 393 K is not an oxide-related center introduced by water corrosion. ESE modulation data was used to probe the structure of the hole trap responsible for the so-called "central line". From the observed aluminum modulation it is concluded that the defect site is located near an aluminum cation in the glass structure.

INTRODUCTION

Over the past decade oxide-based glasses have been used for fabricating low-loss optical waveguide fibers. In recent years, however, heavy metal fluoride glasses have been extensively investigated with the aim of developing ultra-low loss i.r. transmitting optical waveguides.[1-3] Compared to oxide-based fibers which have a minimum attenuation of 0.15 dB/km at 1.55 μm, heavy metal fluoride glasses have lower scattering loss from combined Rayleigh, Brillouin and Raman scattering mechanisms and in addition, a multiphonon edge that is shifted to longer wavelengths, thus permitting a theoretical minimum loss of $\sim 10^{-3}$ dB/km at 2.55 μm.[4-7]

One of the fundamental materials issues concerning the use of heavy metal fluoride glasses for optical waveguide applications has been the elimination of oxide anion impurities which may be responsible for the observed scattering loss in unirradiated glass.[8,9] Various glass processing procedures have been developed for forming heavy metal fluoride melts which are free of such anion impurities as OH^- and O^{2-} and impurities associated with the reduction of ZrF_4 (e.g. ZrF_2 and ZrF_3). One of the more successful methods is the reactive atmosphere processing (RAP)[10] technique which utilizes a variety of gas mixtures which are reactive at high temperatures such as CCl_4/HF, SF_6/He and CF_4/O_2. These reactive component gases are efficient for removing OH^- and O^{2-} impurities from the melt as well as any H_2O present as an impurity in the gases or from outgassing the system and in addition, for preventing the reduction of ZrF_4. However, the CCl_4/HF mixture has a serious drawback since the use of CCl_4 results in the introduction of Cl^- impurities into the melt by the replacement of OH^- with Cl^-. The added Cl^- is deleterious because it produces a higher crystallization tendency, and also reduces the resistance to attack from environmental moisture.

Recently, the effects of ionizing radiation on the properties of heavy metal fluoride glasses have been studied by both optical[11-14] and electron paramagnetic resonance (EPR)[11,12,15-17] spectroscopies. In particular, it has been observed that the nature and stability of the defects produced by ionizing radiation are strongly correlated with glass preparation/processing techniques. Here we expand on previously reported work,[17] and present new EPR results on γ-induced paramagnetic defects. We particularly focus on the correlation of oxide impurities with the observed radiation-induced paramagnetic defects.

EXPERIMENTAL

In this study high-purity heavy metal fluoride glass samples were prepared using procedures described in detail elsewhere.[7] High-purity starting materials were typically prepared by nonaqueous conversion of oxide or carbonate to fluoride by dry HF.[18] Either sublimation or melting in dry HF followed by soaking at high temperatures with subsequent slow cooling to room temperature yielded high-purity metal fluorides. In a typical preparation, chunks of ZrF_4 (53 mol %), BaF_2 (20 mol %), LaF_3 (4 mol %), AlF_3 (3 mol %) and NaF (20 mol %) were loaded in a vitreous carbon crucible which was then placed in a closed-end silica reaction tube fitted with a standard-taper ground-glass joint that permitted input of the reactive atmosphere. The reaction vessel containing the starting materials was heated to 800–900°C during which the resulting melt was exposed to a flowing reactive atmosphere of SF_6/He. The melt was then rapidly cooled through the devitrification temperature T_x to 250°C at a rate of ~200°C/min to

form a glass of approximately the same composition as the melt. The glass, called ZBLAN (ZrF_4, BaF_2, LaF_3, AlF_3, NaF), was then annealed at 250°C for 6 h. All samples were irradiated at 77 K by ^{60}Co γ-radiation at a dose rate of ~1 Mrad/h.

EPR spectra at X-band were obtained with either an IBM Instruments ESP/300 spectrometer employing 100 kHz magnetic field modulation or a Varian Century Series E-9 spectrometer using 25 kHz modulation. Microwave frequencies were measured with a Hewlett-Packard 5342A automatic microwave frequency counter and the magnetic field measurements were made with a Varian nuclear magnetic resonance gaussmeter. EPR spectra at 77 K were obtained using a quartz insertion Dewar. The estimated error in the measured g-values is ± 0.0004. X-band ESE spectra were obtained at 4.2 K on a home-built spectrometer that has been described previously.[19,20] The nominal pulse widths for the two-pulse ESE decay spectrum were 30 ns for both pulses.

EXPERIMENTAL RESULTS AND DISCUSSION

The corrosive attack by water on heavy metal fluoride glasses has recently been investigated by Robinson and Drexhage.[21] They observed that surface degradation occurs only when water condenses on the glass surface. In order to probe the effects of water contamination on the radiation damage process in ZBLAN glass, polished specimens were maintained in direct contact with liquid water at room temperature for approx. 48 h. Samples subjected to water contamination along with pristine samples chosen as "controls", were then remelted under an argon atmosphere in an attempt to uniformly distribute the oxide impurities throughout the contaminated glass. In order to confirm oxide contamination oxygen analyses were performed by monitoring the evolved CO and CO_2 from samples vaporized in graphite crucibles.

Shown in Fig. 1 are EPR spectra of ZBLAN glass recorded at 77 K immediately following γ-irradiation at 77 K and prior to warming. The spectrum in Fig. 1a was observed from the ZBLAN control sample and that in Fig. 1b from the water-treated sample. Indicated in Fig. 1a are the transitions associated with the hole trapping centers F_2^- and F_i^0, and an electron trapping center, Zr^{3+}.[11,12,15,16] Here, F_2^-, characterized by the two outer lines, represents a molecular fluorine radical anion also termed a V_k center, formed by trapping a hole on nonbridging fluorine atoms. The F_i^0 center corresponds to an interstitial defect also termed a V_H center, formed by trapping a hole on a nonbridging fluorine atom which subsequently moves to an interstitial position.[22] It is clear that the spectra shown in Fig. 1 are nearly identical except in the $g = 2.0289$ region which appears to be enhanced in the water-treated sample (Fig. 1b).

When the samples are heated to room temperature for about 15 min and then cooled to 77 K the spectra in Figs 2a,b are obtained for the control and water-treated samples, respectively. These spectra clearly indicate that for both the control and water-treated samples the F_2^- and F_i^0 centers disappear; whereas the feature assigned to the Zr^{3+} center has not significantly changed. A striking difference is clearly evident in the $g = 2.0289$ region ($g = 2.010$ at zero crossing) which appears to be a superposition of two different resonances. Figure 2c depicts the difference spectrum obtained by subtracting the spectrum of the control from that of the water-treated specimen. Before discussing the origin of this "central resonance" centered at $g = 2.010$ the results of higher temperature (393 K) anneal experiments will be presented.

When both the control and the water-treated glasses are annealed at 393 K for about 15 min, a powder glass averaged signal typical of a paramagnetic defect possessing a nearly axial symmetric g-tensor is easily distinguished in Figs 3a,b. It is important to note that these spectra were from samples which were irradiated with the same γ-dose (~3 Mrad) and which were approximately the same weight. From the measured g-values it is clear that this signal is present in the room temperature annealed spectrum (Figs 2a and 2b) where it overlaps the central resonance ($g = 2.010$ spectral region). It has recently been suggested by Cases *et al.*,[16] that the high-temperature annealed signal may be associated with a hole trapped on an oxide-related impurity. Since the EPR absorption intensities for both the water-treated and control samples are essentially the same, our experiments suggest that this signal is not associated with an oxide impurity introduced via the corrosive attack of water.

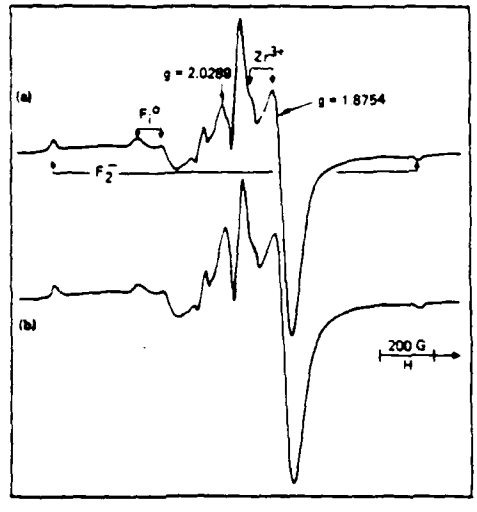

Fig. 1. EPR spectra obtained at 77 K of heavy metal fluoride glass γ-irradiated at 77 K to ~3 Mrad: (a) control sample; (b) water-treated sample.

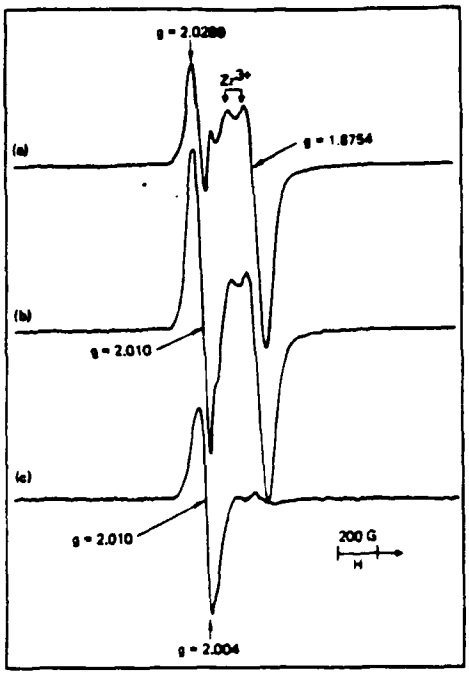

Fig. 2. EPR spectra measured at 77 K of heavy metal fluoride glass γ-irradiated at 77 K to ~3 Mrad and warmed to room temperature (~295 K) for ~15 min: (a) control sample; (b) water-treated sample; (c) difference spectrum [(b) − (a)].

An interesting feature of the "central resonance" is that it grows in intensity with the disappearance of the F_2^- and F_1^0 centers (see Figs 1a,b and Figs 2a,b). This has been observed in heavy metal fluoride glass in which NaF is replaced by LiF and is discussed in more detail by Cases *et al.*[16] These authors also observed that the lineshape of the central resonance at X-band (~9 GHz) is very similar to that measured at Q-band (~35 GHz), thus ruling out a contribution due to a distribution in g-values. Cases *et al.*[16] suggest that the central line may arise from a hole delocalized over several fluorine atoms, each exhibiting a small hyperfine interaction and hence, a lineshape which is inhomogeneously broadened due to unresolved fluorine hyperfine structure.

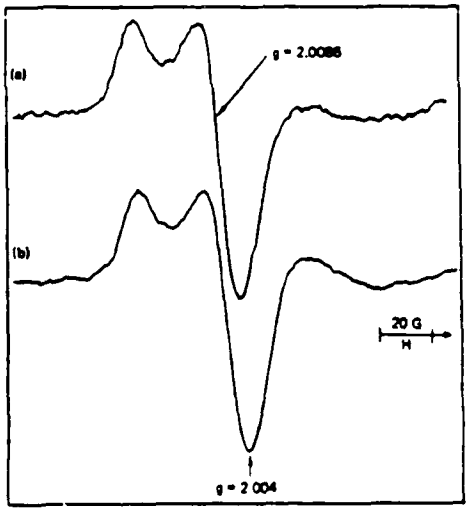

Fig. 3. EPR spectra recorded at 77 K of heavy metal fluoride glass γ-irradiated at 77 K to ~3 Mrad followed by warming to 393 K for ~15 min: (a) control sample; (b) water-treated sample. Both spectra were recorded with the same instrument settings.

Figure 4 is the ESE decay spectrum observed with the magnetic field positioned at $g = 2.0289$ in the spectrum in Fig. 1b. The principles of ESE spectrometry are described in detail elsewhere.[23] In this technique a sequence of resonant microwave pulses are applied to the spin system resulting in microwave echoes corresponding to the reformation of the macroscopic magnetization. For a two-pulse sequence, the echo forms at a time 2τ after the first pulse ($\pi/2$), τ being the interpulse time interval between the first and second (π) pulses. The observed ESE decay spectrum is obtained by sweeping the time interval, τ. In a matrix containing nearby precessing magnetic nuclei, a time-dependent local magnetic field is produced at the unpaired electron spin during the application of the pulse sequence. This results in a modulation of the ESE decay envelope; the modulation frequency being approximately the Larmor precessional frequency of the nearby interacting nuclei.[24] The ESE decay spectrum shown in Fig. 4 is a superposition of two modulation periods; a fast modulation corresponding to the ^{19}F nuclear-free precession frequency ($\nu_F^{-1} \simeq 77$ ns) and a slow one due to nearby ^{27}Al nuclei ($\nu_{Al}^{-1} \simeq 278$ ns) in a magnetic field of 3246.6 G.

The ESE results are important for several reasons. Firstly, the observation of ^{19}F modulation provides direct experimental evidence that the central resonance is inhomogeneously broadened by unresolved hyperfine structure which supports the model pro-

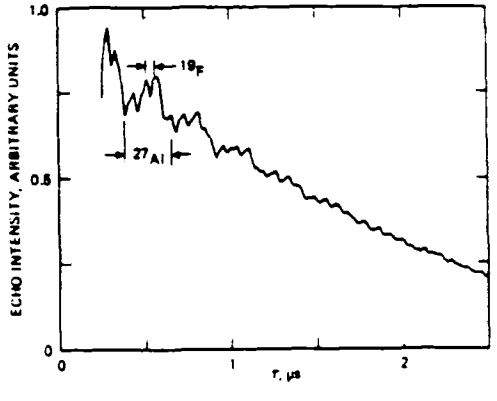

Fig. 4. Two-pulse electron spin echo decay spectrum taken at a fixed magnetic field (3246.6 G) set at the $g = 2.0289$ position of the EPR spectrum in Fig. 1b.

posed by Cases *et al.*[16] Secondly, the observed ^{27}Al modulation provides unique structural information since it indicates that the hole trap is stabilized in the vicinity of a site containing aluminum. It is interesting to note that the heavy metal fluoride glass used in our experiments contains only 3 mol % of aluminum (AlF_3). It is believed that a trivalent cation such as Al^{3+} improves the glass-forming tendency of a melt by reducing the strain of the glass structure.[25] The reduction in strain is due to the fact that the Al^{3+} cation can exhibit a wide range of Al—F bond angles in the immediate coordination environment, thus providing the necessary flexibility to connect the ZrF_n ($5 < n \leqslant 9$) polyhedra to form a three-dimensional, aperiodic network. Molecular dynamics simulations indicate that in the immediate vicinity of the network-forming aluminum cation structural disorder is enhanced.[25] Our results suggest that it is this structural disorder around Al^{3+} which provides the required environment for effective hole trapping.

The final issue to be addressed concerns the incorporation of oxide impurities into the heavy metal fluoride glass structure. As shown by the EPR spectra in Figs 1 and 2, the intensity of the central line ($g = 2.0289$) is larger for the water-treated glass than for the control (see Figs 1 and 2). This observation suggests that the chemical structure of the hole trap responsible for the central resonance may be even more complex than described above since in addition to F^- and Al^{3+} ions, O^{2-} may be involved. Additional experiments involving ^{17}O, which has a nuclear spin of $I = 5/2$, may prove useful for confirming this model. The hyperfine interaction, resulting from the coupling of the unpaired electron spin with the ^{17}O nuclear spin, should provide additional spectral structure for characterizing the hole trap.

SUMMARY AND CONCLUSIONS

We have investigated the effects of water contamination on the radiation-damage process in heavy metal fluoride glass. EPR and ESE spectrometry were used to study the paramagnetic defects generated by γ-irradiation. We have found that the center remaining after annealing irradiated samples at 393 K is not associated with an oxide impurity introduced by water corrosion. The so-called "central line" has been probed using the two-pulse ESE technique. We have observed both ^{19}F and ^{27}Al modulation on the ESE decay curve. The fluorine modulation indicates that the central resonance is inhomogeneously broadened by unresolved fluorine hyperfine structure. This corroborates the EPR results of Cases *et al.*[16] The aluminum modulation provides additional structural information about the hole trap center not anticipated from previous EPR measurements. Finally, we observed that the EPR intensity of the central line in the water-treated sample is stronger than in the pristine sample. This leads us to suggest that the hole trapping site associated with the central resonance may also involve O^{2-}, in addition to F^- and Al^{3+}.

Acknowledgements—We thank the Army Research Office under contract DAAG29-84-C-0005 for support of this research. The ESE studies were supported by the National Science Foundation. The authors wish to thank K. W. Fuller and F. V. Lee for preparing the samples and Paul Tick of Corning Glass Works for carrying out the oxygen analyses.

REFERENCES

1. M. Poulain and M. Poulain, *Mater. Res. Bull.* 1975, **10**, 243.
2. M. Poulain and J. Lucas, *Verres Refract.* 1978, **32**, 505.
3. M. Poulain, *J. Non-Cryst. Solids* 1983 **56**, 1.
4. M. E. Lines, *J. Appl. Phys.* **55**, 1984, 4052, 4058.
5. *Idem, A. Rev. Mater. Sci.* 1986, **16**, 113.
6. J. R. Gannon, *Proc. Soc. Photo-Opt. Instrum. Eng.* 1981, **266**, 63.
7. M. G. Drexhage, in *Treatise on Materials Science and Technology*, Vol. 26 (Edited by M. Tomazawa and R. H. Doremus) p. 151. Academic Press, New York, 1985.
8. T. Nakai, Y. Mimura, H. Tokiwa and O. Shimbori, *J. Lightwave Technol.* 1985, **LT-3**, 565.
9. *Idem, Jpn J. Appl. Phys.* 1986, **25**, L704.
10. R. C. Pastor and A. C. Pastor, *Mater. Res. Bull.* **10**, 251 1975.
11. P. E. Fisanich, L. E. Halliburton, L. N. Feuerheim and S. M. Silbey, *J. Non-Cryst. Solids* 1985, **70**, 37.
12. T. Tanimura, W. A. Silbey, M. Suscavage and M. Drexhage, *J. Appl. Phys.* 1985, **58**, 4544.
13. K. Tanimura, M. Ali, L. F. Feuerheim, S. M. Silbey and W. A. Silbey, *J. Non-Cryst. Solids* 1985, **70**, 397.
14. E. J. Frieble and D. C. Tran, *J. Non-Cryst. Solids* 1985, **72**, 221.
15. D. L. Griscom and D. C. Tran, *J. Non-Cryst. Solids* 1985, **72**, 159.
16. R. Cases, D. L. Griscom and D. C. Tran, *J. Non-Cryst. Solids* 1985, **72**, 51.
17. R. N. Schwartz, M. Robinson and G. L. Tangonan, *Mater. Sci. Forum* 1987, **19–20**, 275.
18. M. Robinson, *J. Cryst. Growth* 1986, **75**, 184.
19. T. Ichikawa, L. Kevan and P. A. Narayana, *J. Phys. Chem.* 1980, **83**, 84.
20. P. A. Narayana and L. Kevan, *J. Magn. Reson.* 1983, **46**, 84.
21. M. Robinson and M. G. Drexhage, *Mater. Res. Bull.* 1983, **18**, 1101.
22. D. L. Griscom, *Solid State Commun.* 1972, **11**, 899.
23. L. Kevan and R. N. Schwartz (Eds), *Time Domain Electron Spin Resonance*. Wiley-Interscience, New York, 1979.
24. L. Kevan, in *Time Domain Electron Spin Resonance* (Edited by L. Kevan and R. N. Schwartz) Chap. 8. Wiley-Interscience, New York, 1979.
25. I. Yasui and H. Inoue, *Mater. Sci. Forum* 1987, **19–20**, 103.

APPENDIX G

AGING EFFECTS IN BULK AND FIBER T2Br-T2I

Aging effects in bulk and fiber TlBr-TlI

Joseph A. Wysocki, Robert G. Wilson, Arlie G. Standlee, Antonio C. Pastor, and Robert N. Schwartz
Hughes Research Laboratories, 3011 Malibu Canyon Road, Malibu, California 90265

Arthur R. Williams
Los Alamos National Laboratory, Los Alamos, New Mexico 87545

Guan-Dao Lei and Larry Kevan
Department of Chemistry, University of Houston, Houston, Texas 77004

(Received 4 November 1987; accepted for publication 4 January 1988)

A study of optical aging in bulk and extruded fibers of thallium bromo-iodide (TlBr-TlI) is presented. A variety of techniques including secondary ion mass spectrometry (SIMS), powder neutron and x-ray diffraction, infrared spectroscopy, and electron paramagnetic resonance (EPR) spectroscopy are used to probe the chemical and structural properties of both pristine and aged material. High concentration levels of a hydrogen bearing impurity have been detected by SIMS and neutron scattering in aged TlBr-TlI, and have been shown to be localized in the surface layers of fibers as well as bulk samples. We present EPR evidence which indicates that the hydrogen bearing impurity is water.

I. INTRODUCTION

A variety of nonsilica-based optical materials is presently the focus of intensive research because of potential application as low loss fibers for infrared communications. Among the most promising materials is the metal halogenide TlBr-TlI system (KRS-5).[1] This crystalline material is known to transmit from 0.6 to 40 μm, and due to low intrinsic scattering losses from Rayleigh and Brillouin mechanisms[2] and a multiphonon edge[3] that is shifted to longer wavelengths, it has a theoretical transmittance loss of $\sim 10^{-3}$ dB/km at 10.6 μm.[4]

Fiber optic waveguides made from TlBr-TlI, however, have optical losses at 10.6 μm that are orders of magnitude higher than predicted by theory. In addition, the optical loss increases with time ($\sim$6 dB/m per year). The focus of this investigation is the phenomenon of optical aging of TlBr-TlI. Our primary concern is correlating changes in the physical and chemical properties of TlBr-TlI with changes in optical attenuation. Freshly prepared and aged optical waveguide fibers and bulk starting material were examined using x-ray and neutron powder diffraction, secondary ion mass spectrometry, infrared spectroscopy, and electron paramagnetic resonance spectroscopy.

II. EXPERIMENTAL PROCEDURES AND RESULTS

A. Sample preparation and selection

The samples used in this study were either supplied by Harshaw or BDH (British Drug House) or grown at Hughes. A description of the method used at Hughes for growing KRS-5 crystals is outlined in the Appendix. Samples of both freshly prepared and aged bulk starting material were extruded into polycrystalline fibers suitable for optical transmission studies. The bulk material, as well as the fibers, were either examined after aging under a variety of conditions or examined in a near pristine state. Samples of the KRS-5 (bulk and fiber) were then examined by either surface analysis techniques such as secondary ion mass spectrometry or x-ray diffraction and/or bulk analysis techniques such as neutron diffraction or electron paramagnetic resonance spectroscopy. In addition, all samples were measured for optical transmission using either infrared spectroscopy or by single point measurements at 10.6 μm.

Table I lists the types of sample used for measurements. Each of these sample types was used for surface and/or bulk analysis as described in the following sections.

The fibers were prepared from the bulk material using hot extrusion, a previously described[1] process. Optical transmission measurements at 10.6 μm were taken using the experimental equipment shown in Fig. 1. These measurements were used as a reference for the starting quality of the fibers. The fibers were then placed in a variety of gaseous environments including helium, argon, hydrogen, and ammonia. Fibers were also placed in vacuum at room temperature and at 77 K and some fibers were placed in opaque containers. The fibers were periodically remeasured for optical aging. A summary of the data for the environmental dependence of the optical aging experiments is shown in Fig. 2. In addition, Fig. 3 shows a plot of the average attenuation of fibers versus the time interval in weeks between the receipt of pristine starting material and the date the bulk material was extruded into fiber.

Samples of these fibers were then used for subsequent analysis after the measurements at 10.6 μm were made. In this way, the measurements at 10.6 μm were used as criterion for deciding how the fibers were responding to the various environments.

TABLE I. Sample types.

Starting materials	Fiber	
New bulk	New	Aged
Aged bulk	New	Aged

 0021-8979/88/094365-07$02.40

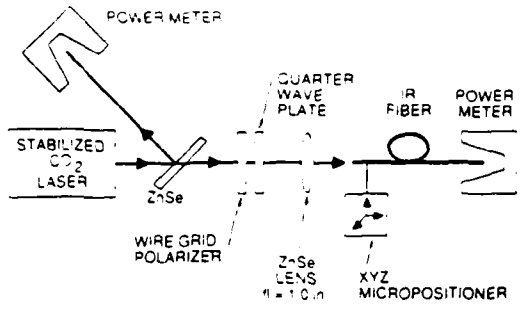

FIG. 1. Experimental apparatus for insertion loss measurements of polycrystalline TlBr-TlI fibers at 10.6 μm.

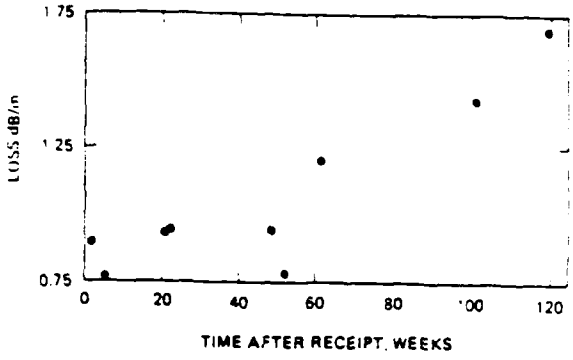

FIG. 3. The average optical attenuation at 10.6 μm vs time interval between receipt of KRS-5 bulk material and its extrusion into fiber.

B. Secondary ion mass spectrometry

The secondary ion mass spectrometry (SIMS) measurements were made with a CAMECA 3f instrument at Charles Evans and Associates. We determined the components of samples of bulk TlBr-TlI by performing full mass scans to 300 amu using both oxygen primary ions and positive ion mass spectrometry, and cesium primary ions and negative ion mass spectrometry. These measurements show both the high intensity matrix components (Tl, Br, and I) and impurities, with detection sensitivities that vary in the range between about 100 ppb and 10 ppm, depending on the ionization potential (for positive mass spectrometry) or the electron affinity (for negative ion mass spectrometry) of the impurity atoms.

The results of these measurements show that the bulk TlBr-TlI material is quite pure. The matrix lines observed in these measurements were Br^+, Tl^{++}, I^+, Tl^+, I_2^+, and $TlBr^+$ in positive ion spectrometry, and Br^-, I^-, Br_2^-, Tl^-, BrI^-, and I_2^- in negative ion spectrometry. The impurities observed were H^+, C^+, N^+, O^+, Na^+, Mg^+, Al^+, Ca^+, Cu^+, and TlO^+ in positive ion spectrometry, and H^-, O^-, and Cl^- in negative ion spectrometry. The impurity elements with the highest concentration levels were H, Al, and Cl.

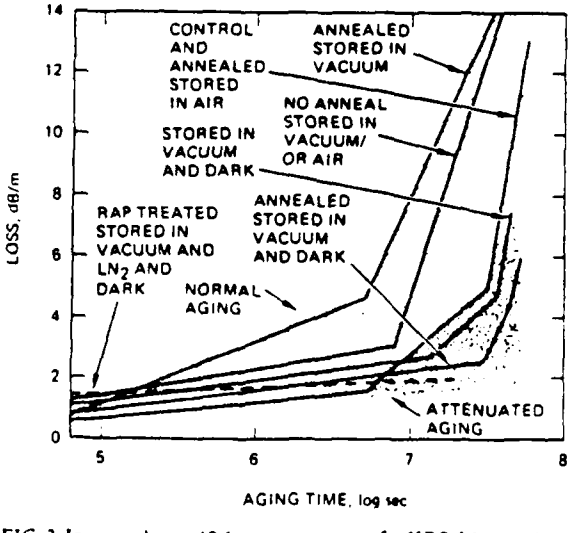

FIG. 2. Insertion loss at 10.6 μm vs aging time for KRS-5 fibers subjected to different aging conditions. The shaded area depicts the overall general trend these fibers are following. The heavily shaded region represents those aging environments which effectively reduce optical aging.

Hydrogen depth profiles from the surface of both bulk material and extruded fibers were measured using a cesium primary ion beam and negative ion mass spectrometry. High sputtering rates were possible for this material and had to be controlled to 1 μm/s or less in order to prevent decomposition. Hydrogen profiles were sometimes measured to depths of 200 μm before a constant density was reached. The depth scales were determined from surface profilometry (Dektak) measurements of the crater depths; the error in the depth scales is about $\pm$ 12% in this material. The hydrogen atom densities were estimated by using the measured intensities of the matrix components (Tl, Br, and I) and the impurities, and their known ionization potentials (positive spectrometry) or electron affinities (negative spectrometry) and the measured curves of SIMS sensitivity factor versus ionization potential or electron affinity for several other materials, determined using ion implantation calibration standards. This approach saved the difficult task of implanting all the ions of interest into polished surfaces of TlBr-TlI and SIMS profiling them.

Hydrogen depth profiles were measured for TlBr-TlI samples grown or prepared in a variety of ways, some to determine the effects of growth technique and some to determine the effects of surface preparation on aging (H in- or out-diffusion with time). Hydrogen depth profiles were also measured to compare the amount of H in material that exhibited high or low loss in separate optical fiber transmission experiments.

Shown in Figs. 4–6 are plots of the relative hydrogen density versus depth from the surface for a variety of KRS-5 samples. In these figures the "relative hydrogen density" is the ratio of H^- ion intensity to the constant $^{79}Br^-$ ion intensity in the same sample, $\times 10^{-7}$; therefore, the relative H densities may all be intercompared. The SIMS results for the three KRS-5 fibers with their relative optical loss characterization and bulk material are summarized in Figs. 4 and 5, respectively.

In Fig. 6 the SIMS relative H density profiles for two different reactive atmosphere processed (RAP; see Appendix) bulk KRS-5 samples are displayed. The unaged sample

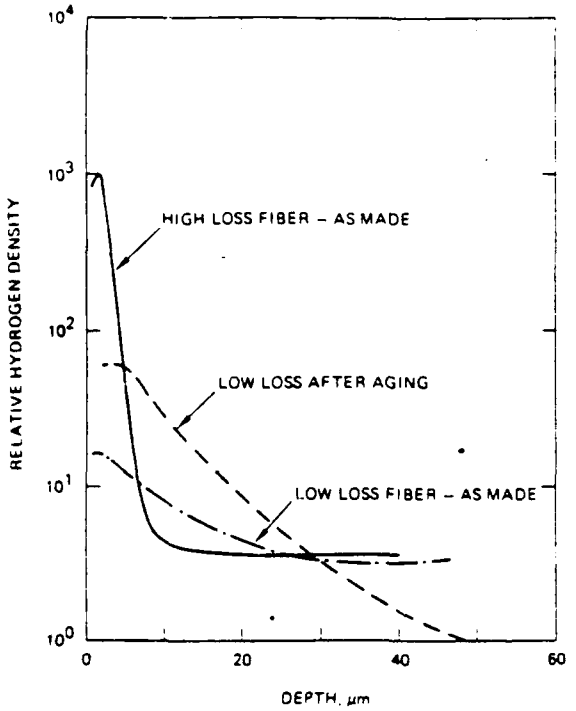

FIG. 4. SIMS depth profiles of KRS-5 fiber samples.

was kept sealed in its ampoule until 10 min before SIMS analysis to prevent interaction with the ambient atmosphere, while the aged sample was exposed to the ambient atmosphere for 24 h before analysis. The unaged sample showed no hydrogen or a significantly reduced relative H density at the surface, while the aged sample showed more than 10× more hydrogen. This is to be contrasted with the non-RAP treated and aged samples which showed an additional order of magnitude increase in hydrogen and where it is estimated that the bulk H density is between about 8% and 16%.

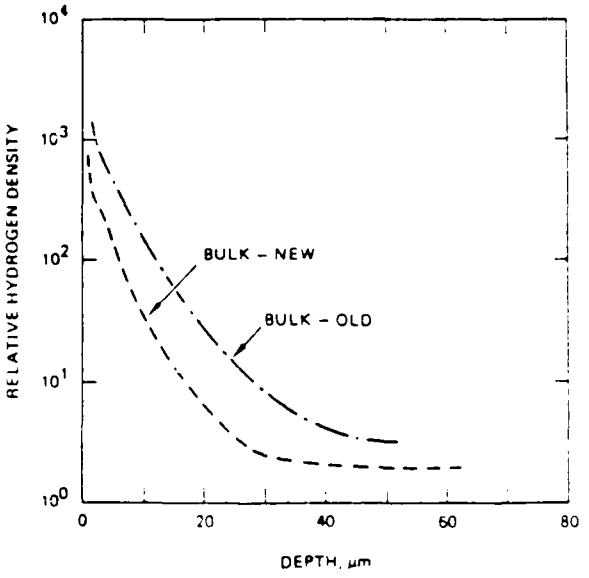

FIG. 5. SIMS depth profiles of KRS-5 bulk material.

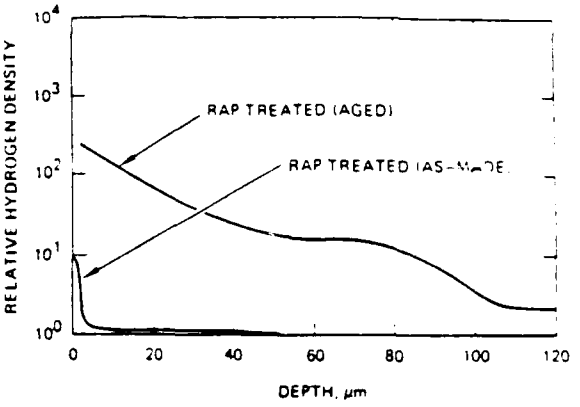

FIG. 6. SIMS depth profiles of RAP treated KRS-5 bulk material.

C. Neutron and x-ray powder diffraction

Neutron powder diffraction experiments were performed on the high intensity powder diffractometer (HIPD) at the Los Alamos Neutron Scattering Center. The samples were in the form of extruded fibers which were cut into pieces about 7 mm long and sealed into a vanadium tube sample holder in a dry helium atmosphere. Neutron diffraction data were then obtained at room temperature and at 12 K. For aged fiber samples, it was estimated from the very high incoherent neutron scattering background shown in Fig. 7 that the polycrystalline material contained between 5- and 10-at. % hydrogen. A measurement of the incoherent neutron scattering from a piece of the aged single-crystal starting material revealed a comparable amount of hydrogen.

Rietveld refinement of the neutron diffraction data was performed using the generalized crystal structure and analysis (GSAS) programs developed at Los Alamos.[5] The refinement of the low-temperature data included 324 reflections (16 033 observations) and 29 parameters were used in the fit. The agreement between the observed data and the Rietveld refinement is very good and has an R factor of 3% at 12 K and 5% at room temperature. The CsCl (space group

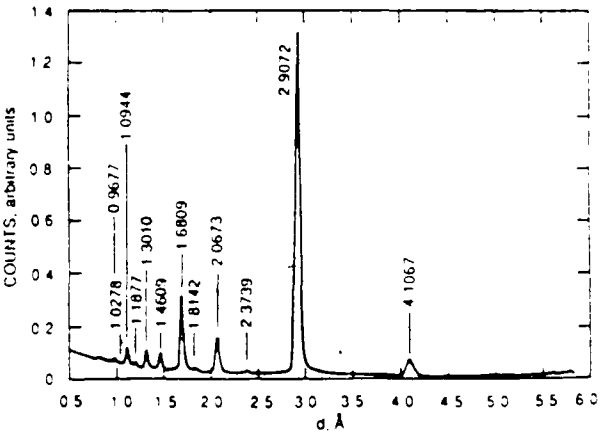

FIG. 7. Neutron powder diffraction pattern from KRS-5 fibers at 300 K.

$Pm3m$) structure was confirmed for this material with no evidence for interstitial or substitutional hydrogen or OH^- anions. Several very weak diffraction peaks that could not be indexed suggest the presence of a very small amount of a second phase (less than 1%). We propose that the hydrogen must therefore be primarily on the surface of the sample or concentrated along grain boundaries in a potentially amorphous gel phase. There was no observable particle size broadening, which indicates that there can be no substantial number of grains in the fibers which are smaller than about 100 nm. Similarly, no extinction was observed, suggesting an upper limit of about 3 μm for the grain size.

A substantial amount of peak broadening is observed in all diffraction patterns which can be attributed to strain. The fractional strain was computed from the broadening of the Bragg peaks and found to be in the range 0.25%–0.32% in both the fibers and bulk starting materials. The values of fractional strain are quite high and may be related to the different sizes of the halogen anions. It should also be pointed out that the neutron refinements show no evidence for anion ordering.

Apparently, the extruded fibers do not exhibit any additional strain in spite of the extrusion process. This may not be too surprising since both the extrusion temperature and the storage (room ambient) temperature are reasonably close to the melting temperature ($T/T_m \sim \frac{1}{2}$) suggesting that annealing may be a continuous process after fabrication.

Figure 8 shows a comparison between the x-ray powder diffraction data (Cu$K\alpha$ radiation) of the freshly extruded fibers [Fig. 8(a)] and the aged fibers [Fig. 8(b)] used in the neutron diffraction experiments. The extra diffraction peaks appearing in Fig. 8(b) are indicative of a possible second phase localized near the surface of the aged fibers.

D. Electron paramagnetic resonance spectroscopy

Electron paramagnetic resonance (EPR) spectra at X band were obtained using a Varian Century Series E-9 spectrometer using 25-kHz magnetic field modulation. Microwave frequencies were measured using a Hewlett-Packard 5342A automatic microwave frequency counter and the magnetic field measurements were made using a Varian nuclear magnetic resonance Gaussmeter. EPR spectra at 77 K were obtained using a quartz insertion Dewar. The estimated error in the measured g values is $\pm$ 0.0004. Samples were irradiated to levels as high as $\sim$6 Mrad at 77 K by ^{60}Co γ radiation at a dose rate of $\sim$ 1 Mrad h^{-1}.

In order to probe the chemical nature of the hydrogen incorporated in KRS-5, bulk and fiber samples of the material were γ irradiated at 77 K and subsequently studied using EPR spectroscopy. Samples for γ irradiation at 77 K were prepared in two ways. The first and simplest involves immersing the sample of KRS-5 directly in the liquid N_2, which is contained in the irradiation Dewar. The second method involves placing the sample in a quartz tube, which is then evacuated for approximately 24 h before sealing under vacuum. The sample in the quartz tube is then γ irradiated at 77 K. In order to anneal out the radiation-induced centers in the quartz tube, one end of the tube was heated with an oxygas torch while keeping the end with the KRS-5 immersed in liquid N_2. The KRS-5 sample was then transferred to the annealed end without warming. Shown in Fig. 9(a) is an EPR spectrum obtained at 77 K of *aged* bulk KRS-5 γ irradiated to a dose of $\sim$3 Mrad. This spectrum clearly resembles that of the $\cdot$OH radical in γ-irradiated polycrystalline ice[6,7] shown in Fig. 9(b). Also discernible in Fig. 9(a) is a signal at $g = 1.9623$, of unknown origin. Upon warming to room temperature, the EPR signals disappeared.

Similar experiments were also carried out on aged fibers

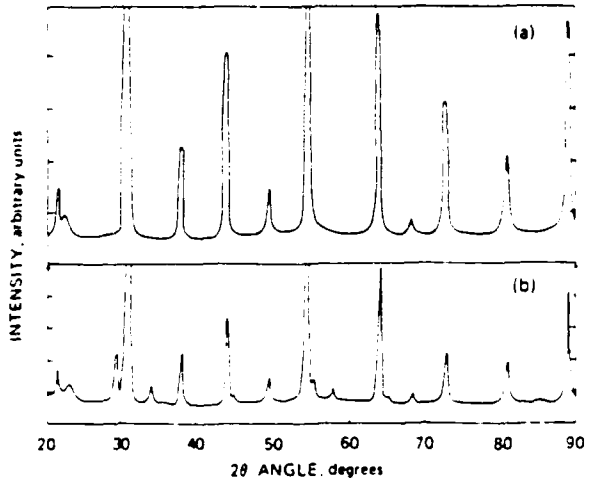

FIG. 8. Room-temperature x-ray powder diffraction pattern from KRS-5 fibers. (a) pristine fibers, (b) aged fibers.

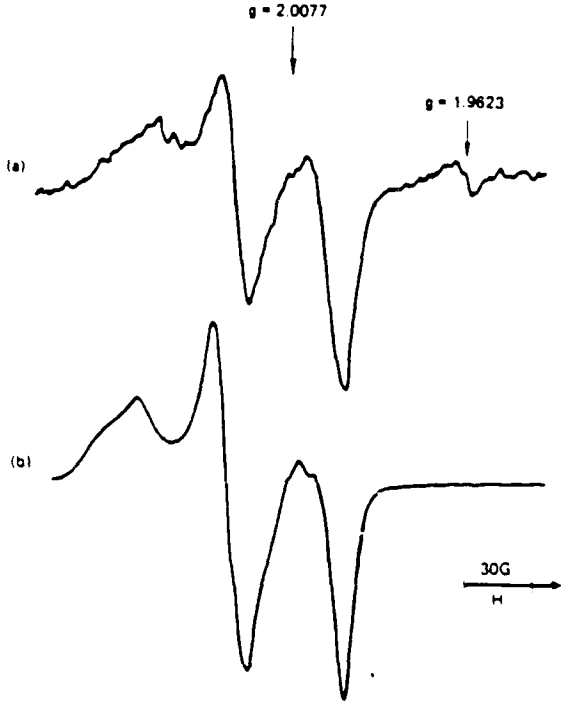

FIG. 9. X-band EPR spectra obtained at 77 K. (a) Aged bulk KRS-5 γ irradiated at 77 K and (b) ice γ irradiated at 77 K.

and gave identical results. In contrast, EPR measurements on γ-irradiated pristine bulk samples gave, in general, variable results. However, from most of the pristine samples examined, the EPR spectrum of the ·OH radical was not observed.

III. DISCUSSION

Figure 2 is a summary of the trends of the behavior of over 300 KRS-5 fibers, in over a dozen different combinations of environments, and monitored over a time period of approximately two years. Because of the schematic nature of this figure, it is necessary to only note the behavior of the optical attenuation of each environment as it compares with the *control* sample. It becomes apparent that it is possible to both accelerate and decelerate the aging compared with storage in normal ambient environments. The variability in the aging suggests that the behavior is not intrinsic, but rather is a result of either the thermodynamic state of the system (chemistry, stress corrosion, etc.) or the extrusion process itself, which induces residual strains, surface defects, grain boundaries, etc.

The data illustrated in Fig. 3 are an aid to delineating the two processes. By taking a large initial sample of material, storing it, and extruding fiber at sequentially longer times, one notes that the mean attenuation of the freshly extruded fiber also increases as a function of time. Interestingly, both fiber-aging and bulk-aging exhibit the same type of behavior, i.e., the change in attenuation is relatively small during an *incubation* period followed by a very rapid deterioration. Because of this behavior in the bulk, it is relatively safe to assume that the aging is not strictly coupled to the extrusion process.

It follows from the discussion above that one of the fundamental questions that needs to be addressed concerning the aging of KRS-5 fibers is whether it is a surface driven phenomenon, e.g., a change in the refractive index at the fiber surface, or a bulk phenomenon, e.g., a change in crystal structure. Previous investigators have noted that aging is strongly correlated with increased light scattering from the fiber surface.[5] These observations are consistent with the data presented here.

In addition to optical transmission measurements, IR spectroscopic data of both bulk and fiber samples were taken. For the bulk samples, disks were cut from the starting billet of KRS-5 and polished in a water-free environment. Data were obtained over the range of 2–15 μm using a Beckman IR spectrometer. Measurements at room temperature showed virtually no absorptions in this material. However, performing the same measurements at 77 K resulted in the appearance of absorption bands at 3.3 and 6.6 μm. Details on these measurements as well as Raman and inelastic neutron scattering results will be reported in a future publication.[9]

Short lengths of KRS-5 fiber (10, 12, and 32 cm) were also examined over the same wavelength range using a Nicolet 8000 FFT IR spectrometer at intervals of 2, 6, and 12 months. Although the signal-to-noise ratio for these data was especially poor, two trends were observed. First, as indicated by the optical attenuation measurements, the loss in the 9–11-μm range always increased in the aged samples with the peak occurring at about 9.6 μm. Second, this loss increase was always accompanied by increases in other parts of the IR spectrum. Most notably, for some samples the loss increased at about 3, 6.5, 9.6, and 13 μm, while for others the loss increased in the 2–10-μm spectral range.

As shown in Fig. 4, the SIMS profile data of the as-made high loss fiber have an order of magnitude larger relative H density near the fiber surface as compared with the as-made low loss fiber. Furthermore, it is clear from the data in Fig. 4 that for both the as-made low and high loss fibers, the relative H density first decreases rapidly with distance from the surface and then remains at a constant value throughout the bulk of the fiber. In contrast, the low loss aged fiber has a larger H density near the surface relative to the as-made low loss material, and in addition, the relative H density is significantly reduced within the bulk; after $\sim 40\,\mu$m from the surface the H density is reduced below the limits of SIMS detection. The SIMS profile data illustrated in Fig. 5 for old and new bulk KRS-5 material also show that the H density near the surface is more than two orders of magnitude larger than in the bulk. In addition, it is also clear from this figure that the H density remains constant after a depth of ~ 30–$40\,\mu$m.

For the RAP treated bulk KRS-5 material, the SIMS profile data for the as-made sample (see Fig. 6) indicate that most of the H density is concentrated within $\sim 3\,\mu$m of the surface. In contrast, the SIMS profile for the aged RAP treated sample clearly demonstrates that not only is the H level higher near the surface, but in addition, more uniformly distributed throughout the bulk of the material.

Further supporting evidence for the presence of hydrogen or a hydrogen containing impurity comes from the incoherent component of the neutron scattering. As is well established, it is very difficult to determine the presence of hydrogen using x rays because of the very low scattering power of hydrogen, but for neutrons the coherent hydrogen scattering is quite comparable with that of other atoms.[10] Because the incoherent component of the neutron scattering cross section shows no interference effects, it constitutes a diffuse background that can be reliably measured and subtracted from the total scattering. In Fig. 7, an incoherent background component is clearly discernible at small d spacing values and results from the large incoherent nuclear spin-disorder scattering for hydrogen.[10]

As discussed above, the SIMS profile data indicate that there is a high concentration of an unspecified H-containing impurity near the surface of both the bulk and fiber KRS-5. Since x rays are strongly absorbed by heavy atomic weight solids, the diffracted beams therefore chiefly originate in a thin surface layer determined by the x-ray penetration depth (~ 50–$100\,\mu$m). Hence, information concerning possible structural modifications caused by the accumulation of a H-related impurity in the vicinity of the surface of KRS-5 may be obtained from x-ray powder diffraction measurements. It is clear from the x-ray diffraction patterns shown in Fig. 8 that additional diffraction peaks occur in the aged samples. This suggests that possibly another phase is forming on the surface which gives rise to the additional diffraction peaks observed in the measurements. However, the neutron dif-

fraction data show an almost negligible amount ($\sim 1\%$) of this second phase in the aged samples. This is consistent because the amount of the second phase as measured by neutron scattering is approximately equal to the ratio of the volume probed by x rays (surface limited) to the volume probed by neutrons (bulk). These results support the view that microstructural changes occur near the surface of aged KRS-5 as a result of the accumulation of H-related impurities.

The results of the EPR measurements provide unique information concerning the chemical identity of the H-bearing impurity. Following γ irradiation at 77 K, the EPR spectrum characteristic of the ·OH radical[6,7] is observed (Fig. 9). One possible mechanism for the formation of the hydroxyl radical is the γ radiolysis of H_2O, which yields in addition paramagnetic H atoms (H·). The H atom EPR spectrum consists of a doublet centered about $g \simeq 2$ and split by approximately 500 G; it has been observed in many matrices. We did not observe the H atom spectrum in KRS-5 upon γ irradiation at 77 K, most likely due to the fact that the rapidly diffusing and highly reactive H atoms have encountered another H atom to form H_2 or reacted with the matrix or some other impurity to form an EPR silent species.

Another unique feature of the EPR data is that the ·OH radical spectrum is a typical powder/polycrystalline averaged spectrum, i.e., the spectrum of an array of randomly oriented, nonrotating paramagnetic molecules in a rigid matrix. Because the neutron scattering data indicate that the H-related impurity does not enter, either interstitially or substitutionally, the TlBr-TlI lattice, the EPR results suggest that the H_2O is trapped in a noncrystalline environment, such as would be found at grain boundaries or in an amorphous phase, localized near the surface.

At the present time we can only speculate on the important question concerning the mechanism of water incorporation in bulk and fiber KRS-5. One possibility is that water is formed in the solid phase via an *in situ* chemical reaction involving O_2, which has diffused in from the outside, and H atoms, which have been generated by the photolysis of impurities such as HI and/or HBr. Another plausible mechanism, which has the virtue of being the simplest as well as the most direct, is that H_2O simply diffuses in from the outside. It is clear from Fig. 2 that samples stored in the dark and under vacuum aged the least. The attenuated aging, when stored in the dark, suggests that a photochemical process such as discussed above may be operative. Further work needs to be done in order to establish the mechanism of water contamination as well as the driving force responsible for the accumulation of water in the surface layers of crystalline/polycrystalline TlBr-TlI.

IV. SUMMARY AND CONCLUSIONS

We have used a variety of techniques including SIMS, powder neutron and x-ray diffraction, IR, and EPR spectroscopy to elucidate the chemical and structural basis of optical aging in bulk and fiber KRS-5. It is found that in aged KRS-5 samples, there is an accumulation of a H-bearing impurity in the surface layers of the crystalline/polycrystalline material. From the EPR of γ-irradiated KRS-5 it that the H-bearing impurity is water. (This has been confirmed by recent neutron inelastic scattering measurements.[9])

ACKNOWLEDGMENTS

This work was supported in part by the Army Research Office under Contract No. DAAG29-84-C-0005. The authors gratefully acknowledge S. E. Hodges (Santa Barbara Research Center) for performing the IR spectroscopic measurements.

APPENDIX

For the in-house growth of KRS-5 crystals, commercial unary thallous halide powders were used. In general, these starting grade materials have an unspecified amount of anion impurities. In the growth of mixed crystals with a common cation, high anion impurity levels could lead to the formation of ternary or even higher multicomponent systems and, therefore, inhibit the growth of crack- and void-free, homogeneous single crystals from the melt. Thus, the thallous bromide and thallous iodide starting materials were purified prior to mixing in the appropriate proportions[11] for growth of KRS-5 crystals.

The purification procedure employed was concurrent reactive atmosphere processing (RAP)[12] and zone refining, wherein the flowing reactive atmosphere used was the corresponding hydrogen halide, i.e., HBr for TlBr and HI for TlI, diluted with helium. Of the possible anion group impurities in the powders, it was expected that OH^-, being a pseudohalide, would be the most difficult to segregate in the repetitive crystallization that is the basis of the zone refining process. In the RAP treatment, the hydrogen halide acts as a chemical scavenger of the OH^- anion resident in the raw materials, in accordance with the reactions

$$HX(g) \rightarrow HX(l) ,$$

and

$$HX(l) + OH^-(l) \rightarrow X^-(l) + H_2O(g) ,$$

where g denotes the vapor state and l denotes the liquid or molten state. However, it was not certain that the excess $HX(l)$ would be quantitatively segregated at the crystallization front, for HX could have some solubility in the solid and thus could affect the hygroscopicity of the latter. Therefore, each batch of material was subjected to ten zone passes, and the middle third fraction of each zone refined ingot was used in the compounding.

Crystal growth of the binary halide was effected in a Bridgman mode using vacuum-sealed silica glass crucibles that had inside diameters just less than that of the extrusion die. The growth rate was held to 0.4–0.6 cm h^{-1} to insure monocrystallinity, but even at these slow rates, the terminal 10% of the typical ingot was polycrystalline. This 10%, as well as the nucleating end, was cut off before extrusion.

[1] D. A. Pinnow, A. L. Gentile, A. G. Standlee, A. J. Timper, and L. M. Hobrock, Appl. Phys. Lett. 33, 28 (1978).
[2] M. E. Lines, J. Appl. Phys. 55, 4052, 4058 (1984); Ann. Rev. Mater. Sci. 16, 113 (1986).
[3] B. Bendow, Solid State Phys. 33, 249 (1978).

[7] J. A. Harrington and A. G. Standlee, Appl. Opt. 22, 3073 (1983).
[8] A. C. Larson and R. B. VonDreele, *Generalized Crystal Structure Analysis System* (LAUR 86-748, Los Alamos, NM, 1986).
[9] S. Siegel, J. M. Flournoy, and L. H. Baum, J. Chem. Phys. 34, 1782 (1961).
[10] H. Riederer, J. Huttermann, P. Boon, and M. C. R. Symons, J. Magn. Reson. 54, 54 (1983).
[11] J. A. Harrington (unpublished results).
[12] A. R. Williams and J. A. Wysocki (unpublished).
[13] C. G. Shull and E. O. Wollan, Solid State Phys. 2, 137 (1956).
[14] A. Smakula, J. Kalnajs, and V. Sils, J. Opt. Soc. Am. 43, 698 (1953).
[15] R. C. Pastor and A. C. Pastor, Mater. Res. Bull. 10, 117 (1975).

97/98

APPENDIX H

A SIMULTANEOUS ELECTRON PARAMAGNETIC RESONANCE AND OPTICAL ABSORPTION STUDY OF ULTRAVIOLET-INDUCED DEFECT CENTERS IN Ge-DOPED SILICA FIBERS

TO BE PUBLISHED IN *JOURNAL OF APPLIED PHYSICS, 1988*

A Simultaneous Electron Paramagnetic Resonance and Optical Absorption Study of Ultraviolet-Induced Defect Centers in Ge-Doped Silica Fibers

Robert N. Schwartz and G. Richard Blair
Hughes Research Laboratories
Malibu, CA 90265

ABSTRACT

Simultaneous electron paramagnetic resonance (EPR) and optical absorption studies were carried out at room temperature in a Ge-doped silica fiber-optic waveguide following in situ ultraviolet (UV)-irradiation with 254 nm (4.88 eV) photons. We have observed that the UV-induced EPR is directly correlated with the UV-induced optical loss in the energy range 1.77 to 3.0 eV. No UV-induced loss was observed in the near infrared spectral region (0.7 to 1.38 eV). The problem of correlating the UV-induced loss with the optical bands of the various possible defect centers in Ge-doped silica is discussed.

I. INTRODUCTION

The action of ionizing radiation on doped-silica glasses used for fabricating fiber-optic waveguides has been the subject of numerous investigations.[1,2] Most of these studies have been concerned with the damage produced by high energy radiation (hard radiation) such as x-rays and γ-rays or by energetic particles such as neutrons, protons and electrons. In general the interaction of hard radiation and matter is extremely complex, ranging from the displacement of atoms far from their equilibrium lattice positions as a result of neutron-nucleus collisions, to the generation of secondary fast electrons by Compton scattering of γ quanta. The end result is the production of both transient as well as long-lived defect centers which, as a result of optical absorption and/or scattering, deteriorate the transmission characteristics of fiber-optic waveguides.

In addition to the response of matter to hard radiation, there is an increasing interest in understanding the types of defects created in fiber-optic glasses by low energy radiation, such as ultraviolet (UV) and even longer wavelength photons.[3-8] This interest has arisen because of the potential of radiation-induced damage to fiber-optic waveguide used to transmit high power laser radiation.[7] Also, there is some recent experimental evidence that even the low level UV radiation used for crosslinking fiber prepolymer coatings leads to the formation of color centers in Ge-doped silica optical fibers, which results in losses approaching

several hundred decibel per kilometer over the spectral range of 500 to 1100 nm (4.33 to 1.97 eV).[5,8]

One of the advantages of using UV light to create color centers in Ge-doped silica is that it is more selective in the reactive channels leading to defect formation. As a result only a subset of possible active defect centers are produced; thus, leading to spectral simplification.[3] This spectral simplification is a tremendous aid not only for identifying the molecular structure of the optically/electron paramagnetic resonance (EPR) active defect centers, but also for understanding the microscopic mechanism(s) of color center formation and hence, developing means for minimizing their formation.

In the present study we focus on the radiation-induced EPR and optical absorption in Ge-doped multimode fiber-optic waveguides exposed to UV photons. Because of the long optical pathlength, fiber optic waveguide offers a unique medium for studying color centers in low concentration or with low intrinsic oscillator strength. Recent work in our laboratory[3,4] as well as in others[5,8] has shown that in both bulk and fiber Ge-doped silica, UV-irradiation (254 nm) produces predominantly one type of paramagnetic center, namely Ge(3), which has a structure similar to the E' center (Si-E') in pure silica, and is called the Ge-E' center. Here we describe and utilize a unique technique to measure simultaneously the optical absorption and the EPR in Ge-doped multimode fiber following <u>in situ</u> irradiation with 254 nm

(4.88 eV) photons. What we mean by simultaneous is that the experimental arrangement allows the measurement of both the EPR and optical absorption on the same sample, and without disturbing the experimental configuration. The main objective of this study is to provide direct as well as unambiguous experimental information concerning the correlation of the UV-induced optical absorption with the UV-induced EPR.

II. EXPERIMENTAL

Germanium-doped multimode step-index optical fibers were drawn from optical preforms made by the modified chemical vapor deposition (MCVD) technique. The preforms were made by first depositing silica layers doped with germaninum, using $GeCl_4$ as the source of germanium, inside a Heraeus Amersil TO-8 quartz tube. Doped core preforms were formed by collapse of the substrate tubing, followed by sleaving with an additional quartz tube (TO-8). The fibers were drawn from the preforms under a nitrogen atmosphere in a graphite resistance furnace and were then coated with aluminum metal.[9] The drawing temperature was ~2100°C and the drawing speed was approximately ~90 m min^{-1}. The uncoated fiber diameter was ~123 μm and the doping level in the core was ~10.6 mole % GeO_2 (NA $\simeq$ 0.21).

EPR experiments were carried out at room temperature using an X-band (~9 GHz) homodyne Varian E-line spectrometer employing

25 kHz magnetic-field modulation. A Hewlett-Packard 5342A automatic frequency counter was used to measure the microwave frequency, and the applied magnetic fields were determined by means of a Micro-Now proton nuclear magnetic resonance gaussmeter. The estimated error in the measured g values is $\pm$0.0004.

To first conduct UV irradiations *in situ* and then to measure simultaneously the UV-induced EPR and optical absorption, we mounted a continuous coil of metal-coated multimode Ge-doped silica fiber consisting of 40 turns in a 1.1-cm-O.D. by 15.5-cm-long Heraeus Amersil TO-8 fused quartz tube (see Fig. 1). This quartz tube had a 0.4-cm-wide slot cut along its length to facilitate mounting the fiber coil in the tube. Inside this quartz tube, which served to rigidly position the fiber coil along the axis of the microwave cavity, the fibers formed a tight bundle. In addition to the slot, a section of the 1.1-cm-O.D. tubing wall was removed so that the metal coating on the fiber could be conveniently removed by chemical means. This opening also served as a window for direct irradiation by UV photons. The whole assembly (fiber coil/1.1-cm-O.D. quartz tube) was inserted in a microwave cavity (standard Varian TE_{102} rectangular cavity) which had a slotted window in one wall and therefore permitted *in situ* UV-irradiation of the fiber coil (see Fig. 2). The two ends of the fiber coil served as the input and output for spectral measurements of the transmission over the range 0.7 to 3.0 eV.

Optical measurements were made using a spectrophotometer with a 100-W quartz-iodine lamp source and an Oriel 0.25-m scanning monochromator. Microscope objectives with numerical apertures lower than that of the fibers were used to couple light into and out of the fiber coil. The detector was either an RCA 4832 photomultiplier or a Germaniun p-n junction photodiode. Standard chopping and lock-in phase-sensitive detection techniques were used for signal processing. The UV-irradiation source was a Pen-Ray (11SC-1) lamp with a quartz envelope. The light intensity at the sample was estimated to be ~2.6 mJ $s^{-1}cm^{-2}$, with 92% of the spectral output at λ = 254 nm (4.88 eV). Higher-order mode propagation was effectively suppressed by the bends associated with the fiber coil geometry. In this way the amount of higher mode optical power propagating in the cladding was significantly suppressed, and thereby minimized absorption in the cladding region of the fiber.

Even though the instrumentation for measuring the EPR and optical absorption are independent and therefore, in principle can be recorded simultaneously, we chose to collect the EPR/optical data sequentially Prior to any UV-irradiation, EPR and optical absorption spectra of the fiber coil were taken. The fiber in the microwave cavity was then UV-irradiated for various lengths of time, with EPR and optical absorption measurements sequentially made following each irradiation period. Finally, without disturbing the input coupling to the spectrophotometer, we severed the fiber, leaving approximately 1 m, and this segment

of unirradiated fiber was recoupled to the spectrophotometer/detector optics for the normalization scan.

III. RESULTS AND DISCUSSION

A. EPR spectra

Shown in Fig. 3(a) is the room-temperature EPR spectrum of as-drawn (unirradiated) Ge-doped fiber. The observed lineshape is characteristic of a center having a nearly axially symmetric spin Hamiltonian. This resonance has been well-characterized by several groups and is attributed to the Ge-E' center, which consists of an electron trapped at an oxygen vacancy with the unpaired spin occupying one of the sp^3 hybrid germanium orbitals.[10-12] Figure 3b shows the EPR spectrum following UV irradiation to a total dose of ~5.5 J cm^{-2} (35 min irradiation time). It is clear in Fig. 3(b) that not only has the overall EPR absorption increased, but also the resonance signal in the g_1 = 2.0009 region has increased relative to the absorption, with zero-crossover at $g_2 \simeq g_3 = 1.9950$.

Computer simulation of EPR lineshapes was performed using g value distributions similar to those reported by Tsai and co-workers.[12] By comparing simulated lineshapes with the experimental spectra, we established that the dominant paramagnetic center in the UV-irradiated fiber is the Ge-E'

center. The fact that we did not include in the simulations the spin Hamiltonian parameters for other Ge-related EPR active color centers, such as Ge(1,2) centers, is certainly one source of error leading to the lack of agreement between the computed and experimental spectra. Since the spectral simulations deviate most strongly from the observed lineshape in the region $2.0010 < g \leq 1.9990$, and, furthermore, since there appears to be no appreciable resonance absorption in the vicinity of $g = 1.987$ [the value of g_3 for the Ge(2) center] of the UV-irradiated fiber, we believe that the predominant minor component is the Ge(1) center. The spectrum of the Ge(1) center, having g values of $g_1 = 2.0007$, $g_2 = 1.9994$, and $g_3 = 1.9930$, is expected to overlap and be obscured by that of the Ge-E' center. Based on recent measurements of the ^{73}Ge hyperfine structure in Ge-related defect centers in Ge-doped silica, Kawazoe and co-workers[11] have proposed a model for the Ge(1) consisting of an unpaired electron localized on a four-coordinated germanium atom substitutional for silicon in the silica network.

In order to determine the EPR intensity due to Ge(1) in the overlapped EPR absorption where Ge(3) dominates, we sequentially subjected UV-irradiated fibers to xenon lamp-irradiation, which leads to photobleaching of the Ge(1) centers.[4] By taking the difference between the EPR spectrum after UV-irradiation, and the spectrum recorded after subsequent xenon lamp-irradiation, we obtain the Ge(1) spectrum.[10] From the difference spectrum we estimate that the spectral contribution of Ge(1) ranges from 10 to 25%.

In Fig. 4 the UV-induced EPR intensity, which is proportional to the number of paramagnetic centers, is displayed as a function of the accumulated UV exposure time. Since field modulation/phase-sensitive detection is employed, the intensity was obtained by double integration of the recorded first derivative of the EPR absorption. A clear linear dependence is observed for the UV-induced EPR intensity over the range of exposure times studied, and is in agreement with our earlier work[3] and that reported by Simpson and co-workers.[5]

B. Optical absorption spectra

Optical absorption spectra of Ge-doped silica fiber were recorded over the spectral region from 0.7 to 3.0 eV as a function of UV exposure time. Shown in Fig. 5 are spectra measured over the energy range 1.77 to 3.0 eV, and obtained immediately after recording the EPR spectrum, which was approximately 5 min after *in situ* UV-irradiation. A well-resolved band located in the vicinity of 2.2 to 2.4 eV is clearly discernible in the spectrum of the unirradiated fiber. With increased UV exposure, however, this band becomes less resolved due to the overlap with the radiation-induced UV absorption tail; for the maximum exposure time the optical spectrum of the irradiated fiber is dominated by this featureless UV-absorption band tail.

In the energy region 0.7 to 1.77 eV, the bands identified with the first overtone of the fundamental OH stretch frequency of

Ge-OH and Si-OH located at ~0.88 eV (~1.40 μm), and the first overtone absorption band (Q_2-transition) of molecular H_2 located at ~1.0 eV (~1.24 μm) are the prominent features.[13,14] In contrast to the optical absorption results in the 1.77 to 3.0 eV spectral region, no change in the optical absorption was detectable in this length of fiber over the range 0.7 to 1.38 eV following UV-irradiation.

Figure 6 displays the UV-induced optical absorption measured at 1.82, 2.25, and 2.48 eV as a function of the accumulated UV exposure time. Over the limited range of accumulated dose exposure realized in our experiments, it is clear that the UV-induced optical absorption is linear in the UV-exposure time. Since the optical and EPR measurements were made simultaneously following in situ UV-irradiation, and since for both experiments there is a linear optical and EPR absorption dependence on the accumulated UV exposure time, it follows that a direct as well as unambiguous correlation is established between the Ge(3) and Ge(1) paramagnetic defect centers and the UV-induced optical loss in the energy range 1.77 to 3.0 eV. More convincing evidence for this correlation is provided by the linearity displayed in the plots in Fig. 7 of the UV-induced optical absorption versus the UV-induced EPR absorption.

Friebele and Griscom[15] have recently reported optical absorption data for Ge-doped silica preform (bulk), X-irradiated at 77 K and recorded at 100 K, over the range 1.5 to 6.0 eV.

These authors resolved the spectrum into Gaussian component bands located at 2.4, 4.4, 5.2, and 5.8 eV. From combined EPR and optical thermal isochronal annealing data, they were able to correlate the optical bands at 4.4 and 4.8 eV with the Ge(1) and Ge(2) defect centers, respectively; however, an optical transition correlating with the Ge(3) (Ge-E') center was not found. The results of Friebele and Griscom[15] also indicate that the 2.4 eV band in Ge-doped silica preform is stable only at temperatures below 200 K and correlates with a tentatively assigned paramagnetic oxygen-associated hole center.

C. UV radiation response

In this study we have used sub-band-gap radiation to selectively produce Ge(1,3) defect centers in Ge-doped silica. We observed that the growth of the integrated EPR signal is correlated with the growth in intensity of a UV band tail that is strongly absorbing in the visible but not in the near-infrared region. Two questions are immediately raised concerning these results: (1) What is the mechanism whereby sub-band-gap UV photons are absorbed as the first step and then followed by processes that lead to defect formation; and (2) Is the UV tail associated with the absorption bands of the Ge(1) and Ge(3) defect centers, or is it related to the optical bands of a diamagnetic color center that is produced simultaneously with the paramagnetic Ge(1,3) centers? At this time, at least based on our experimental results, no definitive conclusions can be reached; however, drawing on recent

photoluminescence[16,17] and optical absorption[15,18] studies in Ge-doped silica glasses, we may gain some insight.

Because of the lack of long-range order in structurally disordered vitreous silicon dioxide (a-SiO_2), the sharp features of the density of states commonly associated with crystalline SiO_2 (α-quartz), in both the valence and conduction bands, are smoothed out, and also, because of the disorder, the band gap is reduced by band tailing. In general, however, the reduction in the band gap in a-SiO_2 due to tailing is not significant enough to allow 254 nm (4.88 eV) photons to generate electrons and holes by band-to-band optical transitions. On the other hand, the creation of pseudo-free charge carriers by optical excitation between the valence band and the localized electronic levels of an acceptor defect in the band gap, or between the levels of a donor defect and the conduction band, can occur by sub-band-gap radiation. A variety of intrinsic defects of the vacancy bridge[19] and valence alternation[6] type has been identified[19] and modeled[20] in the host a-SiO_2. These defects, along with their Ge-related counterparts,[21] are possible candidates for interacting with sub-band-gap radiation for electron-hole production.

Migration of the electrons and holes following electronic excitation must occur in order to form an electronic defect. It is well-established that in Ge-doped silica the Ge-E' center is formed by trapping a hole at a precursor oxygen-vacancy site.[10,12]

Since electrons and holes are created in pairs and the glass as a whole is electrically neutral, it is clear that for every hole center formed there must also be a corresponding electron trapping center formed. Possible candidates for the electron trapping center in Ge-doped silica are the paramagnetic germanium electron trapping center (GEC)[11] [i.e., the Ge(1) center], discussed above, and the diamagnetic luminescence centers described by Kohketsu and co-workers.[17] As described above, the composite EPR spectrum in UV-irradiated Ge-doped silica is dominated by the Ge(3) resonance [recall that the Ge(1) contribution is ~10 to 25%]; therefore, it is reasonable to assume that the end product of electron trapping must involve, in addition to Ge(1) centers, other electron trapping diamagnetic (EPR silent) defect centers. It should be also noted that since the Ge(1) defect correlates with an optical band centered at 4.4 eV,[15] it is reasonable to attribute part of the UV-induced optical absorption to the UV tail associated with the Ge(1) absorption band.

The recent work of Kohketsu and co-workers[17] provides further clues regarding the nature of other candidate electron trapping centers in both Ge-doped silica and a-SiO_2. Based on combined photoluminescence and absorption measurements, Kohketsu et al. suggest that reduced species of silicon and germanium, which are electrically neutral as well as diamagnetic, may be the active luminescence centers. The postulated structural configuration of these diamagnetic color centers consists of a lone pair (spin-paired) of electrons localized on a silicon or germanium atom

bonded to two or three oxygen atoms. For Ge-doped glassy SiO_2, Khoketsu et al.[17] report a strong absorption band peaked at 5.17 eV, and a much weaker band with maximum at 3.77 eV. The low energy edge of the strong band at 5.17 eV may give rise to significant absorption in the visible region.

Yuen[17] and Skuja and co-workers[16] have also studied the UV optical properties of Ge-doped silica and have reported similar absorption data. Yuen,[18] however, suggests that the optical bands at ~3.8 and ~5.2 eV are due to GeO (Ge^{2+}) molecules embedded in a SiO_2 matrix. Furthermore, Yuen[18] concludes that the weak band at ~3.8 eV is correlated with a singlet→triplet transition; whereas the strong absorption at ~5.2 eV is related to a singlet→singlet transition. Skuja et al.[16] obtain similar results; however, based on their photoluminescence polarization data, they suggest that the reduced species may be represented by a bent quasi-molecule, such as GeO_2^{2-}.

Finally, it should be pointed out that Tsai, Griscom, and Friebele[22] have recently reported on the mechanism of Si-E' generation in high-purity silica by sub-band-gap radiation. These authors conclude that the observed Si-E' centers are not generated by photoionization of preexisting oxygen vacancies but rather are formed via a mechanism which first involves the formation of mobile excitons by two-photon-absorption of the sub-band-gap UV light. These mobile neutral excitons then undergo non-radiative

IV. SUMMARY

We have measured simultaneously the optical absorption and EPR in a Ge-doped silica fiber-optic waveguide following in situ irradiation with 254 nm (4.88 eV) photons. In the irradiated fiber the EPR is dominated by the resonance of the Ge-E' [Ge(3)] center. Over the limited range of dose exposure in our experiments, we observed a direct correlation between the the UV-induced integrated EPR intensity and the UV-induced optical loss in the visible region (1.77 to 3.0 eV). No UV-induced loss was observed in the near-infrared spectral region (0.7 to 1.38 eV). It is not possible from our experiments to establish whether the UV-induced loss in the visible is derived from the UV tails associated with the absorption bands of the Ge-E' center, or from the tails of different defects, such as the Ge(1) center and EPR silent diamagnetic color centers. We conjecture that part of the UV-induced loss may be associated with the absorption bands of a diamagnetic electron trapping color center.

Additional experimental and theoretical work is required in order to develop a microscopic understanding of the UV radiation response in Ge-doped glassy SiO_2. One of the crucial elements for making progress is the identification and characterization of the diamagnetic electron trapping centers.

ACKNOWLEDGMENTS

We thank the Army Research Office under contract DAAG29-84-C-0005 for support of this contract. The authors wish to thank M.R. Vince for preparing the Ge-doped preforms, and J.A. Wysocki and A. Lee for fiber fabrication.

REFERENCES

1. E.J. Friebele and D.L. Griscom, in Treatise on Material Science and Technology, Vol. 17, Glass II, edited by M. Tomozawa and R.H. Doremus (Academic Press, New York, 1979), p. 257.

2. E.M. Dianov, L.S. Kornienko, E.P. Nikitin, A.O. Rybaltovskii, V.B. Sulimov, and P.V. Chernov, Sov. J. Quantum Electron. 13, 274 (1983).

3. W. Chamulitrat, L. Kevan, R.N. Schwartz, G.R. Blair, and G.L. Tangonan, J. Appl. Phys. 59, 2933 (1986).

4 R.N. Schwartz, G.L. Tangonan, G.R. Blair, W. Chamulitrat, and L. Kevan, in Defects in Glasses, edited by F.L. Galeener, D.L. Griscom, and M.J. Weber (Materials Research Society, Pittsburgh, PA, 1986), p. 197.

5. J. Simpson, J. Ritger, and F. DiMarcello, in Defects in Glasses, edited by F.L. Galeener, D.L. Griscom, and M.J. Weber (Materials Research Society, Pittsburgh, PA, 1986), p. 333.

6. J.H. Stathis and M.A. Kastner, in Defects in Glasses, edited by F.L. Galeener, D.L. Griscom, and M.J. Weber (Materials

7. R.S. Taylor, K.E. Leopold, S. Mihailov, and R.K. Brimacombe, Opt. Commun. 63, 26 (1987).

8. L.L. Blyler, Jr., F.V. DiMarcello, J.R. Simpson, E.A. Sigety, A.C. Hart, Jr., and V.A. Foertmeyer, J. Non-Crystalline Solids 38 and 39, 165 (1980).

9. G.R. Blair and G.L. Tangonan, IEEE Trans. Nuc. Sci., NS-29, 1489 (1982).

10. E.J. Friebele, D.L Griscom, and G.H. Sigel, Jr., J. Appl. Phys. 45, 3424 (1974).

11. Y. Watanabe, H. Kawazoe, K. Shibuya, and K. Muta, Jpn. J. Appl. Phys. 25, 425 (1986).

12. T. Tsai, D.L. Griscom, E.J. Friebele, and J.W. Fleming, J. Appl. Phys. 62, 2264 (1987).

13. D.B. Keck, R.D. Maurer, and P.C. Schultz, Appl. Phys. Lett. 22, 307 (1973).

14. J. Stone, A.R. Chraplyvy, J.M. Wiesenfeld, and C.A. Burrus, AT&T Tech. J. 63, 991 (1984).

15. E.J. Friebele and D.L. Griscom, in Defects in Glasses, edited

16. L.N. Skuja, A.N. Trukhin, and A.E. Plaudis, Phys. Stat. Sol. A84, K153 (1984).

17. M. Kohketsu, K. Awazu, H. Kawazoe, and M. Yamane, J. Non-Crystalline Solids 95 & 96, 679 (1987).

18. M.J. Yuen, Appl. Opt. 21, 136 (1982).

19. D.L. Griscom, J. Non-Crystalline Solids 73, 51 (1985).

20. E.P. O'Reilly and J. Robertson, Phys. Rev. B 27, 3780 (1983).

21. B. Dutta, D.L. Kinser, R.H. Magruder, III, and R.A. Weeks, J. Non-Crystalline Solids 95 & 96, 389 (1987)

22. T.E. Tsai, D.L. Griscom, and E.J. Fiebele, Phys. Rev. Lett. 61, 444 (1988).

FIGURE CAPTIONS

Figure 1. *Optical fiber coil mounted in quartz tube.*

Figure 2. Optical fiber coil in EPR microwave cavity.

Figure 3. X-band room temperature spectra of Ge-doped silica fiber. Spectrum (a) is for as-drawn fiber and (b) for fiber exposed to UV-irradiation for 35 min (~5.5 J cm^{-2}). The instrumental parameters are: ν = 9.40180 GHz, magnetic field modulation amplitude = 3.2 G, microwave power $\simeq$ 1 mW.

Figure 4. Integrated UV-induced EPR intensity versus accumulated UV exposure time. The solid line is a least-squares fit to the data points.

Figure 5. Optical absorption spectra of Ge-doped silica fiber exposed to UV radiation: (a) as-drawn, (b) 1 min, (c) 3 min, (d) 6 min, (e) 11 min, (f) 20 min, and (g) 35 min.

Figure 6. Plots of the UV-induced optical absorption versus accumulated UV-exposure time. The UV-induced optical absorption data were obtained at: (a) 1.82 eV, (b)

Figure 7. Plots of the UV-induced optial absorption versus UV-induced EPR absorption. The UV-induced optical absorption data were obtained at : (a) 1.82 eV, (b) 2.25 eV, and (c) 2.48 eV. The solid lines are guides to the eye.

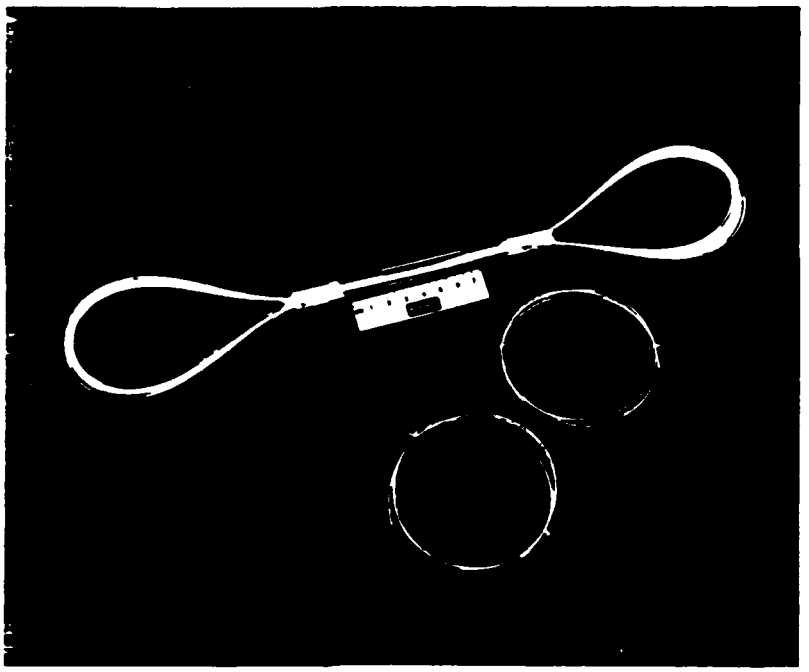

Figure 1

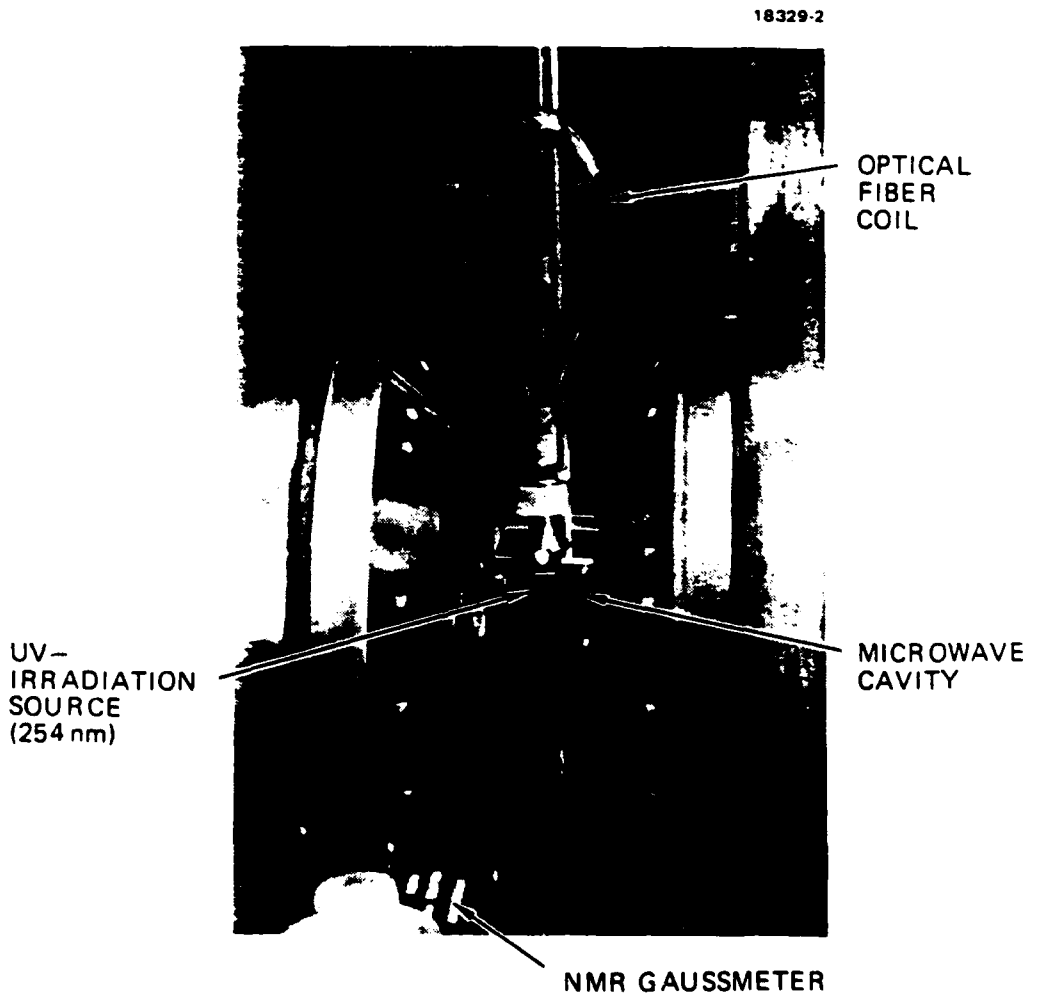
18329-2
OPTICAL FIBER COIL
UV– IRRADIATION SOURCE (254 nm)
MICROWAVE CAVITY
NMR GAUSSMETER

Figure 2

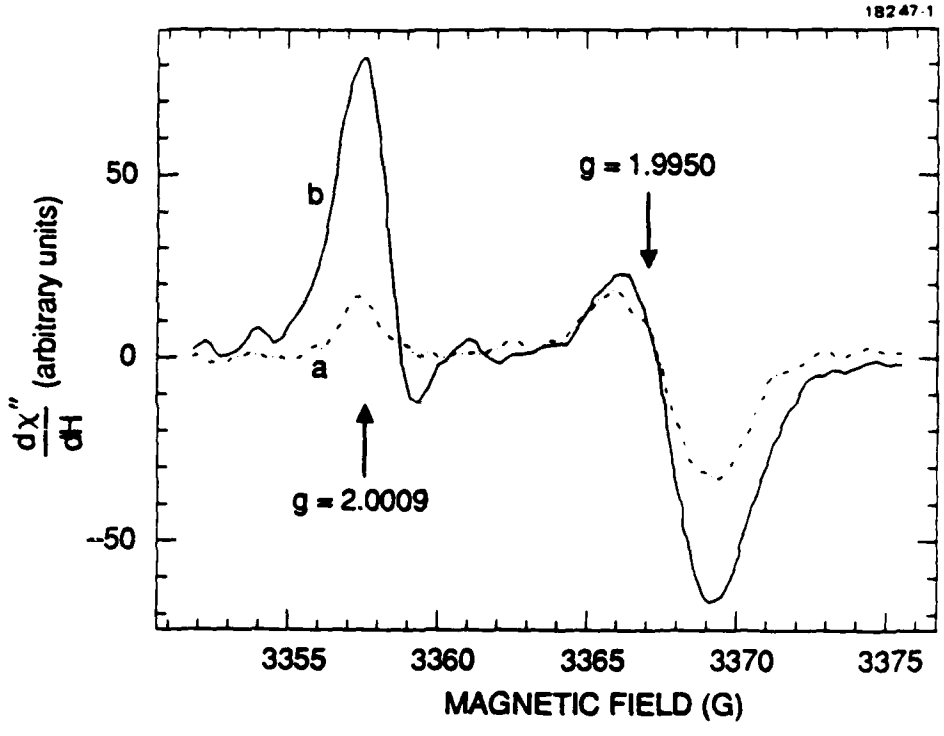
18247-1
50
0
-50
b
a
g = 1.9950
g = 2.0009
$\frac{d\chi''}{dH}$ (arbitrary units)
3355
3360
3365
3370
3375
MAGNETIC FIELD (G)

Figure 3

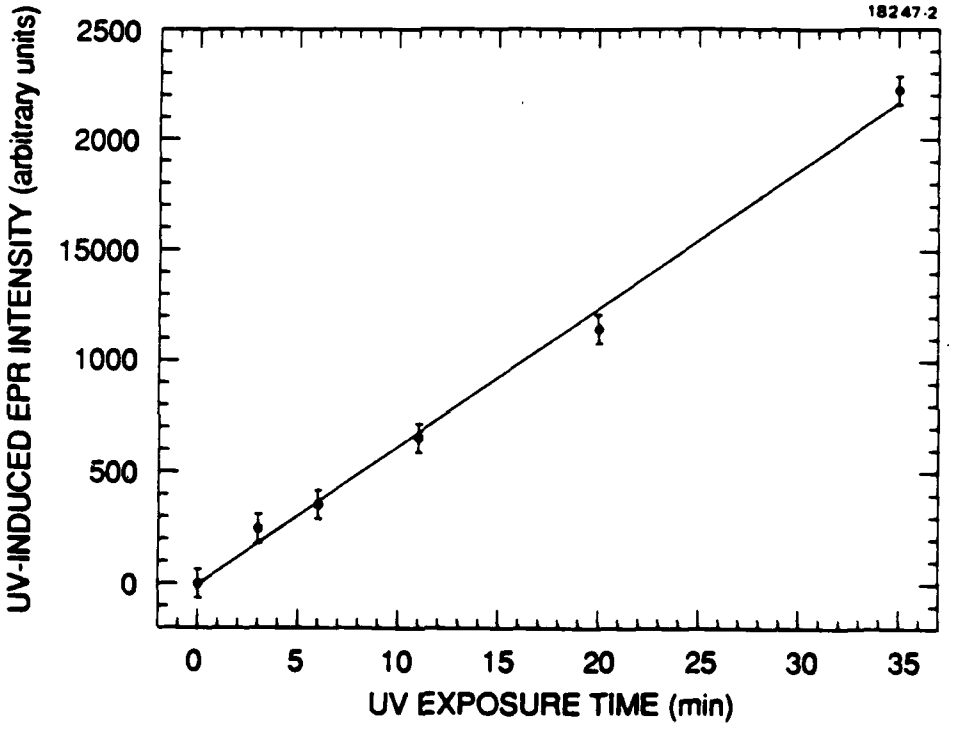
18247-2
UV-INDUCED EPR INTENSITY (arbitrary units)
2500
2000
15000
1000
500
0
0
5
10
15
20
25
30
35
UV EXPOSURE TIME (min)

Figure 4

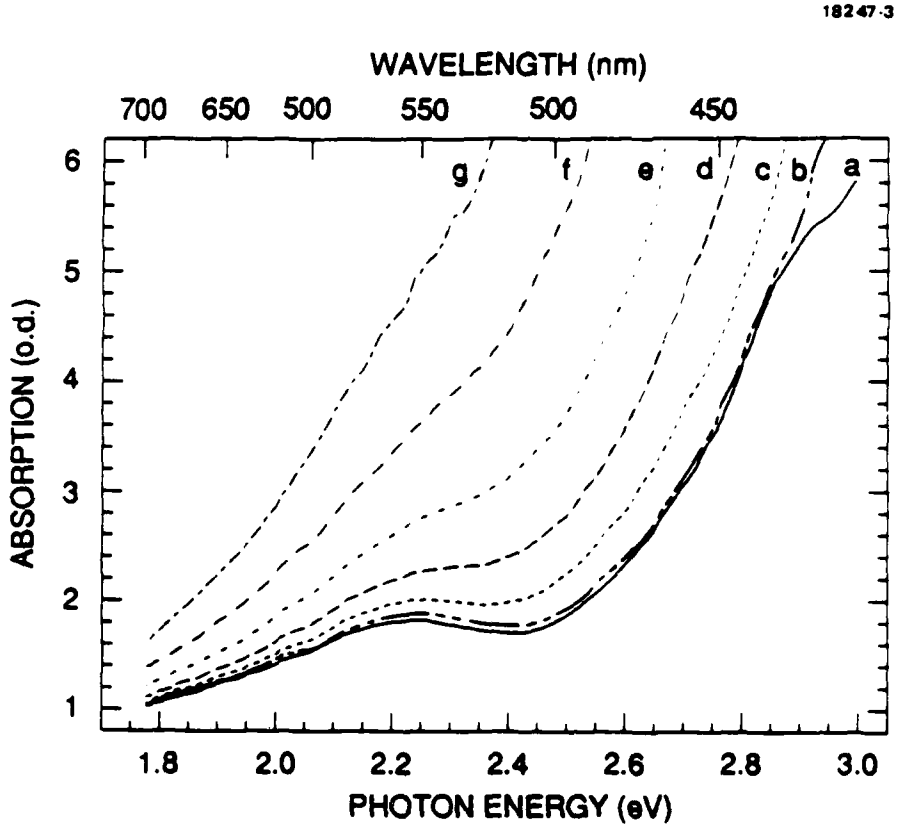
18247-3
WAVELENGTH (nm)
700
650
500
550
500
450
6
5
4
3
2
1
ABSORPTION (o.d.)
g
f
e
d
c
b
a
1.8
2.0
2.2
2.4
2.6
2.8
3.0
PHOTON ENERGY (eV)

Figure 5

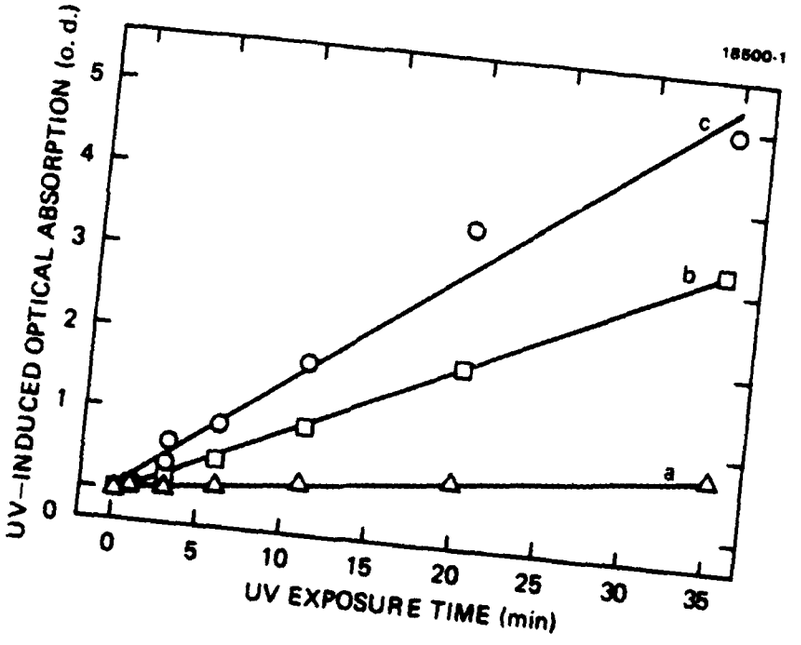
18500-1
UV-INDUCED OPTICAL ABSORPTION (o.d.)
0
1
2
3
4
5
0
5
10
15
20
25
30
35
UV EXPOSURE TIME (min)
a
b
c

Figure 6

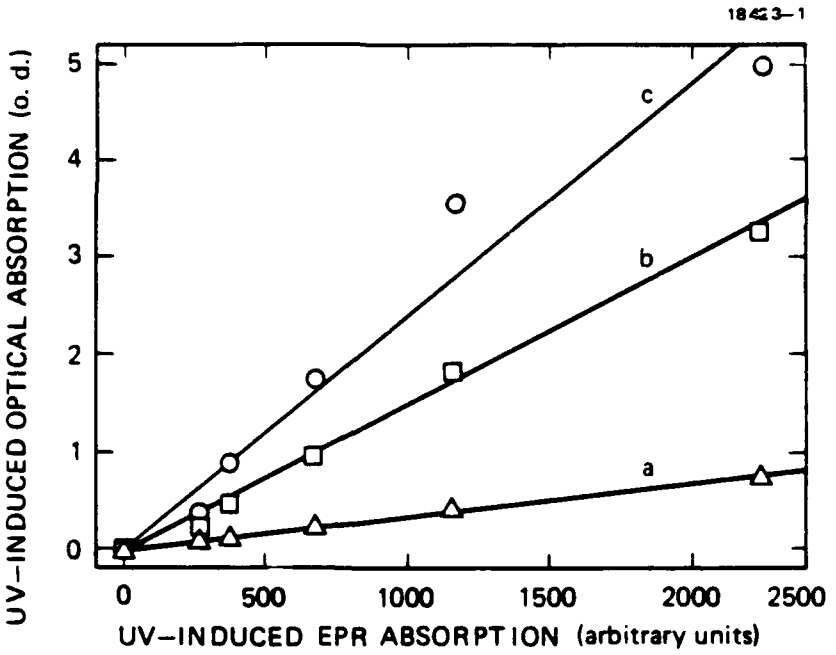
1843-1
UV-INDUCED OPTICAL ABSORPTION (o. d.)
0
1
2
3
4
5
0
500
1000
1500
2000
2500
UV-INDUCED EPR ABSORPTION (arbitrary units)
a
b
c

Figure 7